Ragnhild Skorpa

Hydrogen dissociation under equilibrium and non-equilibrium conditions

A study using molecular dynamics

Doctoral thesis
for the degree of Philosophiae Doctor

Trondheim, October 2014

Norwegian University of Science and Technology
Faculty of Natural Sciences and Technology
Department of Chemistry

NTNU

Norwegian University of Science and Technology

Doctoral thesis
for the degree of Philosophiae Doctor

Faculty of Natural Sciences and Technology
Department of Chemistry

ISBN ISBN 978-82-326-0558-3 (printed version)
ISBN ISBN 978-82-326-0559-0 (electronic version)
ISSN 1503-8181

Doctoral theses at NTNU, 2014:323

Printed by NTNU-trykk

Acknowledgement

First of all I would like to thank Prof. Signe Kjelstrup, who has been the main supervisor for this project and Prof. Em. Dick Bedeaux (co-supervisor), for letting me take part of what turned out to be an interesting journey full of surprises and challenging new methods. I would also like to thank both of you for always having time to discuss new results, and for giving quick and thorough feedback on drafts (even when I specifically ask you to only look at the plots).

Additionally, I would like to thank Prof. Thijs J. H. Vlugt at TU Delft for letting me come and work in his group for 5 months. I learnt a lot about simulations in that period! I would also like to thank Assoc. Prof. Jean-Marc Simon at University of Burgundy for valuable input in the equilibrium simulations and for letting me come to Dijon. Jing Xu is thanked for providing the molecular dynamics code for the potential- and force routine for the hydrogen dissociation reaction. I would also like to thank Storforsk Project Transport nr. 167336 and the Department of Chemistry for financing the PhD.

To all you colleagues, both former and present. Thanks for all the coffee breaks, lunches, help and support, random walks, for listening to my frustration when things are not going according to the plan, and for making D3 a fun place to be! Sondre, thanks for the continuous simulation support.

Family and friends, thanks for all the fun and support these years. Odne, you always make me smile and reminds me of what is important. You really are the best!

Abstract

The aim of this thesis project was to model reactions using classical molecular dynamics simulations under both equilibrium and non-equilibrium conditions and to study the effect of the reaction on the transport properties of the system. The dissociation of hydrogen was chosen as a model system based on its importance for the hydrogen society, and the availability of interaction potentials to model the reaction.

According to procedures described by Stillinger and Weber, a three-particle interaction potential was added to the pair potential. With this it was possible to properly describe the dissociative reaction. Equilibrium studies was performed at different temperatures and densities. From this, a detailed analysis of the interaction potential, the pair correlation functions and the contributions from the two- and three particle interactions on the overall pressure was performed. This made it possible to determine a temperature and density range where the degree of dissociation was significant.

The Small System method was extended to calculate partial molar enthalpies from fluctuations of particles and energies in a subsystem embedded in the simulation box. It was proven that this method worked well for both reacting and non-reacting mixtures. This method was applied to the hydrogen dissociation reaction. From this the reaction enthalpy was determined as a function of temperature, pressure and composition of the reacting mixture for three different densities. The reaction enthalpy was found to be approximately constant (460–440 kJ/mol) for a gas (0.0052 g/cm^3), 410–480 kJ/mol for a compressed gas (0.0191 g/cm^3) and 500–320 kJ/mol for a liquid (0.0695 g/cm^3) for temperatures in the range 4000-21000 K. With knowledge of the reaction enthalpy, the thermodynamic equilibrium constant, and thus the deviation from ideality was found.

Non-equilibrium simulations was used to study the coupled transport of heat and mass both transport of hydrogen through a palladium membrane and for the dissociative reaction in a bulk phase. For the first case, transport coefficients had to be estimated. For the latter case, the coefficients were determined for the first time directly from the fluxes in the system using non-equilibrium molecular dynamics simulations. The transport properties for both systems were then determined from the coefficients. For transport across a membrane, it was illustrated how a temper-

ature gradient could be used to enhance and control the flux of hydrogen through the membrane.

Contents

Chapter 1

Introduction

1.1 Scope

Computer simulations are a useful tool for a realistic study of systems under conditions that are not easy to achieve in a laboratory, such as high temperature, pressure, concentration and other extreme conditions. Quantum mechanics is one option, but as these simulations becomes very time consuming for large systems, or if statistical averages are needed, quantum mechanics is practically not possible. Classical simulations, such as molecular dynamics- and Monte Carlo simulations offer an alternative to the quantum mechanical methods, as they are better in handling both the temperature ranges and the appropriate time scale (ns). However, most molecular dynamics simulations use a classical force field with a harmonic description of the bonds. Since these potentials do not allow formation and breaking of bonds, they are not suited to model chemical reactions. Stillinger and Weber proved in 1985 that by adding three particle interaction to the commonly used two particle interaction potential, they were able to properly describe a chemical reaction [1–3]. Around the same time, several other many body potentials sprung out [4, 5].

A detailed analysis of the equilibrium properties of a chemical reaction, such as variation of the reaction enthalpy with temperature, pressure and composition, and of the transport properties under non equilibrium conditions will be performed. This will serve as a basis for further studies, where a temperature- or concentration gradient is present e.g., in combination with a surface. The hydrogen dissociation reaction was chosen as a model reaction due to its importance in many instances, its simplicity and the availability of interaction potentials for modeling the reaction. This makes the hydrogen dissociation reaction an ideal model reaction for our purpose.

1.2 The hydrogen dissociation reaction

Hydrogen is the most abundant element in the universe and on earth [6,7]. However, the majority of hydrogen is chemically bound (as e.g., H_2O) and less than 1% is present as H_2 [6]. As the ratio of valence electrons to protons is high, the chemical energy gain per electron is high [6], and unlike hydrocarbons, hydrogen can not be destroyed [7].

The hydrogen dissociation reaction is important in many instances, such as for the hydrogen society; as pure hydrogen is needed for fuel cells in electric vehicles. Additionally, as it is a simple reaction, it is also well suited as a model system for chemical reactions. The phase diagram of hydrogen shows that the molecular fluid (H_2) dominates up to approximately 5000 K. Above that, hydrogen spontaneously dissociates to an atomic fluid. Thus, at "normal" temperatures and pressures hydrogen is present as a molecular fluid, while high temperatures, such as those on the surface of the sun, is needed to get a dissociated system. At standard state conditions (1 bar, 298 K) the reaction enthalpy for the dissociative reaction ($H_2 \rightleftharpoons 2H$) is 436 kJ/mol [8]. As will be illustrated in Chapter 6 the reaction enthalpy is of the same magnitude also for higher temperatures and pressures.

Hydrogen, for use in fuel cells etc., is conventionally produced using the water-gas-shift reaction [9] and from water electrolysis. In a membrane reactor, the chemical reaction (to produce hydrogen) and the separation process (from the resulting hydrogen and hydrocarbon stream), is performed in one step, as the palladium membrane is solely selective towards hydrogen. This results in both a higher yield and a lowering of the production cost. An overview of hydrogen production using palladium membranes was given by Basil [10], and a review of the palladium reactors can be found in ref. [11]. One drawback with this method of producing hydrogen, is that palladium is expensive. This makes it more important to understand all the small steps in the production mechanism, such as the dissociative adsorption reaction of hydrogen on the palladium surface. This gives motivation to use the dissociative reaction of hydrogen as a model system for a thorough study of the reaction and the influence of temperature, pressure and molecular concentration on the reaction enthalpy, and on the transport properties. The intention is to establish a model which adds to the description of reactions at both equilibrium and non-equilibrium conditions, in addition to gain knowledge of the hydrogen dissociation reaction, which will be of importance for improving membrane technologies.

1.3 Methods for determination of enthalpies

A goal in the chemical process industry is to completely understand and model the processes in a chemical reactor. Chemical reactions often take place in the presence of a pressure and/or a temperature gradients. The enthalpy is an important parameter to understand thermodynamics of chemical reactions, as it determines the

equilibrium properties of a multicomponent system [12]. This absolute quantity is difficult to measure precisely [13]. One can only determine the enthalpy difference. For a binary mixture at constant temperature and pressure the total enthalpy is given by

$$\Delta H = \sum_{i=1}^{n} N_i \Delta H_i \tag{1.1}$$

where N_i is the number of particles of specie i and ΔH_i is the partial molar enthalpy of component i which can be defined, from the total enthalpy, by

$$\Delta H_i = \left(\frac{\partial \Delta H}{\partial n_i} \right)_{n_{j \neq i}} \tag{1.2}$$

Partial molar enthalpies are usually found (both experimentally and with simulations) by taking a numerical derivation of the total enthalpy with respect to the number (in mol) of particles of one component [14].

Calorimetry is the most common experimental method available to determine enthalpies, and measures the heat change of a chemical reaction, which in turn is related to the change in internal energy and the reaction enthalpy. The calorimetry methods, such as constant volume (bomb calorimetry) and constant pressure, are well described in literature [15–18]. Experimentally, constant pressure is much easier to maintain in laboratory than e.g., constant volume. If the heat change is measured at constant pressure, it is directly proportional to the enthalpy.

$$\Delta H = -C_P \Delta T \tag{1.3}$$

The heat capacity of the calorimeter, C_P, can be found by applying an electric current to the system.

Another way to determine the enthalpy change is to measure the change in vapour pressure as a function of temperature, by e.g., heating up a pure liquid. The enthalpy of vaporisation can then be found from

$$\mathrm{d} \ln P = -\frac{\Delta_{vap} H}{R} \mathrm{d} \left(\frac{1}{T} \right) \tag{1.4}$$

The total enthalpy of a mixture can easily be found from simulations. The partial molar enthalpies are however more troublesome, as they can not be expressed directly as an average of a function of the coordinates and momenta of the particles in a mixture [19]. For a mixture of non-reactive components, the partial molar enthalpies can be found by taking the derivative of the total enthalpy with respect to mol component. However, for reactions and other linear dependent systems, this is not possible. Additionally, the accuracy is dependent of the numerical differentiation [19].

Over the years, several methods to find partial molar enthalpies using molecular simulations have been established in addition to the numerical differentiation, such

as particle insertion and deletion (the Widoms test particle method, see e.g., Frenkel and Smit [20]) and identity changes [19, 21]. The first, requires several simulations at different compositions, which is a disadvantage. Additionally, it is not suited for dense systems, as the acceptance for a particle insertion would be too low. The second method, by changing the identity of a particle of component i to component j is superior as only one simulation is needed. The partial enthalpy is found for both methods by looking at the potential energy change from such operations. The Small System Method, developed by Schnell and coworkers [22–24], has been extended to determine partial molar enthalpies [25] as will be illustrated in Chapter 5. From fluctuations of particle numbers and energies in a small system embedded in a larger reservoir, one can directly calculate the partial molar enthalpies. As the Small System Method has been proven to work well for a chemically reacting system, [25], this method will be used to find partial molar enthalpies and reaction enthalpies for the hydrogen dissociation reaction in Chapter 6. The principles of the Small System Method, along with some usage areas, are outlined in Section 2.2.

1.4 Problem definition and outline of the thesis

The aim of this thesis project is to model reactions using classical molecular dynamics simulations under both equilibrium and non-equilibrium conditions and to study the effect of the reaction on the transport properties. With this the work also aspire to improve knowledge about dissociative reactions, and to add to already existing models. This will be done by first studying a chemical reaction, the dissociation of hydrogen, under equilibrium conditions where the enthalpy of the reaction is determined as a function of pressure, temperature and composition. The hydrogen dissociation reaction will also be studied under non-equilibrium conditions, in the presence of a temperature gradient, where the transport processes will be described and quantified. With this additional study the aim is to lay the basis for further studies, e.g., for a reaction on a surface.

A short theoretical background for the thesis is given in Chapter 2. Chapters 3–6 are based on published or submitted papers. One is still in preparation, Chapter 7. All papers are listed in the next Section.

In Chapter 3 (Paper 1) the transport of hydrogen through a palladium membrane was studied, illustrating the importance of and application for both non-equilibrium thermodynamics and membrane technologies. The hydrogen dissociation on the palladium surface plays an important role in the membrane setup, and it is illustrated how a temperature gradient over the membrane can be used to enhance and control the mass flux of hydrogen through the membrane.

In Chapter 4 (Paper 2) a classical molecular dynamics model of the hydrogen dissociation reaction was developed, based on the previous model of Stillinger and

Weber for fluorine. With this model the equilibrium basis for the dissociation of hydrogen was studied in detail, such as the energy landscape (with both two- and three particle interactions), the pair correlation functions, and the contributions from the two- and three-particle interactions to the pressure. A first estimate of the reaction enthalpy was made from the dissociation constant, assuming ideal conditions.

The Small System Method was extended to find partial molar enthalpies and reaction enthalpies in Chapter 5 (Paper 3). Both a binary mixture and a dummy reaction was used as model systems.

In Chapter 6 (Paper 4) the Small System Method was applied to the dissociation of hydrogen. From this the enthalpy of reaction, Kirkwood-Buff integrals and thermodynamic correction factors for a gas, compressed gas and a liquid density was determined as a function of temperature. All for non ideal systems. From this the thermodynamic equilibrium constant was determined for the lowest density.

In Chapter 7 (Paper 5) the diffusion of heat and mass in a chemically reactive mixture; the hydrogen dissociation reaction was studied. With the use of the analytical procedure given by Xu et al. [26] the temperature profile and the component fluxes was successfully fit to analytical expressions. From this the resistivities of the system, and the transport properties of the system was determined.

A conclusion of the work is given in Chapter 8, and in Chapter 9 some suggestions for further work is given.

1.5 List of papers

The publications made during the PhD is listed below and has been included in the thesis as Chapter 3–6. Papers 1-4 have been published or submitted to international peer-reviewed journals, while paper 5 is in preparation, and has been included as a manuscript.

Paper 1. R. Skorpa, M. Voldsund, M. Takla, S. K. Schnell, D. Bedeaux and S. Kjelstrup. *Assessing the coupled heat and mass transport of hydrogen through a palladium membrane.*. J. Membrane Science, (2012) 394–395:131–139.

Paper 2. R. Skorpa, J.-M. Simon, D. Bedeaux, S. Kjelstrup. *Equilibrium properties of the reaction* $H_2 \rightleftharpoons 2H$ *by classical molecular dynamics simulations.*. PCCP, (2014) 16:1227–1237.

Paper 3. S. K. Schnell, R. Skorpa, D. Bedeaux, S. Kjelstrup, T.J.H. Vlugt and J.-M. Simon. *Partial Molar Enthalpies and Reaction Enthalpies From Equilibrium Molecular Dynamics Simulation.* Submitted to J. Chem. Phys June 2014

Paper 4. R. Skorpa, J.-M. Simon, D. Bedeaux, S. Kjelstrup. *The reaction enthalpy of hydrogen dissociation calculated with the Small System Method from simulations of molecular fluctuations.* PCCP (2014) 16:19681–19693.

Paper 5. R. Skorpa, T. J. H. Vlugt, D. Bedeaux and S. Kjelstrup. *Diffusion of heat and mass in a chemically reactive mixture.* Manuscript in preparation.

1.6 Author contributions

The simulations and programming needed for paper 2, 4 and 5 were done by Ragnhild Skorpa (RS), which is the author of this thesis. The work was supervised by Signe Kjelstrup (SK) (paper 2, 4 and 5), Dick Bedeaux (DB) (paper 2, 4 and 5), Jean-Marc Simon (JMS) (papers 2 and 4) and Thijs J.H. Vlugt (TJHV) (paper 5). All co-authors have been helping with the problem formulation, discussion of the results and with valuable comments on the manuscripts. DB and SK has also helped with writing parts of the manuscripts.

The problem formulation of paper 1 was suggested by SK, and the work done was a joint contribution between RS, Mari Voldsund (MV), Marit Takla (MT) and Sondre K. Schnell (SKS), under supervision of DB and SK. MV and SKS performed the mathematical modeling, and MT and RS took the lead in defining the equations and estimation of the necessary parameters. RS took the lead in writing the final paper.

The problem formulation of paper 3 was suggested by JMS. RS verified the theoretical predictions using molecular dynamics simulations under the supervision of JMS. Once RS had verified the theory, SKS took over and expanded the modeling. The final simulations that appear in the paper was performed by SKS. The writing of the paper was performed mainly by JMS and SKS, all authors have contributed to scientific discussion of the results, and commenting on the manuscript.

Chapter 2

Theoretical background

This chapter gives a short theoretical background of the techniques used in this thesis. A short introduction to molecular dynamics simulations of chemical reactions is given in Section 2.1 followed by a brief introduction to the Small System Method in Section 2.2, which is used to calculate the reaction enthalpy. Finally, a short introduction to non-equilibrium thermodynamics for both bulk and surface is given in Section 2.3.

2.1 Molecular dynamics simulations of reactions

Molecular dynamics simulations is a useful tool to mathematically study complex phenomena over time, and several textbooks have been written on the topic, see e.g., references [20, 27, 28]. Simulations give us the possibility to study systems at very high or low temperatures and pressures. These situations are either not possible, or extremely difficult to achieve in laboratories. Another advantage is that it is cheaper than laboratory experiments, as one does not need chemicals or expensive apparatus, only a computer and access to a supercomputer is needed. This in turn gives the possibility to run several simulations in parallel, and this can be used e.g. to screen molecules for catalysts.

The addition of a three-particle interaction to the commonly used pair potential makes it possible to study the formation and breaking of bonds, and thereby making it possible to study chemical reactions with classical simulations. The first report of a reactive system modeled with a three-particle potential was from Stillinger and Weber in 1987 where they investigated the chemical reactivity in liquid sulphur [2]. In 1988 [3] they continued the procedure with the reaction $F_2 \rightleftharpoons 2F$ as a model system. Kohen et al. used three particle interactions in 1998 to model the interaction of hydrogen with a silicon surface [29]. Xu et al. [26,30–32], investigated

the nature of coupled transfer of heat and mass for a chemical reaction using two- and three particle interactions. As a model system Xu et al. also used the simple reaction $2F \rightleftharpoons F_2$, and the system was exposed to temperature gradients up to 10^{11} K/m. Another example of a three-particle interaction potential is the potential by Axilrod and Teller to describe dispersion interactions from 1943 [33], which has been used to study binary fluids [34, 35].

Another possibility to model chemical reactions is to use bond order potentials, first derived by Abel in 1985 [5]. These potentials uses the bond order to describe different the chemical bonds and can for this reason be used to model chemical reactions. Double and triple bonds are defined by the length of the bonds and not orbital overlap, and the bond length of double and triple bonds are for this reason often predicted to be longer than the experimental values. Over the years this potential type has been expanded and improved [4, 36–40] to be able to describe both radicals and conjugated systems, by including also the coordination of the nearest neighbours. However, until recently these potentials have only been able to describe hydrocarbons, with the exception being the latest versions of ReaxFF [38] and REBO [39]. As ReaxFF has been developed to also describe different oxidation states of metals [41, 42], and reactions catalysed by transition metals [43, 44] it is well suited to model chemical reactions at the interface of different materials, which is interesting in a catalytic point of view.

2.1.1 Interaction potentials

The interactions between particles are described by an interaction potential which gives the interaction energies as a function of the distance between the particles. For a system consisting of N_p-particles, the interaction potential can be divided into contributions from one-, two-, three-particle interactions etc.

$$U_{tot}(1,\ldots,N_p) = \sum_i u_{(1)}(i) + \sum_{i<j} u_{(2)}(i,j) + \sum_{i<j<k} u_{(3)}(i,j,k) + \ldots \tag{2.1}$$

The first term gives the single particle potential which contains the contribution from walls and external forces, and can be ignored when no external force is present.

The pair interaction, the second summation in Eq. (2.1), is only a function of the scalar distances [45]. Kohen et al. [29] gave the pair interaction (Eq.(2.2)), for the hydrogen dissociation reaction [29], based on quantum mechanical results [46].

$$u_{(2)}(r) = \begin{cases} \alpha\left(\beta_2 r^{-p} - 1\right)\exp\left[\frac{\gamma_2}{r-r_c}\right] & \text{if } r < r_c \\ 0 & \text{if } r > r_c \end{cases} \tag{2.2}$$

Where $\alpha = 5.59 \cdot 10^{-21}$ kJ, $\beta_2 = 0.044067$ Å^p, $\gamma_2 = 3.902767$ Å, $r_c = 2.8$ Å and $p = 4$ are constants [29]. α is chosen such that the minimum of the potential gives the binding energy of hydrogen (432.065 kJ mol^{-1}) [29] at the equilibrium

bond distance between two hydrogen atoms, $r_e = 0.74$ Å [47]. When the distance between two atoms is larger than the cut-off distance, $r \geq r_c$, the potential is zero. The reduced units used throughout this thesis (indicated by superscript *) are defined by the particle diameter, σ which is defined by $u_2(\sigma) = 0$, which gives $\sigma = \sqrt[p]{\beta_2} = 0.458$Å, and the potential depth, ϵ based on the binding energy of hydrogen, so that $\epsilon/k_B = 51991$ K.

As stated earlier, a three particle interaction is also needed to describe a chemical reaction, and this interaction must possess full translational and rotational symmetry [45]. For the hydrogen dissociation the three particle interaction was given by Kohen et al. [29].

$$u_{(3)} = h_{i,j,k}(r_{ij}, r_{jk}, \theta_{i,j,k}) + h_{j,i,k}(r_{ji}, r_{ik}, \theta_{j,i,k}) + h_{i,k,j}(r_{ik}, r_{kj}, \theta_{i,k,j}) \tag{2.3}$$

where the middle letter, j, in the subscript i, j, k refers to the atom in the subtended angel vertex. The h-functions are given by

$$h_{j,i,k}(r_{ji}, r_{ik}, \theta_{j,i,k}) = \begin{cases} \lambda a \exp\left[\frac{\gamma_3}{(r_{ji}-r_c)} + \frac{\gamma_3}{(r_{ik}-r_c)}\right] & \text{if } r_{ji} < r_c \text{ and } r_{ik} < r_c \\ 0 & \text{otherwise} \end{cases} \tag{2.4}$$

and

$$a = \left[1 + \mu\cos(\theta_{j,i,k}) + \nu\cos^2(\theta_{j,i,k})\right] \tag{2.5}$$

$\lambda = 2.80 \cdot 10^{-21}$ kJ, $\mu = 0.132587$, $\nu = -0.2997$ and $\gamma_3 = 1.5$ Å are constants [29]. The cut-off distance, r_c, is the same for both the two- and three-particle interactions (2.8 Å).

The total potential for a linear configurations of hydrogen atoms, is illustrated in Figure 2.1, where the minima of the potentials are indicated by U_1-U_3. Only the

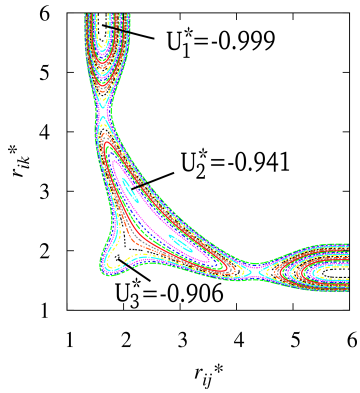

Figure 2.1: Total potential energy surface for a linear configuration of three hydrogen particles using two- and three particle interactions. Superscript * indicate reduced units. U_1-U_3 indicates the minima of the potential. The figure is adapted from ref. [48].

linear configuration of the total potential was considered as Siegbahn and Liu [49] determined that the linear configuration contained the deepest minima.

From the study in Chapter 4 it will be shown that the three-particle interaction lead to a large excluded volume diameter of the molecular fluid. This excluded volume diameter is in agreement with the Lennard-Jones diameter used by others [48].

2.1.2 Pressure calculations

The three-particle interaction potential will give a contribution to the overall pressure in the system [31,48]. From the virial theorem, the expression for the pressure in the presence of two- and three-particle interactions is:

$$P = \frac{k_B T N_p}{V} - \frac{1}{3V} \sum_{i=1}^{N_p} \left[\frac{1}{2} \sum_{j \text{ pair with } i} \frac{\partial u_2(r_{ij})}{\partial r_{ij}} r_{ij} \right. \\ \left. + \sum_{j<k \text{ triplet with } i} \left(\frac{\partial h_i}{\partial r_{ji}} r_{ji} + \frac{\partial h_i}{\partial r_{ik}} r_{ik} + \frac{\partial h_i}{\partial r_{jk}} r_{jk} \right) \right] \tag{2.6}$$

where pairs and triplets under the summation indicates that the summation is performed over all pairs and triplets. The function h_i is a function of the angle and distances of a triplet formation.

$$h_i = h_{j,i,k}(r_{ji}, r_{ik}, \theta_{j,i,k}) \tag{2.7}$$

The first term in Eq. (2.6) gives the ideal contribution to the pressure due to the total number of particles, N_p. The second and the third terms give the contributions from the two- and three particle potentials, respectively. This makes it possible to quantify and compare the separate contributions to the pressure. The first study of the three-particle interaction contribution to the overall pressure for a chemical reaction was made by Xu et al. [30]. In Chapter 4 it will be shown that the magnitude of the three particle contribution to the pressure is dependent on the degree of dissociation [48].

2.2 The Small System Method

In 1963 Hill [50] extended the range of the validity of the thermodynamic functions and the mathematical interrelations between these functions to nonmacroscopic systems, such as colloidal particles or one macroscopic molecule. In this situations U, H and G are no longer extensive variables, and regular thermodynamic functions and relations are not valid. In 1998 Hill and Chamberlin [51–53] defined nanothermodynamics to describe systems that are far from the thermodynamic limit, i.e., systems with only a small number of particles. If the size of the small system increases towards the size of an infinite system ($N_j \to \infty$ or $V_j \to \infty$), the thermodynamical equations for the small system becomes equal to the ordinary thermodynamical equations.

The Small System Method is based on Hills formalism and the first reports of this was made by Schnell and coworkers [22–24] in 2011. This new method is under constant development, with the latest extension to find partial molar enthalpies and reaction enthalpies, and the usage areas increases rapidly. This will be described in detail in Chapter 5, where also a more detailed description of the method is given.

2.2.1 Principles

In the simulation box, periodic boundary conditions, as illustrated in Figure 2.2 for a two-dimensional system, is obeyed. The original system, in the center with red

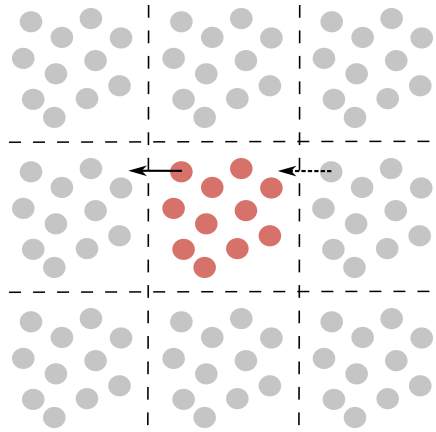

Figure 2.2: A two-dimensional illustration of periodic boundary conditions. The center frame is the frame of reference (red particles) and a copy of this is made in all directions. When a particle leaves the center frame, another particle enters from one adjacent frame as indicated by the arrows (full arrow for the particle leaving the frame of reference and dashed for the one entering). In this manner, the number of particles is conserved.

particles, is surrounded by replicas in such way that if a particle at the left move across the wall to the next replica to the left (indicated by the arrow), a particle from the right immediately enters from the same location (dashed arrow) at the right hand side.

The basic principle of the Small System Method is to create a small system inside a large reservoir (e.g., the original simulation box). For a spherical subsystem, the radius varies from $\sigma < L < 0.5B_i$, where B_i is the shortest length of the simulation box for a non-cubic system, and L is the radius of the sphere . In these subsystems, energy and particle number are allowed to fluctuate, and the original periodic boundary conditions of the box (as illustrated in Figure 2.2) are thus not obeyed. An illustration of this is given in Figure 2.3, for a two-dimensional system. With the reservoir in the N, V, T ensemble, the small systems follow the μ, V, T ensemble. From the fluctuation of particle number and energy in a binary mixture

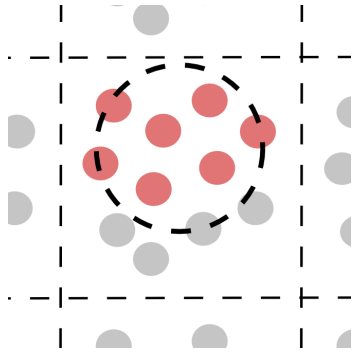

Figure 2.3: Two-dimensional illustration of the boundaries of the Small System Method. A spherical subsystem with fluctuation of energy and particles is embedded in the reservoir. Particles that are inside the small system is indicated by red spheres. For molecules, the center of mass was used to determine whether a molecule is inside or not. The gray spheres indicates particles that are not counted as part of the small system.

the thermodynamic correction factors, Γ_{ij}, and the partial enthalpy of component i, h_i can be found.

$$\Gamma_{ij}^{-1} = \frac{1}{\beta}\left(\frac{\partial \ln\langle N_i\rangle}{\partial \mu_j}\right)_{T,V,\mu_{k\neq i}} = \frac{\langle N_i N_j\rangle - \langle N_i\rangle\langle N_j\rangle}{\langle N_j\rangle} \tag{2.8}$$

$$h_i = \left(\frac{\partial H}{\partial N_i}\right)_{T,V,\mu_{j\neq i}} = -\frac{\langle U N_i\rangle - \langle U\rangle\langle N_i\rangle + k_B T\langle N_i\rangle}{\langle N_i^2\rangle - \langle N_i\rangle^2} \tag{2.9}$$

Where the brackets denote time averages, N_i is the number of particle i inside the subsystem, $\beta = k_B T$ and U is the total energy.

All fluctuations inside the subsystem are dependent on the size of the subsystem in consideration. This means that the thermodynamic properties are found as a function of system size. For the density of an extensive thermodynamic variable, X, we have [25]

$$\frac{X}{V} = A_b + A_s L^{-1} + A_e L^{-2} + A_c L^{-3} \tag{2.10}$$

where L is the radius of the subsystem and V its volume. A_b, A_s and A_e give contributions to X proportional to the volume, surface and the linear diameter, respectively and A_c is a constant. By extrapolating to $1/L = 0$ (infinitely large system) the volume term, A_b, is independent of the size of the small system, and can for this reason be linked to the value in the thermodynamic limit. This means that by changing the size of the small subsystems the thermodynamic limit value of X can be determined by extrapolation, from one simulation alone. This is an extremely important advantage of the method. However, one has to keep in mind that the value in the thermodynamic limit is ensemble dependent, thus these values might need to be transformed to a different ensemble to obtain the correct results. This will be illustrated in Chapters 5 and 6, where the Small System Method is

used to find partial enthalpies at constant T, V, μ_j and then transferred to partial molar enthalpies (at T, P, N_j).

As the fluctuations inside the subsystem are size dependent, it is important to determine a region where size effects are negligible. This region, which is independent of the size of the reservoir, should be used when extrapolating to find the value in the thermodynamic limit. As will be illustrated in Chapters 5 and 6 this region is system dependent and has to be determined individually for each system. This can be verified by running the same simulation with a larger simulation box (with the same density).

2.2.2 Status of the Small System Method

Even though the Small System Method is fairly new (first reported in 2011), and continuously under extension, it has already proven to be useful for chemists. Liu et al. [54, 55] showed how this method could be used to find Fick diffusion coefficients from Maxwell-Stefan diffusivities with the knowledge of the thermodynamic correction factors, which are found from particle fluctuations using the Small System Method. In 2013, Schnell et al. [56] showed that the Small System Method works well for linearly dependent systems, such as the individual species in salt solution, which is an important property of this method compared to other simulation techniques. The Small System Method was extended by Collell and Galliero [57] for in- homogeneous Lennard Jones fluids confined in slit pores to determine the thermodynamic factor of confined fluids. Recently, the method was used by Reif et al. [58] to calculate the thermodynamic correction factors for salt-water and salt-salt interactions. Trinh et al. [59] studied the adsorption of carbon dioxide on a graphite surface and thereby extended the Small System Method to surfaces. The latest extension, to calculate partial molar enthalpies and reaction enthalpies from one single simulation, will be demonstrated in Chapter 5 [25]. In Chapter 6, the method will be used to find reaction enthalpies and as a function of temperature for the dissociation of hydrogen, a system that is far from ideal conditions.

2.3 Non-equilibrium thermodynamics

Non-equilibrium thermodynamics is a useful tool to systematically describe transport processes, as it provides a theoretical description of transport properties for irreversible processes which are out of global equilibrium [12, 60]. Over the years several textbooks have been written on the subject, see e.g., references [12, 60, 61]. The theory was established by Onsager in 1931 [62, 63] to describe transport processes in homogeneous systems. A systematic description of the extension to heterogeneous systems, including transport into and through a surface was given by Kjelstrup and Bedeaux in 2008 [12]. The two chapters that include non-equilibrium thermodynamics in the thesis both contain a chemical reaction, but in different

ways. One reaction is present in the bulk phase (Chapter 7), the other at the surface of a membrane (Chapter 3).

2.3.1 The entropy production of a chemically reacting system

The entropy production rate for a chemical reaction, e.g., $H_2 \rightleftharpoons 2H$, with transport of heat and mass was given by Groot and Mazur [61], and this system will be discussed in detail in Chapter 7.

$$\sigma = J_q \nabla \left(\frac{1}{T}\right) - \sum_i J_i \nabla \frac{\mu_i}{T} - r\frac{\Delta_r G}{T} \geq 0 \tag{2.11}$$

Here, J_q is the total heat flux, and J_i the molar component flux of either H or H_2, with respect to the wall. $\nabla(1/T)$ gives the temperature gradient in the x-,y- and z-direction, and $\nabla\mu_i$ is the gradient in chemical potential of component i. r is the reaction rate, and $\Delta_r G$ is the reaction Gibbs energy. The first two flux-force pairs are vectors, while the third flux-force pair, from the reaction, is a scalar, and does for this reason not couple to the other vectorial flux-force pairs. In the absence of a net mass flux through the system ($J_{\mathrm{H}} = -2J_{\mathrm{H}_2}$), the rate of the reaction is defined as the gradient of the component flux

$$r = -\frac{\partial}{\partial x} J_{\mathrm{H}_2}(x) = \frac{\partial}{\partial x}\frac{1}{2} J_{\mathrm{H}}(x) \tag{2.12}$$

The reaction Gibbs energy for the dissociative reaction is defined as

$$\Delta_r G \equiv 2\mu_{\mathrm{H}} - \mu_{\mathrm{H}_2} \tag{2.13}$$

The measurable heat flux, J'_q, is defined as

$$J_q = J'_q - J_{\mathrm{H}_2}\Delta_r H \tag{2.14}$$

If only transport in the x-direction is considered, the entropy production rate of the reacting mixture can be rewritten

$$\sigma = J'_q \frac{\partial}{\partial x}\left(\frac{1}{T}\right) + \frac{1}{T} J_{\mathrm{H}_2} \frac{\partial}{\partial x}\left(\Delta_r G\right)_T - r\frac{\Delta_r G}{T} \tag{2.15}$$

Form the entropy production the following force-flux relations for transport of heat and mass [12] can be defined

$$\frac{\mathrm{d}}{\mathrm{d}\,x}\frac{1}{T} = r_{qq} J'_q + r_{q\mu} J_{\mathrm{H}_2} \tag{2.16}$$

$$\frac{\mathrm{d}}{\mathrm{d}\,x}\frac{\Delta_r G}{T} = r_{\mu q} J'_q + r_{\mu\mu} J_{\mathrm{H}_2} \tag{2.17}$$

where r_{ii} and r_{ij} are the main- and coupling coefficients, respectively, which describes resistance to transport (here, heat and mass). The coupling coefficients gives the possibility describe and quantify coupled transport, and are linked by the Onsager reciprocal relations, $r_{ij} = r_{ji}$ [62, 63]. For a chemically reactive system, the reaction rate can be regarded as a linear function of the driving forces if $\Delta_r G < RT$ [60]. In Chapter 7 a complete analytical procedure to describe chemical reactions [26] is given. According to the definition by Onsager, the coefficients are only dependent on state variables, such as temperature and density, and not on the fluxes and forces. This means that a a temperature gradient can be used to increase- or even to stop the mass flux. This will be discussed in detail in Chapter 3, where transport of hydrogen through a palladium membrane will be studied.

The transport properties of the system, such as the diffusivity, thermal conductivity and heat of transfer etc., can all be found if the phenomenological coefficients are known, this will be show in Chapters 3 and 7. However, these are not always known from experiments and often have to be estimated. This will be illustrated in Chapter 3, where it will be shown how non-equilibrium thermodynamics makes it possible to define experiments for finding both transport properties and the phenomenological coefficients.

With local chemical equilibrium, $\Delta_r G = 0$, the entropy production reduces to a one flux-force expression

$$\sigma = J'_q \frac{\partial}{\partial x}\left(\frac{1}{T}\right) \tag{2.18}$$

2.3.2 Transport of a reacting mixture through a membrane

For transport of a mixture through a membrane, the entropy production (for one side of the membrane) is given as

$$\sigma^m = J_q^m \frac{\partial}{\partial x}\frac{1}{T} + \sum_j J_j^m \frac{\partial}{\partial x}\frac{\mu_j}{T^m} \tag{2.19}$$

where superscript m indicates the membrane. The force-flux relations for the membrane can be set up in a similar manner as described in the previous section. In the membrane, the enthalpy of the components is constant, and for this reason no coupling effect of the heat- and mass flux is observed in the membrane, [12, 64].

At the membrane surface, the situation is more complex. In non-equilibrium thermodynamics, Gibbs definition of a dividing surface, "a geometrical plane, going through points in the interfacial region, similarly situated with respect to to conditions of adjacent matter" [65], is used. With this definition, in terms of the excess densities, the surface is treated as an autonomous thermodynamic system. One consequence of this is that the surface has its own temperature, and that all its properties depend on this temperature alone, and not on the temperature of the adjacent phases. Consider a surface, s, separating two phases, i and o, as illustrated

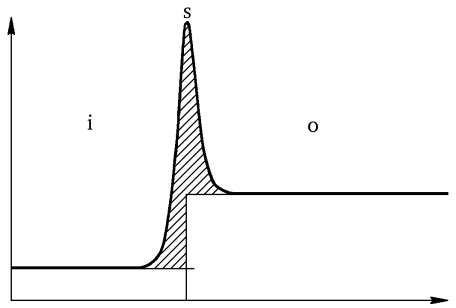

Figure 2.4: The density profile of a surface (shaded area), i and o indicate the adjacent phases. The excess surface density can be found by integration of the density profile. The figure has been reprinted and modified with permissions from the authors, ref. [12].

in Figure 2.4 for the excess surface density. With Gibbs definition of the excess surface densities, normal thermodynamic relations, such as the first and second laws are valid [65]. The excess entropy production for a non-polarized surface in the absence of an electric field has five independent flux-force pairs;

$$\sigma^s = J_q^{i,o}\left(\frac{1}{T^s}-\frac{1}{T^{i,o}}\right)+J_q^{o,i}\left(\frac{1}{T^{o,i}}-\frac{1}{T^s}\right) \tag{2.20}$$
$$+\sum_{j=1}^{n} J_j^{i,o}\left[-\left(\frac{\mu_j^s}{T^s}-\frac{\mu_j^{i,o}}{T^{i,o}}\right)\right]+\sum_{j=1}^{n} J_j^{o,i}\left[-\left(\frac{\mu_j^{o,i}}{T^{o,i}}-\frac{\mu_j^s}{T^s}\right)\right]+r^s\left(-\frac{\Delta_n G^s}{T^s}\right)$$

for transport perpendicular to the surface. From the above equation, it can be seen that coupling between $-\Delta_n G/T^s$ and $\Delta\mu/T$ is now possible, unlike the situation in the bulk phase and the membrane. This will be examined in Chapter 3, where it will also be shown that for transport of hydrogen across a palladium membrane, the entropy production reduces to two independent flux-force pairs.

Chapter 3

Assessing the coupled heat and mass transport of hydrogen through a palladium membrane

Ragnhild Skorpa[1], Mari Voldsund[1], Marit Takla [1], Sondre K. Schnell[2], Dick Bedeaux[1] and Signe Kjelstrup[1,2]

1. Department of Chemistry,
Norwegian University of Science and Technology,
NO-7491 Trondheim, Norway

2. Process & Energy Laboratory,
Delft University of Technology,
Leeghwaterstraat 39, 2628CB Delft,
The Netherlands

This chapter was published in
J. Mem. Sci. (2012) 394–395:131–139

Abstract

We have formulated the coupled transport of heat and hydrogen through a palladium membrane, including the dissociative adsorption of hydrogen at the surface. This was done using the systematic approach of non-equilibrium thermodynamics. We show how this approach, which deviates from Sieverts' law, makes is possible to calculate the direct impact that a temperature gradient, or a heat flux, has on the hydrogen flux. *Vice versa*, we show how the dissociative adsorption reaction leads to heat sinks and sources at the surface.

Using a set of transport coefficients estimated from experimental values available in the literature, calculations were performed. An enhancement of the hydrogen flux through the membrane with 10% and 25%, by transmembrane temperature differences of 24.8 K and 65.6 K, respectively, was predicted with a feed temperature of 673 K. Similarly, a transmembrane temperature difference of -176.5 K was observed to stop the hydrogen flux (Soret equilibrium). The calculations are done with estimated transport properties for the surfaces. The results show that an effort should be put into determination of these. Such experiments are discussed.

3.1 Introduction

With increasing energy prices, and a limited supply of oil, it is of importance to improve the efficiency of the most common industrial processes. In this situation, membrane reactors are interesting. In a membrane reactor, a chemical reaction and the separation of resulting products can be performed in one process step. The products are removed continuously along the reactor. This *in situ* removal of the products (or of unwanted by-products from the chemical reaction), as well as the possibility of a high yield from equilibrium limited reactions, makes this a very interesting alternative to traditional reactors.

Membrane reactors can be put into two categories: porous and dense. Porous membranes can be *e.g.* zeolite-based membranes [66,67], while the palladium membrane is a typical example of a dense membrane. In industrial applications, there are several situations where one wishes to extract hydrogen from a reaction; the water-gas-shift reaction [9] is one of the most important. For other examples, see Basile [10]. The palladium membrane is a thin layer of palladium, often on a porous support of either steel or alumina. For a recent review of state of the art palladium membrane reactors, see Yun and Oyama [11]. Palladium is purely selective towards transport of H_2. In order to give a high flux of hydrogen through the membrane, the palladium-layer should be as thin as possible; typically a few micro meter or less. In a palladium reactor hydrogen is transported as hydrogen atoms in the palladium, and as hydrogen molecules in the gas phases on each side of the membrane [11, 68]. The heat of adsorption is significant ($-87\,\mathrm{kJ\,mol^{-1}}$ [69]), including the splitting of molecular hydrogen and adsorption at the surface. This dissociative

adsorption is likely to influence the mass flux. There is a need to study this in a systematic manner for several reasons. It is known that surface effects can hamper experiments [70]. Also, permeability studies often show deviation from Sieverts' law [71]. Furthermore, while it is known how the absolute temperature affects a chemical reaction, little is known on how a temperature gradient affects the reaction rate. With a thin membrane and large heat sinks and sources at the interfaces, such gradients may be large. The coupling of chemical reactions to fluxes of heat and mass is possible in principle [60], but has not been described in detail for a real system before.

In their now seminal paper, Ward and Dao [72], presented a model for hydrogen permeation through a palladium membrane which accounted for all kinetic steps in the permeation and reaction process. This model has been modified and improved to also include mass transfer through the support by others, and has been further used a basis for incorporating the surface and a reaction in reactor models [73–77]. Many of the existing models for hydrogen permeation neglects the effect of the surface, see *e.g* [78, 79]. None of these works deal with transport of heat in combination with transport of mass across surfaces, however.

This gives us a motivation to apply non-equilibrium thermodynamics to study the transport in a palladium membrane. The work of de Groot and Mazur [61] outlines how to describe homogeneous systems. During the last decade, the field has been further developed to also include heterogeneous systems, such as systems with membranes [12]. In the extension, dynamic boundary conditions for the crossing from one layer to the next were defined. The coupling, or the interaction of fluxes and forces at the surface, is often overlooked in the literature, while it is now known that it can be substantial [80]. It is, however, relevant to ask whether linear force-flux relations apply when a chemical reaction takes place in the system. Chemical reactions have normally rates which are non-linear functions of their driving force, meaning that we then need to go to a mesoscopic level of description to capture this property [60]. In the present case, we shall see that there is no need to invoke this level of complication for operating conditions that are typical for palladium transport.

After a short description of the system and the system conditions used in Section 3.2, we proceed in Section 3.3 to derive transport equations, using non-equilibrium thermodynamics, across a palladium membrane. Details concerning the calculations and solution procedures are given in Section 3.4. In Section 3.5 we present and discuss the results obtained from applying the model to different sets of boundary conditions. We study in particular the effect the surface has on the transport across the membrane. In Section 3.6, we draw conclusions.

3.2 The system

Consider a palladium membrane separating two gas phases. For simplicity, we assume pure H_2 gas on each side. Hydrogen is transported from gas phase to gas phase, and the transport is considered to be 1-dimensional, in the direction perpendicular to the membrane. The membrane is considered to be a homogeneous system with thickness δ^{m}. The region between the gas phase and the palladium defines the membrane *surface*. There are two such planar layers of molecular thickness; one at each side of the membrane. The surface in equilibrium was described already by Gibbs as a two-dimensional system using excess thermodynamic properties. The same terminology is adopted here, following Kjelstrup and Bedeaux [12] for surfaces outside equilibrium. Figure 3.1 illustrates the system with the different phases and with fluxes entering and leaving the system. Superscript s is used to denote the surface, while f and p stands for the feed- and the permeate sides, respectively. We shall not model the diffusion layers in the gas phase external to the surfaces. These layers might well be diffusion limiting, but this will not be adressed in the present paper.

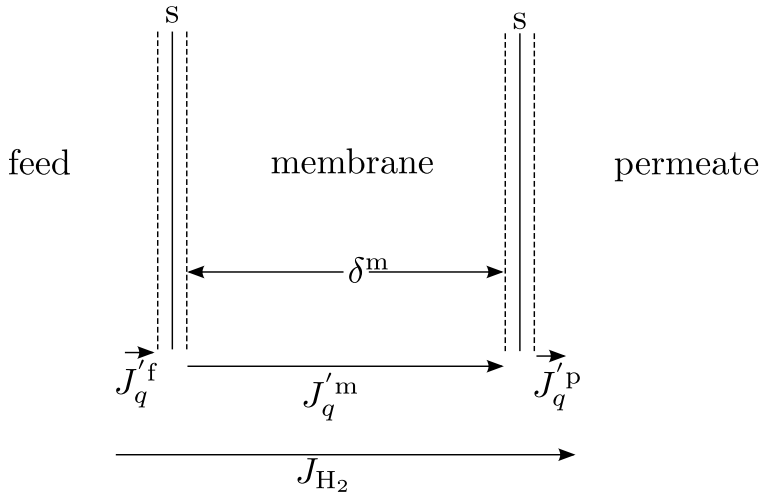

Figure 3.1: A schematic illustration of the system. A palladium membrane of thickness δ^m is bounded by two planar surfaces of molecular thickness. The planes have no extension in the direction of transport on the scale used. The mass flux, $J_{\mathrm{H_2}}$, is constant at stationary state, while the measurable heat flux, J_q', depends on the position in the system.

Prior to membrane transport, hydrogen is adsorbed at the surface. The dissociative adsorption can be written as:

$$\mathrm{H_2}(g) \rightleftharpoons 2\mathrm{H}(ads). \tag{3.1}$$

The Gibbs energy difference, ΔG, for the dissociative adsorption at the feed side

can then be defined as

$$\Delta G = 2\mu_{\mathrm{H}}^{\mathrm{m}} - \mu_{\mathrm{H_2}}^{\mathrm{f}}, \tag{3.2}$$

where μ_j^{i} is the chemical potential of component j in phase i evaluated close to the surface (here surface at the feed side). As only equations for the feed side of the membrane is given in detail in this paper, the superscripts indicating the phase (f, m or p) have been dropt for ΔG throughout the paper. For the permeate side, a similar expression as given in Eq.(3.2) can be obtained.

We shall study the stationary state, where there is no accumulation of mass anywhere in the system, and

$$r^s = \frac{1}{2} J_{\mathrm{H}} = J_{\mathrm{H_2}}. \tag{3.3}$$

Here r^s is the rate of the dissociative adsorption, J_{H} is the flux of atomic hydrogen through the membrane, and $J_{\mathrm{H_2}}$ is the rate of which $\mathrm{H_2}$ enters and leaves the system per m^2.

The total heat flux, J_q, through the system is also constant in the stationary state, giving

$$J_q = J_q'^{\mathrm{f}} + J_{\mathrm{H_2}} H_{\mathrm{H_2}}^{\mathrm{f}} = J_q'^{\mathrm{m}} + J_{\mathrm{H}} H_{\mathrm{H}}^{\mathrm{m}} = J_q'^{\mathrm{p}} + J_{\mathrm{H_2}} H_{\mathrm{H_2}}^{\mathrm{p}}, \tag{3.4}$$

which rearranged gives

$$J_q'^{\mathrm{f}} = J_q'^{\mathrm{m}} + \Delta H J_{\mathrm{H_2}} = J_q'^{\mathrm{p}}, \tag{3.5}$$

where H_j^{i} is the enthalpy of component j in phase i, $\Delta H = 2H_{\mathrm{H}}^{\mathrm{m}} - H_{\mathrm{H_2}}^{\mathrm{f}} = 2H_{\mathrm{H}}^{\mathrm{m}} - H_{\mathrm{H_2}}^{\mathrm{p}}$ is the heat of dissociative adsorption and $J_q'^{\mathrm{i}}$ is the measurable heat flux in phase i. Constant enthalpy in each phase was assumed.

3.3 A thermodynamic description of transport

In Sections 3.3.1 (for the membrane) and 3.3.2 (for the surface) we present the entropy production for each subsystem. The entropy production determines the relevant forces and fluxes, and their interactions. For details in the derivation we refer to the literature [12]. All the presented equations are given for the feed side of the membrane and for the surface at the feed side only. Equations for the permeate side are analogous and can be found in a similar manner. The force-flux relationships defines the necessary and sufficient experiments for determining transport coefficients. We shall further make a link to the experimental data we take from the literature.

3.3.1 The membrane

The general expression for entropy production in a homogeneous phase is defined as the linear combination of fluxes and forces, and is described in several texts

on non-equilibrium thermodynamics, see *e.g.* [12, 61]. For transport of heat and atomic hydrogen in the membrane, we have the following expression, choosing the representation with the measurable heat flux, $J_q'^{\mathrm{m}}$

$$\sigma^{\mathrm{m}} = J_q'^{\mathrm{m}} \frac{\partial}{\partial x}\left(\frac{1}{T}\right) + J_{\mathrm{H}}^{\mathrm{m}}\left(-\frac{1}{T^{\mathrm{m}}}\frac{\partial \mu_{\mathrm{H},T}}{\partial x}\right). \tag{3.6}$$

Here, J_{H} is the flux of atomic hydrogen, while $\partial\mu_{\mathrm{H},T}/\partial x$ is the gradient in chemical potential for atomic hydrogen at a constant temperature, T^{m}. The derivation is shown for the corresponding processes across the surface in 3.B. The expression means, that dissipative processes at stationary state are connceted to heat transport and transport of atomic hydrogen.

We express the flux of atomic hydrogen from the surface through the membrane with the flux of molecular hydrogen outside the membrane, J_{H_2}, using Eq.(3.3). We see that taking the measurable heat flux constant across the membrane simplifies the integration. We find that it results in a calculation error of less than 2% for the entropy balance. For the whole membrane, we obtain the entropy production per surface area

$$\sigma^{\mathrm{m}}\delta^{\mathrm{m}} = J_q'^{\mathrm{m}}\Delta_{\mathrm{m}}\left(\frac{1}{T}\right) + J_{\mathrm{H}_2}\left(-\frac{2}{T^{\mathrm{m}}}\Delta_{\mathrm{m}}\mu_{\mathrm{H},T}\right), \tag{3.7}$$

where Δ_{m} means the difference between the right and left hand side in the membrane phase. The force-flux relations for the membrane phase are

$$\Delta_{\mathrm{m}}\left(\frac{1}{T}\right) = r_{qq}^{\mathrm{m}} J_q'^{\mathrm{m}} + r_{q\mu}^{\mathrm{m}} J_{\mathrm{H}_2}, \tag{3.8}$$

$$-\frac{2}{T}\left(\Delta_{\mathrm{m}}\mu_{\mathrm{H},T}\right) = r_{\mu q}^{\mathrm{m}} J_q'^{\mathrm{m}} + r_{\mu\mu}^{\mathrm{m}} J_{\mathrm{H}_2}, \tag{3.9}$$

where r_{ii} and r_{ij} are the main- and cross coefficients, respectively, which describe resistance to transport. The cross coefficients describe coupling between the different fluxes, here the mass- and heat flux, and are linked by the Onsager reciprocal relations, $r_{ij} = r_{ji}$ [62, 63].

In order to solve Eqs.(3.8) and (3.9), we need values for the main- and cross coefficients. Only three coefficients are independent, given the validity of the Onsager relations. The first coefficient, r_{qq}^{m}, can be found from the membrane thermal conductivity, λ^{m}, which is defined at zero mass flux

$$\lambda^{\mathrm{m}} = -\left[\frac{J_q'^{\mathrm{m}}}{\Delta_{\mathrm{m}}T/\delta^{\mathrm{m}}}\right]_{J_{\mathrm{H}_2}=0} = \frac{1}{T^2 r_{qq}^{\mathrm{m}}}. \tag{3.10}$$

The second coefficient, the coupling coefficient, can best be found via the measurable heat of transfer in the membrane, $q_{\mathrm{H}}^{*\mathrm{m}}$. This property is defined as the ratio

between the measurable heat flux and mass flux at zero temperature gradient [12]

$$q_{\mathrm{H}}^{*\mathrm{m}} = \left(\frac{J_q'^{\mathrm{m}}}{J_{\mathrm{H_2}}}\right)_{\Delta_{\mathrm{m}}T=0} = -\frac{r_{q\mu}^{\mathrm{m}}}{r_{qq}^{\mathrm{m}}}. \tag{3.11}$$

From Eq.(3.11) the measurable heat of transfer is also equal to the negative ratio between the cross coefficient and the resistivity of the heat flux.

The coupling coefficient makes it possible to describe mass transport that takes place due to a temperature gradient, the Soret effect. The Soret effect is described by the Soret cefficient, s_T, which is defined according to [12] for a system in stationary state as

$$s_T = -\left(\frac{\partial c_{\mathrm{H_2}}/\partial x}{c_{\mathrm{H_2}}\partial T/\partial x}\right)_{J_{\mathrm{H_2}}=0} = \frac{q_{\mathrm{H}}^{*\mathrm{m}}}{c_{\mathrm{H_2}}}\left(\frac{\partial \mu_{\mathrm{H_2},T}}{\partial c_{\mathrm{H_2}}}\right)^{-1}, \tag{3.12}$$

where $c_{\mathrm{H_2}}$ is the concentration of molecular hydrogen. This means that a temperature gradient in principle can be used to stop the mass flux. We define such a condition as the Soret equilibrium. This condition can be used to experimentally determine the coupling coefficient.

The third independent coefficient is the mass transfer resistance $r_{\mu\mu}^{\mathrm{m}}$. It is now common to report the membrane permeability, Π^{m}, of molecular hydrogen using Sieverts' law for the isothermal interface

$$J_{\mathrm{H_2}}|_{\Delta T=0} = -\Pi^{\mathrm{m}}\left(\frac{\left(p_{\mathrm{H_2}}^{\mathrm{p}}\right)^{0.5} - \left(p_{\mathrm{H_2}}^{\mathrm{f}}\right)^{0.5}}{\delta^{\mathrm{m}}}\right). \tag{3.13}$$

Here $p_{\mathrm{H_2}}^{\mathrm{i}}$ is the partial pressure of hydrogen in the bulk gas phase i (feed or permeate). We specify in 3.A the conditions for which this equation is valid.

The expression in Eq.(3.13) can be used to find $r_{\mu\mu}^{\mathrm{m}}$ from Π^{m}, by neglecting any pressure gradient in the diffusion layer next to the surface. At isothermal conditions and with chemical equilibrium at the surfaces, the force-flux equations, Eqs.(3.8) and (3.9), reducees to

$$J_{\mathrm{H_2}}|_{\Delta T=0} = -\frac{2R}{\delta^{\mathrm{m}}}\ln\left(\frac{p_{\mathrm{H_2}}^{\mathrm{p}}}{p_{\mathrm{H_2}}^{\mathrm{f}}}\right)^{0.5}\left(r_{\mu\mu}^{\mathrm{m}} - \frac{r_{q\mu}^{\mathrm{m}} r_{\mu q}^{\mathrm{m}}}{r_{qq}^{\mathrm{m}}}\right)^{-1}, \tag{3.14}$$

where R is the universal gas constant. We have used the definition of the chemical potential, $\mu_{\mathrm{H}} = \mu_{\mathrm{H}}^0 + RT\ln a_{\mathrm{H}}$, where $a_{\mathrm{H}} = K\left(p_{\mathrm{H_2}}/p^0\right)^{0.5}$ (*cf.* 3.A), p^0=1 bar is the standard state pressure and K is the equilibrium constant for the reaction given in (3.1).

When these conditions apply, we find $r_{\mu\mu}^{\mathrm{m}}$ from Π^{m}, setting Eqs.(3.13) and (3.14) equal, knowing r_{qq}^{m} (λ^{m}) and $r_{q\mu}^{\mathrm{m}}$ ($q^{*,\mathrm{m}}$). The result is:

$$r_{\mu\mu}^{\mathrm{m}} = \frac{\left(q^{*,\mathrm{m}}\right)^2}{T^2\lambda^{\mathrm{m}}} - \frac{R\ln\left(\frac{p_{\mathrm{H_2}}^{\mathrm{p}}}{p_{\mathrm{H_2}}^{\mathrm{f}}}\right)}{\Pi^{\mathrm{m}}\left(\left(p_{\mathrm{H_2}}^{\mathrm{f}}\right)^{0.5} - \left(p_{\mathrm{H_2}}^{\mathrm{p}}\right)^{0.5}\right)}. \tag{3.15}$$

The result can be used under arbitrary conditions, as the transport coefficients do not depend on the forces or the fluxes, according to the basic postulates of non-equilibrium thermodynamics.

3.3.2 The surfaces

The excess entropy production of the surface, has in the outset five independent conjugate flux-force pairs for transport of heat and mass in the presence of a surface reaction, see Kjelstrup and Bedeaux [12]. We show in 3.B, how the five pairs can be reduced to two at stationary state conditions. For the surface at the feed side, we obtain:

$$\sigma^{\mathrm{s}} = J_q'^{\mathrm{f}} \Delta_{\mathrm{f,m}} \left(\frac{1}{T} \right) + J_{\mathrm{H_2}} \left[-\frac{1}{T^{\mathrm{m}}} \Delta G(T^{\mathrm{m}}) \right], \tag{3.16}$$

where $J_q'^{\mathrm{f}}$ is the measurable heat flux. Gibbs energy difference, ΔG, was defined in Eq.(3.2), and $\Delta G(T^{\mathrm{m}})$ means that it is evaluated at the temperature in the membrane close to the surface at the feed side.

The resulting force-flux relations for the surface at the feed side are then

$$\Delta_{\mathrm{f,m}} \left(\frac{1}{T} \right) = r^{\mathrm{s}}_{qq} J_q'^{\mathrm{f}} + r^{\mathrm{s}}_{q\mu} J_{\mathrm{H_2}}, \tag{3.17}$$

$$-\frac{1}{T^{\mathrm{m}}} \Delta G(T^{\mathrm{m}}) = r^{\mathrm{s}}_{\mu q} J_q'^{\mathrm{f}} + r^{\mathrm{s}}_{\mu\mu} J_{\mathrm{H_2}}. \tag{3.18}$$

The surface excess resistivities have the dimensionality of membrane resistivities times a length. They can be found in a similar manner as shown for the membrane.

For the right-hand side surface, the excess entropy production can be derived in an analogous manner as illustrated for the left-hand side surface in 3.A. The resulting expression is similar. The force-flux relations follow from this in a similar manner as shown for the other surface.

3.4 Calculation details

3.4.1 Determination of resistivities

The resistivities for the membrane and the surfaces were calculated using the relations described in Section 3.3 and data from the literature given in Table 3.1. The resulting resistivities are given in Table 3.2.

Each set of coefficients (in phase i) was tested for consistency with the second law of thermodynamics using [12]

$$D^{\mathrm{i}} = r^{\mathrm{i}}_{\mu\mu} r^{\mathrm{i}}_{qq} - r^{\mathrm{i}}_{\mu q} r^{\mathrm{i}}_{q\mu} \geq 0. \tag{3.19}$$

Table 3.1: Coefficient values for a palladium membrane from the literature. Π^{m} is the membrane permeability for a 7.2 μm membrane, λ^{m} the thermal conductivity at 673 K, ΔH is the heat of adsorption, and U is the overall heat transfer coefficient.

Symbol	Value	Units	Ref.
Π^{m}	$1.22 \cdot 10^{-8}$	$\mathrm{mol\,m^{-1}\,s^{-1}\,Pa^{-0.5}}$	[71]
λ^{m}	82	$\mathrm{W\,m^{-1}\,K^{-1}}$	[81]
ΔH	-87	$\mathrm{kJ\,mol^{-1}}$	[69]
U	2.4	$\mathrm{W\,m^{-2}\,K^{-1}}$	[78]

Table 3.2: Estimated resistivities. r_{ii} are the main coefficients while r_{ij} are the coupling coefficients. Superscript s and m denotes surface and membrane, respectively.

Coefficient	Value	Units
r^{m}_{qq}	$2.7{\cdot}10^{-8}$	$\mathrm{m\,s\,J^{-1}\,K^{-1}}$
$r^{\mathrm{m}}_{q\mu}$	0	$\mathrm{m\,s\,mol^{-1}\,K^{-1}}$
$r^{\mathrm{m}}_{\mu\mu}$	$3.79{\cdot}10^{6}$	$\mathrm{J\,m\,s\,mol^{-2}\,K^{-1}}$
r^{s}_{qq}	$9{\cdot}10^{-13}$	$\mathrm{m^2\,s\,J^{-1}\,K^{-1}}$
$r^{\mathrm{s}}_{q\mu}$	$1.6{\cdot}10^{-8}$	$\mathrm{m^2\,s\,mol^{-1}\,K^{-1}}$
$r^{\mathrm{s}}_{\mu\mu}$	$4{\cdot}\ 10^{-3}$	$\mathrm{J\,m^2\,s\,mol^{-2}\,K^{-1}}$

Estimating membrane resistivities

The main coefficients, r^{m}_{qq} and $r^{\mathrm{m}}_{\mu\mu}$, were calculated from Eqs.(3.10) and (3.15), respectively. The cross coefficient or the measurable heat of transfer, $q^{*\mathrm{m}}_{\mathrm{H}}$ is not known for hydrogen in palladium. According to Kjelstrup and Bedeaux [12], q^* is a fraction of the enthalpy change. As the enthalpy of the component to a good approximation is constant in the membrane, we expect that $q^{*\mathrm{m}}_{\mathrm{H}}$ is very small. Thus, in lack of any further information, we shall use $r^{\mathrm{m}}_{\mu q}$=$r^{\mathrm{m}}_{q\mu} = 0$, see Eq.(3.11).

Estimating surface resistivities

To the best of our knowledge, no data for the surface transport properties are available. The direct coefficients for the surface resistivities have been estimated by multiplying the resistivity in the rate determining phase next to the surface with the surface thickness, δ^{s} (1nm).

$$r^{\mathrm{s}} = \delta^{\mathrm{s}} r^{\mathrm{i}}, \tag{3.20}$$

where r^{i} is an arbitrary resistance in the rate determining phase i. Using this we get a resistance per length unit in the surface area that is twice the resistance in phase i.

For the resistance to heat transport, r_{qq}, the gas phase next to the surface (feed or permeate) will be rate determining, as the membrane is a well conducting metal.

Thus, we used the overall heat transfer coefficient, U, given for a similar system by Johannessen and Jordal [78], to determine the thermal conductivity in the gas phase, λ^{g}. The resistance in the membrane is neglected.

$$\lambda^{\mathrm{g}} = U\delta^{\mathrm{tot}}. \tag{3.21}$$

Here δ^{tot} is the total thickness of the system (1 mm) from bulk to bulk phase. δ^{tot} was used as an estimate for the thickness of the gas phase, as the membrane under investigation is thin ($\delta^{\mathrm{m}} = 7.2\,\mu$m).

$$\delta^{\mathrm{g}} = \delta^{\mathrm{tot}} - \delta^{\mathrm{m}} - 2\delta^{\mathrm{s}} \simeq \delta^{\mathrm{tot}}. \tag{3.22}$$

The resistance to heat transfer in the gas phase, r^{g}_{qq}, was then calculated analogous to the relation given in Eq.(3.11). When this was known, it was possible to estimate r^{s}_{qq} from r^{g}_{qq} according to Eq. (3.20).

The rate determining layer for resistance to mass transfer, is the membrane. Hence, $r^{\mathrm{s}}_{\mu\mu}$ was then estimated from $r^{\mathrm{m}}_{\mu\mu}$ according to Eq. (3.20).

According to Kjelstrup and Bedeaux [12], the heat of transfer, q^*, for the whole surface, defined analogous as in Eq.(3.11), can also be written as

$$q^{*\mathrm{s}} = -k\Delta H, \tag{3.23}$$

(*cf.* Eq.(11.24) in [12]). Thus, $q^{*\mathrm{s}}$ can be expressed as a fraction, k, of the enthalpy change over the interface. Kinetic theory predicts that $k = 0.2$, see [12]. In lack of better information, we have used the kinetic theory-value also in this case.

It is known that the surface has a high resistivity, thus we shall increase the value of the set of coefficients by a factor $\alpha = 10$ or 100. The set with $\alpha = 10$ shall be called the basis set.

A major difference between the transport properties of the surface and the homogeneous phases is that the coupling coefficients can be neglected in the homogeneous phase, but not at the surface, due to surface properties described above. In the state-of-the art description the coupling coefficients are neglected also at the surface, and we shall examine the effect of this assumption.

3.4.2 Investigated cases

In order to investigate the effect of coupling and thermal driving forces on the membrane performance, we started with a typical set of operating conditions, determined from reported values by Gade *et al.* [71] for a 7.2 μm thick membrane. The pressure at the permeate side was calculated based on values in [71]. The values are given in Table 3.3.

The following cases were studied:

Table 3.3: Typical operating conditions. δ^{m} is the membrane thickness, p^{i} the pressure in phase i, T is the temperature in the gas phase and $J_{\mathrm{H_2}}$ the hydrogen flux. Values are based on reported data from Gade *et al.* [71]. The permeat pressure was calculated.

Symbol	Value	Units
δ^{m}	7.2	μm
p^{f}	2.2	bar
p^{p}	0.72	bar
T	673	K
$J_{\mathrm{H_2}}$	340	mmol $\mathrm{m^{-2}s^{-1}}$

1. The basis set of coefficients ($\alpha = 10$) at typical operating conditions, $\Delta p \neq 0, \Delta T = 0$. The purpose of this case was to examine conditions for determination of the permeability Π^m. The effect of removing the coupling coefficients was studied to compare with available experiments.

2. The added effect of a temperature difference on the hydrogen flux at typical operating conditions, $\Delta p \neq 0, \Delta T \neq 0$ was studied for the basis case of surface resistivities ($\alpha = 10$). The overall temperature difference needed to enhance the hydrogen flux with 10% and 25% were found. The possibility to reach Soret equilibrium was investigated, to test if this condition is experimentally within reach, *cf.* Eq.(3.12).

3. Case 2 was repeated for $\alpha = 10$ with $k = 0.4$ (from Eq.(3.23)) and for $\alpha = 100$. This was done to illustrate the role of the surface.

To explicitly see the contribution from coupling on the mass fluxes, the mass fluxes were expressed as function of all resistivities and all gradients throughout the system, and divided into *direct terms*, $J_{H_2}(\mathrm{main})$, and *coupling terms*, $J_{H_2}(\mathrm{coupling})$.

$$J_{H_2} = J_{H_2}(\mathrm{main}) + J_{H_2}(\mathrm{coupling}). \tag{3.24}$$

The direct terms are the terms with gradients in chemical potential

$$J_{H_2}(\mathrm{main}) = \frac{-\frac{1}{T^{\mathrm{mf}}}\Delta G^{\mathrm{f}}(T^{\mathrm{mf}}) + \frac{1}{T^{\mathrm{mp}}}\Delta G^{\mathrm{p}}(T^{\mathrm{mp}}) - \frac{2}{T^{\mathrm{mf}}}\left(\Delta\mu_{\mathrm{H},T}(T^{\mathrm{mf}})\right)}{2\frac{D^{\mathrm{s}}}{r^{\mathrm{s}}_{qq}} + \delta^{\mathrm{m}}\frac{D^{\mathrm{m}}}{r^{\mathrm{m}}_{qq}}}, \tag{3.25}$$

here, D^{i} was defined in Eq.(3.19) and $\Delta G^{\mathrm{i}}(T^{\mathrm{mi}})$ is the Gibbs energy difference over the surface at the i side of the membrane, evaluated at the temperature, T^{mi}, in the membrane close to the surface of phase i. The coupling terms are the terms with temperature gradients

$$J_{H_2}(\mathrm{coupling}) = -\frac{\frac{r^{\mathrm{s}}_{\mu q}}{r^{\mathrm{s}}_{qq}}\left(\Delta_{\mathrm{m,f}}\left(\frac{1}{T}\right) + \Delta_{\mathrm{p,m}}\left(\frac{1}{T}\right)\right) + \frac{r^{\mathrm{m}}_{\mu q}}{r^{\mathrm{m}}_{\mu\mu}}\Delta_{\mathrm{m}}\left(\frac{1}{T}\right)}{2\frac{D^{\mathrm{s}}}{r^{\mathrm{s}}_{qq}} + \delta^{\mathrm{m}}\frac{D^{\mathrm{m}}}{r^{\mathrm{m}}_{qq}}} \tag{3.26}$$

We see that a coupling of the heat- and mass flux can enhance or reduce the total mass flux, depending on its direction. This shall be tested.

3.4.3 Solution procedure

We have two transport equations for each layer; one for heat and one for mass. Eqs.(3.8) and (3.9) describe the transport in the membrane. The transport at the feed side of the surface is described by Eqs.(3.17) and (3.18), and we have similar equations for the other surface. Altogether we have six transport equations for the whole system. As we have stationary state conditions, we also have the relation given in Eq.(3.5).

With constant resistivities and constant enthalpies in each phase and known conditions at the gas side, the above equations were integrated across each layer, and solved for J_{H_2}, $J_q'^{\mathrm{f}}$ and temperature and hydrogen activity in the membrane close to the surface at each side. This was done numerically.

3.5 Results and discussion

3.5.1 Operating conditions for permability studies with the basis set of coefficients

Permeability experiments are normally done with relatively small pressure differences and for isothermal conditions. Under such conditions one may expect that Sieverts' law applies, *cf.* 3.A. In case 1, we examined the local conditions for transport, for experiments where $T^{\mathrm{f}} = T^{\mathrm{p}}$.

The temperature profile across the membrane was first calculated with the basis set of resistivity coefficients ($\alpha = 10$). The result is shown in Figure 3.2 and Table 3.4, for the operating conditions given in Table 3.1. The profile is antisymmetric around the plane through the membrane center, as expected from the heat source we have on the left and the heat sink on the right-hand side. The temperature jumps at the surfaces are, however, insignificant in magnitude, meaning that the membrane in practice is isothermal, as assumed in Eq.(3.14). Experiments with $\Delta T = 0$ should thus give resonable values for Π^{m}. The same applies to the jumps in the chemical potential. The ΔG at the surface was observed to be -8.46 $\mathrm{J\,mol^{-1}}$ and -9.13 $\mathrm{J\,mol^{-1}}$ with and without coupling, respectively. The assumption of chemical equilibrium at the surface is thus approximately valid for this set of coefficients. The corresponding hydrogen flux is therefore also not altered by including coupling, as can be seen from Table 3.4.

In spite of the seemingly small effects from coupling on the temperature profiles, it is interesting to note that the heat flux vary largely between the membrane and its surroundings. The measurable heat flux in the membrane is positive and large, 23 $\mathrm{kJ\,mol^{-1}}$, while on the feed side it is -6.3 $\mathrm{kJ\,mol^{-1}}$, meaning that heat is transported into the feed side. The measurable heat flux on the permeate side is also

Table 3.4: Hydrogen flux, J_{H_2}, calculated for the basis case with a scaling factor for the surface resistivities, $\alpha = 10$. The calculations were performed with and without coupling at no overall temperature difference, $\Delta T = 0$. The contribution to J_{H_2} from direct terms is constant, $J_{H_2}(\text{main}) = 339.387\,\text{mmol}\,\text{m}^{-2}\,\text{s}^{-1}$. $J_q'^{\text{i}}$ is the measurable heat flux for phase i, and ΔG the Gibbs energy difference over the surface at the feed side.

Case	ΔT	J_{H_2}	$J_q'^{\text{f}}$	$J_q'^{\text{m}}$	ΔG
$\alpha = 10$	K	$\text{mmol}\,\text{m}^{-2}\,\text{s}^{-1}$	$\text{kJ}\,\text{m}^{-2}\,\text{s}^{-1}$	$\text{kJ}\,\text{m}^{-2}\,\text{s}^{-1}$	$\text{J}\,\text{mol}^{-1}$
base	0	339.39	-6.28	23.24	-8.46
no coupling	0	339.32	-0.32	29.21	-9.13

negative (and equal to $J_q'^{\text{f}}$), here pointing into the membrane. The discontinuity is due to the enthalpy of dissociative adsorption at the surface. The source propagates in both directions according to $q*^s$, see Eq.(3.23). The values of the measurable heat flux in the homogeneous phases means that in order to maintain isothermal conditions, the feed side must be continuously cooled to remove this heat, while on the permeate side we need to supply this amount of heat.

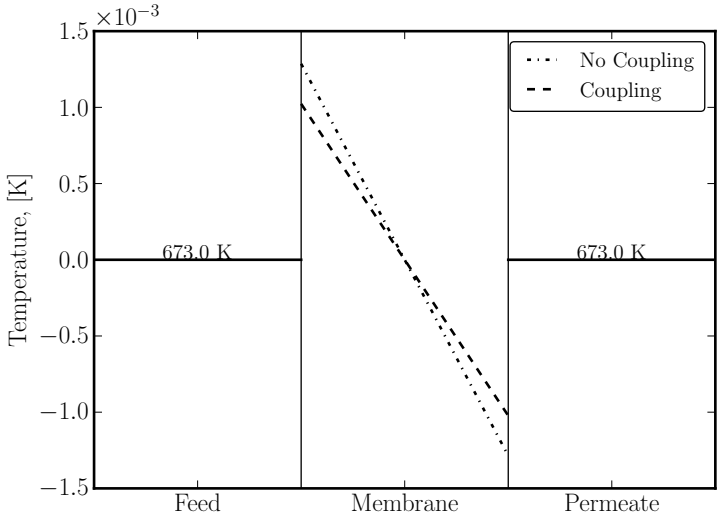

Figure 3.2: Temperature profile across the membrane for identical feed and permeate temperatures, calculated with the basis set of coefficients and for operating conditions as given in Table 3.1.

We conclude that permeability experiments, or experiments to determine $r^{\text{m}}_{\mu\mu}$, can be performed when the feed and permeate phases have the same temperature, while the feed is continuously cooled and the permeate is continuously heated. A temperature difference between the two sides, have a large impact on the mass flux, however, as can be seen from the results below.

3.5.2 Non-isothermal operating conditions with the basis set of coefficients

Using the basis set of coefficients ($\alpha = 10$), we calculated temperature differences required to enhance the mass flux by 10% and 25%, and the temperature difference required to stop the hydrogen flux (Soret equilibrium, Eq.(3.12)). The results are given in Table 3.5. From Table 3.5 we see that a positive temperature difference will enhance the mass flux, while a negative temperature difference is required to obtain Soret equilibrium. A positive temperature difference implies that the temperature shall be higher at the permeate side than at the feed side. According to Le Chatelier's principle, increasing the temperature at the permeate side shifts the endothermic desorption reaction towards the product. In the same way, the exothermic adsorption reaction will be shifted towards products by lowering the temperature at the feed side. This facilitates the formation of H in the membrane at the feed side, and the formation of H_2 at the permeate side, thereby increasing J_{H_2}.

Table 3.5: Hydrogen flux, J_{H_2}, and overall temperature difference, ΔT, calculated for scenarios with mass flux increased by 10% and 25% and Soret equilibrium (zero mass flux). $J_q'^{\mathrm{i}}$ is the measurable heat flux in phase i, and ΔG is Gibbs energy difference over the surface at the feed side. For the basis case, the surface resistivities are multiplied with a factor, $\alpha = 10$. The contribution to J_{H_2} from direct terms is constant, $J_{H_2}(\mathrm{main}) = 339\,\mathrm{mmol\,m^{-2}\,s^{-1}}$.

Case	ΔT	J_{H_2}	$J_q'^{\mathrm{f}}$	$J_q'^{\mathrm{m}}$	ΔG
$\alpha = 10$	K	$\mathrm{mmol\,m^{-2}\,s^{-1}}$	$\mathrm{kJ\,m^{-2}\,s^{-1}}$	$\mathrm{kJ\,m^{-2}\,s^{-1}}$	$\mathrm{J\,mol^{-1}}$
+10%	24.8	373	-2909	-2877	308
+25%	65.6	424	-7264	-7227	806
Soret	-176.5	0	29021	29021	-2657

It was observed that a temperature difference of -176 K was needed to stop the hydrogen flux (Soret equilibrium), *cf.* Table 3.5. From the table we observe that when $J_{H_2} = 0$, $J_q'^{\mathrm{f}} = J_q'^{\mathrm{m}} = J_q'^{\mathrm{p}} = J_q$ (*cf.* Eqs.(3.4) and (3.5)). This situation may be achieved in the laboratory, and can then be used to find the coupling coefficient, which is the direct cause of this effect.

A plot of J_{H_2} and $J_{H_2}(\mathrm{main})$ versus temperature difference is given in Figure 5.4. From the figure we see that the fraction of the flux caused by direct terms ($J_{H_2}(\mathrm{main})$) is constant in spite of temperature changes in the system. Variation with temperature is seen for the total flux, and is thus caused by coupling terms (*cf.* Eq.(3.24)). Thus, application of a temperature gradient gives a significant contribution to the overall mass transfer across the membrane.

The reaction Gibbs energy difference was observed to be smaller than RT in all scenarios (see Table 3.5). This means that the reaction rate can be regarded as a linear function of the driving force [60], justifying that the linear version of non-equilibrium thermodynamics is sufficient for a good description. It was observed

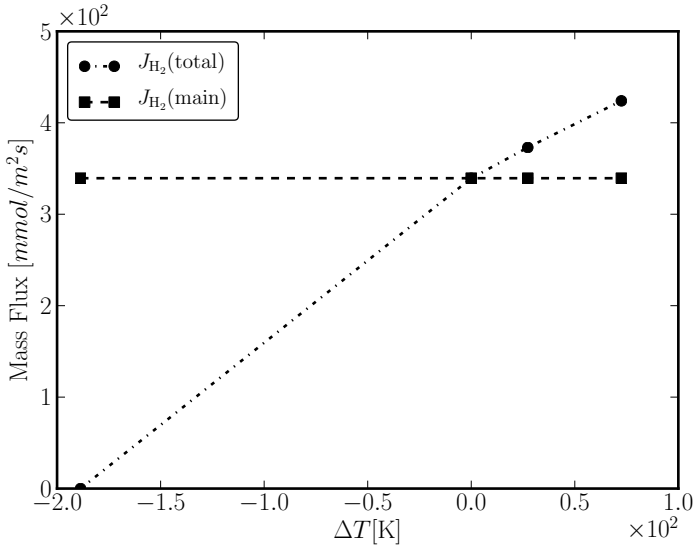

Figure 3.3: J_{H_2} and J_{H_2}(main) as function of overall temperature difference.

that ΔG at both the feed and permeate sides were to a good approximation the same. Thus, only the values for the feed side are reported.

A transmembrane temperature difference may, however, be difficult to maintain in practice in the present system. This is indicated by the large amounts of heat supply or removal that are needed to maintain the gradient.

The removal of coupling effects, makes it impossible for our model to see the importance of a temperature gradient. It is remarkable to observe that the heat fluxes in the various phases using this approach differ by orders of magnitude from fluxes that would have been obtained by only using the energy balance in combination with Fick's and Fourier's laws. Therefore, a description without coupling can give a serious error in models where the energy balance is central. Vice versa, if experimental data are interpreted with an insufficient set of equations for determination of transport properties, the determined properties may be wrong. Effort should thus be made to determine the resistivities, and especially the coupling coefficients.

3.5.3 Increasing the coupling coefficient

The sensitivity of the model was investigated by increasing the value of k (in Eq.(3.23)) from 0.2 to 0.4. The results are shown in Table 3.6. From the table we see that the temperature differences needed to increase the mass flux, and to obtain Soret equilibrium (Eq.(3.12)) is smaller when $k = 0.4$ rather than $k = 0.2$, *cf.* Table 3.5. We also observe that the measurable heat flux (both in the membrane

Table 3.6: Hydrogen flux, J_{H_2}, and overall temperature difference, ΔT, calculated for scenarios with mass flux increased by 10% and 25% and Soret equilibrium (zero mass flux). The basis case for the surface resistivities where used, but the coupling coefficient were doubled. $J_q'^{\mathrm{i}}$ is the measurable heat flux in phase i and ΔG the reaction Gibbs energy difference at the feed side of the surface. The contribution to J_{H_2} from direct terms is constant, $J_{H_2}(\mathrm{main}) = 339.599\,\mathrm{mmol\,m^{-2}\,s^{-1}}$.

Case $\alpha = 10, k = 0.4$	ΔT K	J_{H_2} $\mathrm{mmol\,m^{-2}\,s^{-1}}$	$J_q'^{\mathrm{f}}$ $\mathrm{kJ\,m^{-2}\,s^{-1}}$	$J_q'^{\mathrm{m}}$ $\mathrm{kJ\,m^{-2}\,s^{-1}}$	ΔG $\mathrm{J\,mol^{-1}}$
base	0	339.60	-12.26	17.28	-6.50
no coupling	0	339.32	-0.32	29.21	-9.13
+10%	12.2	374	-1464	-1432	308
+25%	31.3	425	-3645	-3608	791
Soret	-101.5	0	14513	14513	-2873

and in the feed) is smaller along with an observed decrease in ΔG, compared to Table 3.5. This is expected, as a larger coupling at the surface will enhance the surface effects.

3.5.4 Increasing the resistivities

We also studied the effect of increasing the resistivities from the basis set with $\alpha = 10$ to a set with $\alpha = 100$. The results are given in Table 3.7.

Table 3.7: Hydrogen flux, J_{H_2}, and overall temperature difference, ΔT, calculated for scenarios with mass flux increased by 10% and 25% and Soret equilibrium (zero mass flux). $J_q'^{\mathrm{i}}$ is the measureable heat flux in phase i and ΔG the reaction Gibbs energy difference at the feed side of the surface. The surface resistivities are multiplied with a factor, $\alpha = 100$. The contribution to J_{H_2} from direct terms is constant, $J_{H_2}(\mathrm{main}) = 331.290\,\mathrm{mmol\,m^{-2}\,s^{-1}}$.

Case $\alpha = 100$	ΔT K	J_{H_2} $\mathrm{mmol\,m^{-2}\,s^{-1}}$	$J_q'^{\mathrm{f}}$ $\mathrm{kJ\,m^{-2}\,s^{-1}}$	$J_q'^{\mathrm{m}}$ $\mathrm{kJ\,m^{-2}\,s^{-1}}$	ΔG $\mathrm{J\,mol^{-1}}$
+10%	24.6	364	-297	-266	226
+25%	64.9	414	-733	-697	709
Soret	-175.2	0	2902	2902	-2658

We observe a small difference for the mass flux between two sets of surface resistivities ($\alpha = 10$ and $\alpha = 100$) by comparing Tables 3.5 and 3.7. Thus, when looking at the mass flux, the overall picture is not much changed. The observed temperature jumps (ΔT) become smaller along with a smaller contribution from coupling. The effect was, however, not proportional to the change in surface resistivities. For $J_q'^{\mathrm{i}}$ the observed effect was proportional to the change in surface resistivities (a decrease by a factor ten was observed compared to Table 3.5). A decrease was also observed for ΔG.

3.6 Conclusion

We have modelled transport of hydrogen through a palladium membrane using the framework of non-equilibrium thermodynamics. The model gives a systematic approach to quantify surface effects, in particular the thermal effects associated with transport, but also of the dissociative adsorption at the surface.

The calculations were based on estimated resistivities, and given that these are realistic, we have found that the chemical reaction is most likely described by a linear flux-force regime. We also found that a transmembrane temperature difference can obstruct the validity of Sieverts' law.

Our calculations predict that heating at the permeate side will increase the flux of hydrogen. The overall temperature difference needed for enhancing the mass flux with 10% and 25%, for the basis case, was found to be 27.3 K and 72.5 K, respectively, with an initial feed temperature of 673 K. Similarly, an overall temperature difference of -176.5 K will stop the hydrogen flux. Thus, cooling the permeate side gives a negative temperature gradient and a decrease in the mass flux.

When the scaling factor for the surface resistivities were changed from $\alpha = 10$ to $\alpha = 100$, a small decrease was seeen for the overall temperaure differences. Only increasing the coupling coefficient ($\alpha = 10$, $k = 0.4$), however, lead to larger changes in the observed overall temperature difference.

As the results depend on the estimated resistivities, effort should be put into a more exact determination of these, to bring this work further. The coupling coefficient leading to Soret equilibrium, is unknown for the surfaces as well as for the membrane transport of hydrogen. The surface main resistivies to mass and heat transfer are also not known, and needs to be determined for a more exact description of the system.

Acknowledgments

SKS and SK acknowledge financial support from NWO-CW through an ECHO grant, and computational resources were sponsored by the Stichting Nationale Computerfaciliteiten (National Computing Facilities Foundation, NCF), with financial support from the Nederlandse Organisatie voor Wetenschappelijk onderzoek (Netherlands Organization for Scientific Research, NWO).

3.A Conditions for application of Sieverts' law

Sieverts' law gives the equilibrium concentration for atomic hydrogen, c_{H}, in the metal [82] as:

$$c_{\mathrm{H}} = K(p^{\mathrm{p}}_{\mathrm{H_2}})^{0.5} \tag{3.27}$$

Here, $p^{\mathrm{p}}_{\mathrm{H_2}}$ is the partial pressure of molecular hydrogen at the permeate side, and K is the equilibrium constant for reaction (3.1). As $p^{0}_{\mathrm{H_2}} = 1\mathrm{bar}$, it has been removed from the equality and the rest of the appendix.

When this relation (Eq. (3.27)) is introduced into Fick's law (the first equality below), we find the equation commonly used to describe hydrogen permeability in membranes:

$$\begin{aligned} J_{\mathrm{H_2}}|_{\Delta T=0} &= -D^{\mathrm{m}}_{\mathrm{H}} \left(\frac{c^{\mathrm{p}}_{\mathrm{H}} - c^{\mathrm{f}}_{\mathrm{H}}}{\delta^{\mathrm{m}}} \right) \\ &= -D^{\mathrm{m}}_{\mathrm{H}} K \left(\frac{\left(p^{\mathrm{p}}_{\mathrm{H_2}}\right)^{0.5} - \left(p^{\mathrm{f}}_{\mathrm{H_2}}\right)^{0.5}}{\delta^{\mathrm{m}}} \right) \\ &= -\Pi^{\mathrm{m}} \left(\frac{\left(p^{\mathrm{p}}_{\mathrm{H_2}}\right)^{0.5} - \left(p^{\mathrm{f}}_{\mathrm{H_2}}\right)^{0.5}}{\delta^{\mathrm{m}}} \right). \end{aligned} \tag{3.28}$$

Here $J_{\mathrm{H_2}}$ is the flux of molecular hydrogen, $D^{\mathrm{m}}_{\mathrm{H}}$ is the diffusion constant for atomic hydrogen in palladium, δ^{m} is the thickness of the membrane, Π^{m} is the membrane permeability of atomic hydrogen, $p_{\mathrm{H_2}}$ is the partial pressure of hydrogen in the homogeneous phases (feed or permeate). Some authors also denote this equation as Sieverts' law. We shall specify the conditions for which the equation is valid.

At chemical equilibrium, the chemical potential differences for adsorption and reaction over the surface obey

$$\Delta G = 2\mu^{\mathrm{m}}_{\mathrm{H}} - \mu^{\mathrm{f}}_{\mathrm{H_2}}, \tag{3.29}$$

where ΔG is the Gibbs energy difference for the dissociative adsorption at the surface.

The chemical potential for molecular hydrogen in the gas phase, $\mu^{\mathrm{f}}_{\mathrm{H_2}}$, assuming ideal gas, is

$$\mu^{\mathrm{f}}_{\mathrm{H_2}} = \mu^{0,\mathrm{f}}_{\mathrm{H_2}} + RT \ln p_{\mathrm{H_2}}, \tag{3.30}$$

where $\mu^{0,\mathrm{i}}_{j}$ is the chemical potential at standard state conditions for component j in phase i. The chemical potential for atomic hydrogen adsorbed at the membrane surface is defined by

$$\mu^{\mathrm{m}}_{\mathrm{H}} = \mu^{0,\mathrm{m}}_{\mathrm{H}} + RT \ln a_{\mathrm{H}}, \tag{3.31}$$

where a_{H} is the activity of hydrogen on the surface.

By introducing Eqs.(3.30) and (3.31) for the chemical potentials into Eq.(3.2), and with $\Delta G = 0$, we obtain for the feed side

$$2\mu_{\mathrm{H}}^{0,\mathrm{m}} - \mu_{\mathrm{H_2}}^{0,\mathrm{f}} = RT \ln \frac{a_{\mathrm{H}}^2}{p_{\mathrm{H_2}}} = \Delta G^0. \tag{3.32}$$

Here ΔG^0 is the standard state Gibbs energy.

We rearrange and obtain the following expression for the activity of atomic hydrogen near the membrane surface at equilibrium conditions

$$a_{\mathrm{H}} = \left[\exp\left(\frac{\Delta G^0}{RT}\right)\right]^{0.5} p_{\mathrm{H_2}}^{0.5} = K p_{\mathrm{H_2}}^{0.5}. \tag{3.33}$$

The activity of atomic hydrogen at the surface is further defined by

$$a_{\mathrm{H}} = c_{\mathrm{H}} \gamma, \tag{3.34}$$

where c_{H} is the concentration of atomic hydrogen near the surface and γ is the activity coefficient. For an ideal surface $\gamma = 1$. For Langmuir adsorption, $\gamma = 1/(1-\theta)$ where θ is the surface coverage [83]. With γ equal unity or constant, we have

$$c_{\mathrm{H}} = K' p_{\mathrm{H_2}}^{0.5}, \tag{3.35}$$

where K' is the equilibrium constant divided by the activity coefficient. For low coverage it is the equilibrium constant, and Eq.(3.35) is reduced to Eq.(3.27) (Sieverts' law [82]).

Experimental results give often values for the exponent that deviates from 0.5 [71]. We have seen that Eq.(3.28) can be expected to hold, when there is equilibrium for adsorption and reaction in the surface, when the conditions are isothermal, when the hydrogen gas is ideal, and when the surface activity coefficient is unity (the coverage is small or nearly constant).

3.B The entropy production for a palladium surface with hydrogen

We are interested in the excess entropy production, σ^{s}, for hydrogen and heat transport through a palladium surface, and start with the general expression derived by Kjelstrup and Bedeaux [12]. For a non-polarized surface, in the absence of an electric current, we have

$$\begin{aligned}\sigma^{\mathrm{s}} = {} & J_q^{\mathrm{i}} \left(\frac{1}{T^{\mathrm{s}}} - \frac{1}{T^{\mathrm{i}}}\right) + J_q^{\mathrm{o}} \left(\frac{1}{T^{\mathrm{m}}} - \frac{1}{T^{\mathrm{s}}}\right) + \sum_{j=1}^{n} J_j^{\mathrm{i}} \left[-\left(\frac{\mu_j^{\mathrm{s}}}{T^{\mathrm{s}}} - \frac{\mu_j^{\mathrm{i}}}{T^{\mathrm{i}}}\right)\right] \\ & + \sum_{j=1}^{n} J_j^{\mathrm{o}} \left[-\left(\frac{\mu_j^{\mathrm{o}}}{T^{\mathrm{o}}} - \frac{\mu_j^{\mathrm{s}}}{T^{\mathrm{s}}}\right)\right] + r^{\mathrm{s}} \left(-\frac{1}{T^{\mathrm{s}}} \Delta G^{\mathrm{s}}\right).\end{aligned} \tag{3.36}$$

Here J_q is the total heat flux, J_j is the flux of component j, μ_j is the chemical potential of component j, T is the temperature, r^{s} is the reaction rate and ΔG^s is the reaction Gibbs energy for a possible surface reaction. Superscripts i, o and s refers to the adjacent phase at left and right hand side of the surface and the surface, respectively. Transport is perpendicular to the surface. The normal components of the vector fluxes, which are scalar, will couple to the scalar chemical reaction.

Consider first the left hand side surface of our system in Figure 3.1.

$$\sigma^{\mathrm{s}} = J_q^{\mathrm{f}} \Delta_{\mathrm{f,s}} \left(\frac{1}{T}\right) + J_q^{\mathrm{m}} \Delta_{\mathrm{s,m}} \left(\frac{1}{T}\right) + J_{\mathrm{H_2}}^{\mathrm{f}} \left[-\left(\frac{\mu_{\mathrm{H_2}}^{\mathrm{s}}}{T^{\mathrm{s}}} - \frac{\mu_{\mathrm{H_2}}^{\mathrm{f}}}{T^{\mathrm{f}}}\right)\right] + J_{\mathrm{H}}^{\mathrm{m}} \left[-\left(\frac{\mu_{\mathrm{H}}^{\mathrm{m}}}{T^{\mathrm{m}}} - \frac{\mu_{\mathrm{H}}^{\mathrm{s}}}{T^{\mathrm{s}}}\right)\right] + r^{\mathrm{s}} \left(-\frac{1}{T^{\mathrm{s}}} \Delta G^{\mathrm{s}}\right). \tag{3.37}$$

Here, super- and subscripts f and m respectively designates the feed side and the membrane.

At stationary state we have the following relation between the reaction rate and the fluxes of molecular hydrogen and atomic hydrogen

$$r^{\mathrm{s}} = J_{\mathrm{H_2}} = \frac{1}{2} J_{\mathrm{H}}, \tag{3.38}$$

where r^s has dimensions mol m^{-2} s^{-1}.

At stationary state conditions we also have a constant total heat flux through the system.

$$J_q = J_q'^{\mathrm{f}} + H_{\mathrm{H_2}}^{\mathrm{f}} J_{\mathrm{H_2}}^{\mathrm{f}} = J_q'^{\mathrm{m}} + H_{\mathrm{H}}^{\mathrm{m}} J_{\mathrm{H}}^{\mathrm{m}}. \tag{3.39}$$

Here J_q' is the measureable heat flux and H_j is the enthalpy of component j.

The reaction Gibbs energy is defined at the tempertaure of the surface, T^{s}:

$$\Delta_r G^{\mathrm{s}} = 2\mu_{\mathrm{H}}^{\mathrm{s}} \left(T^{\mathrm{s}}\right) - \mu_{\mathrm{H_2}}^{\mathrm{s}} \left(T^{\mathrm{s}}\right). \tag{3.40}$$

The surface temperature is normally not known. By introducing Eqs.(3.38), (3.39) and (3.40) into equation Eq.(3.37) we avoid T^{s} and use instead:

$$\sigma^{\mathrm{s}} = J_q \Delta_{\mathrm{f,m}} \left(\frac{1}{T}\right) - J_{\mathrm{H_2}} \left(2\frac{\mu_{\mathrm{H}}^{\mathrm{m}} \left(T^{\mathrm{m}}\right)}{T^{\mathrm{m}}} - \frac{\mu_{\mathrm{H_2}}^{\mathrm{f}} \left(T^{\mathrm{f}}\right)}{T^{\mathrm{f}}}\right). \tag{3.41}$$

A problem is that the heat flux is not absolute; it depends on a reference state. We want to express the entropy production in terms of the measurable heat flux into the surface from the feed side and the flux of molecular hydrogen. By using

Eq.(3.39), we eliminiate the total heat flux and obtain

$$\begin{aligned}\sigma^{\mathrm{s}} &= J_q'^{\mathrm{f}}\Delta_{\mathrm{f,m}}\left(\frac{1}{T}\right) + J_{\mathrm{H_2}}\left[\Delta_{\mathrm{f,m}}\left(\frac{1}{T}\right)H^{\mathrm{f}}_{\mathrm{H_2}} - \left(2\frac{\mu^{\mathrm{m}}_{\mathrm{H}}\left(T^{\mathrm{m}}\right)}{T^{\mathrm{m}}} - \frac{\mu^{\mathrm{f}}_{\mathrm{H_2}}\left(T^{\mathrm{f}}\right)}{T^{\mathrm{f}}}\right)\right] \\ &= J_q'^{\mathrm{f}}\Delta_{\mathrm{f,g}}\left(\frac{1}{T}\right) + J_{\mathrm{H_2}}\left(-\frac{1}{T^{\mathrm{m}}}\left(2\mu^{\mathrm{m}}_{\mathrm{H}}\left(T^{\mathrm{m}}\right) - \mu^{\mathrm{f}}_{\mathrm{H_2}}\left(T^{\mathrm{m}}\right)\right)\right) \\ &\equiv J_q'^{\mathrm{f}}\Delta_{\mathrm{f,g}}\left(\frac{1}{T}\right) + J_{\mathrm{H_2}}\left(-\frac{1}{T^{\mathrm{m}}}\Delta G\left(T^{\mathrm{m}}\right)\right), \end{aligned} \tag{3.42}$$

after using the identity

$$\Delta_{\mathrm{i,o}}\left(\frac{\mu_{\mathrm{j}}}{T}\right) = \frac{1}{T^{\mathrm{o}}}\Delta_{\mathrm{i,o}}\mu_{j,T} + H^{\mathrm{i}}_{j}\Delta_{\mathrm{i,o}}\left(\frac{1}{T}\right). \tag{3.43}$$

The resulting entropy production in the surface is a sum of two independent terms. It contains the combined effect of adsorption and reaction. The measurable heat flux on the feed side, and the temperature of the membrane can be found, and so can the Gibbs energy change, ΔG, from equilibrium isotherms, see Appendix 3.A. The result applies to stationary states only, but does not assume chemical equilibrium at the interface.

The expression for the right hand side is completely analogous.

Chapter 4

Equilibrium properties of the reaction $H_2 \rightleftharpoons 2H$ by classical molecular dynamics simulations

Ragnhild Skorpa[1], Jean-Marc Simon[2], Dick Bedeaux[1] and Signe Kjelstrup[1,3]

1. Department of Chemistry,
Norwegian University of Science and Technology,
NO-7491 Trondheim, Norway

2. Laboratorie Interdisciplinaire Carnot de Bourgogne,
UMR, CNRS-Université de Bourgogne,
Dijon, France.

3. Process & Energy Laboratory,
Delft University of Technology,
Leeghwaterstraat 39, 2628CB Delft,
The Netherlands

This chapter was published in
PCCP (2014) 16:1227–1237

Abstract

We have developed a classical molecular dynamics model for the hydrogen dissociation reaction, containing two- and three- particle potentials derived by Kohen,Tullu and Stillinger. Two fluid densities were investigated for a wide range of temperatures, and 11 fluid densities were considered for one temperature. We report the temperature range where the degree of reaction is significant, and also where a stable molecule dominates the population in the energy landscape. The three-particle potential, which is essential for the reaction model and seldom studied, together with the two-particle interaction lead to a large effective excluded volume diameter of the molecules in the molecular fluid. The three-particle interaction was also found to give a large positive contribution to the pressure of the reacting mixture at high density and/or low temperatures. From knowledge of the dissociation constant of the reaction and the fluid pressure, we estimated the standard enthalpy of the dissociation reaction to 430 kJ/mol ($\rho = 0.0695$ g cm^{-3}) and 380 kJ/mol ($\rho = 0.0191$ g cm^{-3}). These values are in good agreement with the experimental vaule of 436 kJ/mol under ambiant pressure. The model is consistent with a Lennard-Jones model of the molecular fluid, and may facilitate studies of the impact of chemical reactions on transport systems.

4.1 Introduction

By computer simulations one can study systems under conditions that are difficult to achieve in a laboratory. For instance, at very high temperatures, above 3000 K (at 1 bar), there is a significant dissociation of hydrogen into atoms [8], but this is difficult to measure. Likewise, it is difficult to measure at 300 GPa where hydrogen becomes metallic [84]. Simulation techniques are indispensable in such cases. The aim of this paper is to find a simulation tool that can help address problems that arise when chemical reactions take place in the presence of gradients in pressure, temperature and concentration. This is the case in most chemical reactors.

To quantitatively model a chemical reaction requires quantum mechanics. Such models are computationally expensive, however, and allow no easy interaction with flow fields. The aim of this paper is therefore to help establish a classical model for a chemical reaction using equilibrium molecular dynamics. Doing this, we hope to facilitate future studies of reactions and transport in combination. A first effort in this direction was made by Xu et al. [30,31] in their study of the reaction $F_2 \rightleftharpoons 2F$. The interesting result was that transport properties, like thermal conductivity and diffusion coefficients of the components in the mixture, were largely affected by the presence of the chemical reaction. It is therefore of interest to examine to which degree this effect also applies to other systems.

We have chosen the hydrogen dissociation reaction as example in the present work. The properties of hydrogen are for instance important for the envisioned hydrogen

society [85, 86]. A selective separation of hydrogen (H_2) from the main product stream of the water gas shift reaction is then central. Such a separation can occur via a palladium (Pd) membrane [11, 64, 72]. At the palladium surface, hydrogen dissociates to atomic hydrogen, and atoms are transported through the metal lattice [11, 68, 72]. At the other side, the reverse reaction takes place; molecular hydrogen is formed from atoms, and removed from the surface by an inert sweep gas. Equilibrium and transport data for simulations of these steps are not available, and are also not easily accessible from experiments. A classical model for the hydrogen dissociation reaction may then facilitate the modelling of such coupled transport phenomena.

The purpose of this paper is therefore to establish a model for the chemical reaction ($H_2 \rightleftharpoons 2H$) using molecular dynamics simulations at equilibrium. The aim is to find the range of conditions where the reaction takes place, and where the molecular hydrogen fluid dominates.

Few equilibrium studies have been performed on the nature of chemical reactions using classical equilibrium molecular dynamics (EMD). Cummings and Stell [87] studied chemical reactions ($A + B \rightleftharpoons AB$) with the use of statistical mechanical models. To the best of our knowledge, no thorough study of the equilibrium properties of the hydrogen dissociation reaction has been done. High temperature hydrogen dissociation has however been studied. In 1996 Magro et al. studied molecular dissociation in hot, dense hydrogen, using path-integral Monte Carlo [88]. Delaney et al. studied the liquid-liquid phase transition between the molecular and atomic fluid phases in high-pressure hydrogen using quantum Monte Carlo [89] in 2006. None of these studies contains three particle interactions, however. In 1978 Siegbahn and Liu [49] obtained a 3-dimensional potential energy surface for H_3. In 1992 and 1994 Diedrich and Anderson studied the barrier height [47], and the potential energy surface [46], respectively, of the reaction $H + H_2 \Leftrightarrow H_2 + H$ using quantum Monte Carlo calculations. Stillinger and Weber [3] studied equilibrium conditions for the dissociation of fluorine using a classical model of the reaction. They concluded that combinations of two- and three-particle potentials suffice to represent the main features of chemical binding. Other examples of such three particle interactions is the Axilrod and Teller potential to describe dispersion interactions [33], and the effect of this potential has been studied for binary fluids by Sadus [34, 35]. A comparison of several many-body potentials for silicon (Si_n-clusters, $n = 2-6$) was studied by Balamane in 1992 [90]. In 1998 Kohen et al. [29] gave analytic expressions for the two- and three-particle potentials of hydrogen in a study of reactions on silicon surfaces. We shall build on these works in an effort to obtain a good model for the reaction. Work has been done on the H_4 potential by Boothroyd et al. [91], but given the results of Stillinger and Weber we restrict ourselves to the two- and three-particle interactions.

We shall examine the interaction energy landscape of the model derived from Kohen et al. [29], characterizing its states and their occupancy in terms of pair correlation functions, at various temperatures, for a density just below the triple point and for a moderately compressed gas density. Focus will be given on the particular effects

of three-particle interactions, which are seldom studied in molecular simulations. We shall see that they have interesting effects on the pair-correlation functions, and therefore on the properties of the reacting mixture. We shall discuss in detail the effect on the pressure. The pressure calculation from particle interactions in a mixture where particles constantly are formed or disappear, is by no means trivial. In this context we shall benefit from the existing methodology [31,92]. The temperature variation of the reaction shall also be studied.

The paper has been organized as follows. First we present the details of the hydrogen potential in Section 4.2 Section 4.3 discusses the details of the molecular dynamics simulations. In Section 4.4 we give results for the pair correlation function, the system pressure, the dissociation constant and the reaction enthalpy. Conclusions are given in Section 4.5.

4.2 Interaction potentials

For the computer simulations, we need an analytical form of the potential which describes essential interactions between particles in the system, based on an acceptable approximation to the electronic ground state potential of the collection of atoms involved [3, 26, 29, 31]. Following Stillinger and Weber [3], we use an interaction potential, U, which is the sum of two- and three-particle interaction contributions:

$$U(\mathbf{r}_1, ..., \mathbf{r}_N) = \sum_{i<j} u_{(2)}(r_{ij}) + \sum_{i<j<k} u_{(3)}(\mathbf{r}_i, \mathbf{r}_j, \mathbf{r}_k) \tag{4.1}$$

where $u_{(2)}$ and $u_{(3)}$ are the two- and three-particle potentials, respectively and $\mathbf{r}_i$ are the positions of the hydrogen atoms. The spherically symmetric pair potential, $r_{ij} = |\mathbf{r}_i - \mathbf{r}_j|$, describes the interaction between two particles, and defines the bonded and non-bonded pairs. The pair-potential used in the calculations was given by Kohen et al. [29]:

$$u_{(2)}(r) = \begin{cases} \alpha\left(\beta r^{-p} - 1\right) \exp\left[\frac{\gamma_2}{r - r_c}\right] & \text{if } r < r_c \\ 0 & \text{if } r > r_c \end{cases} \tag{4.2}$$

where $\alpha = 5.59 \cdot 10^{-21}$ kJ, $\beta = 0.044067$ Å^p, $\gamma_2 = 3.902767$ Å, $r_c = 2.8$ Å and $p = 4$ are constants [29]. α is chosen such that the minimum of the potential gives the binding energy of hydrogen (432.065 kJ mol^{-1}) [29] at the bond distance between two hydrogen atoms, $r_e = 0.74$ Å [47]. When the distance between two atoms is larger than the cut-off distance, $r \geq r_c$, the potential is zero. For convenience in the calculation procedures, reduced units based on the pair potential have been used. σ is defined by $u_{(2)}(\sigma) = 0$, which implies that $\sigma = \sqrt[p]{\beta} = 0.458$ Å. The value of ϵ , based on the bond energy of hydrogen, gives $\epsilon/k_B = 51991$ K. Thus, the reduced pair potential has a minimum of -1 at $r^*_{ij} = 1.6$.

The mass of one hydrogen atom, $m_0 = 1.67 \cdot 10^{-27}$ kg, is used to define the reduced total mass density $\rho^* = \rho\sigma^3/m_0$. This implies that the reduced total mass density equals the reduced total molar density in terms of $(N_{\mathrm{H}} + 2N_{\mathrm{H_2}})$. Reduced units are indicated by superscript *, and the relation between real and reduced units is given in Table 6.1.

Table 4.1: Relation between reduced and real units, ϵ/k_B = 51991 K, σ=0.458 Å and $m_0 = 1.67 \cdot 10^{-27}$ kg.

Reduced vaiable	Formula
mass	$m^* = m/m_0$
distance	$r^* = r/\sigma$
energy	$u^* = u/\epsilon$
time	$t^* = (t/\sigma)\sqrt{\epsilon/m_0}$
temperature	$T^* = k_B T/\epsilon$
density	$\rho^* = \rho\sigma^3/m_0$
pressure	$P^* = P\sigma^3/\epsilon$
velocity	$\mathrm{v}^* = \mathrm{v}\sqrt{m_0/\epsilon}$

The major role of the 3-particle potential is to prevent formation of more than one bond to each hydrogen atom. This is done by making it energetically non-favorable for a third atom to be close to two chemically bonded atoms. The three-particle potential given by Kohen et al. [29] is:

$$u_{(3)} = h_{i,j,k}(r_{ij}, r_{jk}, \theta_{i,j,k}) + h_{j,i,k}(r_{ji}, r_{ik}, \theta_{j,i,k}) + h_{i,k,j}(r_{ik}, r_{kj}, \theta_{i,k,j}) \tag{4.3}$$

The h-functions are given by

$$h_{j,i,k}(r_{ji}, r_{ik}, \theta_{j,i,k}) = \begin{cases} \lambda a \exp\left[\frac{\gamma_3}{(r_{ji}-r_c)} + \frac{\gamma_3}{(r_{ik}-r_c)}\right] & \text{if } r_{ji} < r_c \text{ and } r_{ik} < r_c \\ 0 & \text{otherwise} \end{cases} \tag{4.4}$$

where

$$a = \left[1 + \mu\cos(\theta_{j,i,k}) + \nu\cos^2(\theta_{j,i,k})\right] \tag{4.5}$$

in real units, and $\lambda = 2.80 \cdot 10^{-21}$ kJ, $\mu = 0.132587$, $\nu = -0.2997$ and $\gamma_3 = 1.5$ Å are constants [29]. The cut-off distance, r_c, is the same for both the two- and three-particle interactions (2.8 Å).

In the triad subscript j, i, k the middle letter i refers to the atom at the subtended angle vertex. The distances have been written with respect to the center atom. The interaction energy is plotted for the triad j, i, k in Figure 4.1 for a linear configuration of three hydrogen atoms. Only linear configurations of the three H atoms (j, i and k) are plotted, as it was established in the paper by Siegbahn and Liu that the linear configuration contained the lowest minima [49]. The figure shows three minima, taking the symmetry in the plot into consideration. The lowest minimum, $U_1^* = -0.999$, corresponds to the minimum seen for the pair potential,

where two atoms (j and i) are chemically bonded, $r^*_{ji} = 1.6$, while the third atom (k) is far away, $r^*_{ik} = 6$. The second minimum, $U^*_2 = -0.941$, shows that two atoms (j and i) are close, $r^*_{ji} = 2.2$, while the third atom (k) is located further away, $r^*_{ik} = 3.0$. The last minimum, $U^*_3 = -0.906$, found on the symmetry axis, corresponds to distances $r^*_{ji} = r^*_{ik} = 1.9$. Such extra minima were not observed for fluorine [3]. We will comment on the second and the third minima in Section 4.4 (Results and discussion). The total potential was used to determine the distance of

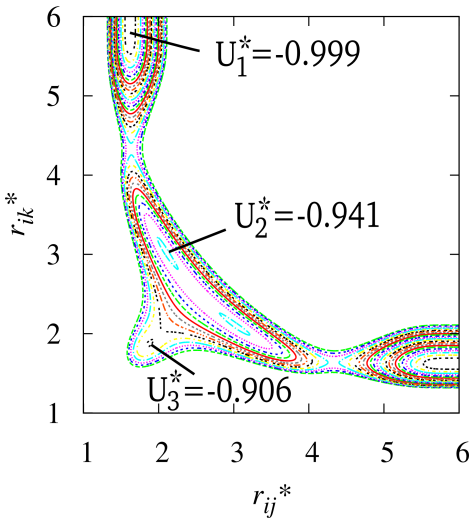

Figure 4.1: Total interaction energy, U^*, for a linear configuration of 3 hydrogen atoms j, i and k as a function of the distances r^*_{ji} and r^*_{ik}. Three minima is observed, U^*_i, when the symmetry of the plot is taken into consideration. Reduced units are used, cf. Table 6.1.

chemically bonded particles. When the distance between two particles was shorter than $r^*_{ji} \leq 4.0$ they were labeled as part of a molecule, see Figure 4.1. This choice is in agreement with the procedure used by Stillinger and Weber [3], and is further confirmed by the results for the pair correlation function in Section 4.4.

4.3 Simulation details

The system consisted of 1000 hydrogen atoms (for all densities) in a non cubic box with dimensions $L_x = 2L_y = 2L_z$, in the x, y and z direction, respectively. The volume of the box was $V = L_xL_yL_z = N_pm_0/\rho$, where ρ is the overall mass density ($\rho = N_pm_0/(V)$), N_p is the total number of particles ($N_p = N_{\mathrm{H}} + 2N_{\mathrm{H}_2} = 1000$) and m_0 is the mass of one hydrogen atom. Periodic boundary conditions were applied to the x-, y- and z-directions [93]. Data were sampled every 20 steps after the system had been equilibrated. A time step length of 0.1 in reduced units (0.22 fs), see Table 6.1, was used.

The velocity Verlet algorithm [94] was used to integrate Newton's equations of motion. A list of all pairs who were closer to each other than a set distance, $r^*_{list} = 6.5$, was made to save computational time, as many particles are further away from each other than the cut-off distance, $r^*_c = 6.11$. Pair interactions were then only calculated when $r^* \leq r^*_{list}$. A similar algorithm, called NEIGHBOUR3, which was developed by Xu et al. [31], was used to compute 3-particle interactions. In this algorithm a list of triplets is made by combining pairs from the pair list, which have one particle in common. As long as the displacement of the particles was less than half of $r^*_{list} - r^*_c = 0.4$, we did not need to update the two lists. This procedure avoided unnecessary calculation of particle interactions.

The program gave the temperatures in the box within ± 0.1 %. During the equilibration period the temperature was scaled to the set temperature every step by velocity scaling. After this, the temperature was adjusted every 100 steps, by scaling the velocities with the scaling factor given in Eq. (4.6), to maintain the wanted temperature [28].

$$scale = \sqrt{T_{inst}/T_{wanted}} \tag{4.6}$$

Here T_{inst} is the instantaneous temperature and T_{wanted} is the wanted temperature. This does not give a perfect canonical distribution, but we assume that the influence of this procedure on the calculated structural- and thermodynamic properties is negligible. In order to test system size dependence, we repeated some of the equilibrium simulations for the same density with 4096 particles.

The pair correlation function along with the dissociation constant and reaction enthalpy was studied at a density just below the triple point density ($\rho^* = 0.004$) and approximately a fourth of this density ($\rho^* = 0.0011$), following the procedures of Stillinger and Weber [3]. For both densities temperatures were chosen in the range $0.003 \leq T^* \leq 0.3$. Additionally, a run was performed near the triple point of the molecular fluid ($\rho^* = 0.004$ and $T^* = 0.000268$).

For the calculation of the pressure (with the different contributions), densities in the range $0.00001 \leq \rho^* \leq 0.004$ were studied at $T^* = 0.03$. For the densities, $\rho^* = 0.0011$ and 0.004 additional runs in temperature range $0.002 \leq T^* \leq 0.4$ were performed.

For the high density cases, $0.0003 \leq \rho^* \leq 0.004$, three million MD steps were used for equilibration of the system and the simulations were run a total of five million steps, including the equilibration. For the lower density cases, $0.00001 \leq \rho^* \leq 0.0001$, up to seven million MD steps were used for equilibration, and a total of up to ten million steps were used for the simulation run.

Figure 4.2 shows snapshots from the simulations for the reduced densities $\rho^* = 0.0011$ (left) and $\rho^* = 0.004$ (right) at $T^* = 0.003$ ($T = 156$ K). We see that the high density system is a dense liquid, while the low density system can be compared to a compressed gas.

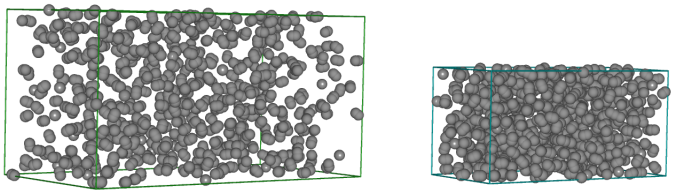

Figure 4.2: Snapshot from simulations illustrating the density, $\rho^* = 0.0011$ (left) and $\rho^* = 0.004$ (right), at $T^* = 0.003$ ($T = 156$ K). A disordered system is clearly seen for both densities. Conditions are such that the dissociation is negligible.

4.3.1 Calculation details

The temperature T was found from the average kinetic energy per degree of freedom of all particles:

$$T = \frac{1}{3k_B N_p} \sum_{i=1}^{N_p} m_i \mathrm{v}_i^2 \tag{4.7}$$

where $\mathrm{v}_i^2 = \mathrm{v}_{x,i}^2 + \mathrm{v}_{y,i}^2 + \mathrm{v}_{z,i}^2$. From the virial theorem, the expression for the pressure in the presence of two- and three-particle interactions is:

$$\begin{aligned} P = \frac{k_B T N_p}{V} - \frac{1}{3V} \sum_{i=1}^{N_p} \Bigg[& \frac{1}{2} \sum_{j \text{ pair with } i} \frac{\partial u_2(r_{ij})}{\partial r_{ij}} r_{ij} \\ & + \sum_{j<k \text{ triplet with } i} \Bigg(\frac{\partial h_{j,i,k}(r_{ji}, r_{ik}, \theta_{j,i,k})}{\partial r_{ji}} r_{ji} \\ & + \frac{\partial h_{j,i,k}(r_{ji}, r_{ik}, \theta_{j,i,k})}{\partial r_{ik}} r_{ik} + \frac{\partial h_{j,i,k}(r_{ji}, r_{ik}, \theta_{j,i,k})}{\partial r_{jk}} r_{jk} \Bigg) \Bigg] \end{aligned} \tag{4.8}$$

The first term in Eq. (4.8) is the ideal contribution to the pressure, while the second and the third terms give the contributions from the two- and three particle potentials, respectively. As the angle $\theta_{j,i,k}$, and the distance r_{ik} are constant in $h_{j,i,k}$ when we take the derivative with respect to r_{ji}, this derivative is easy to calculate; and similarly for the other two contributions. The contributions to the pressure will be calculated separately and compared.

In the calculation of the pressure we used the atomic method [92]. This implies that we took the kinetic contributions of all atoms to give the ideal contribution to the pressure, $N_P k_B T/V$. To this, we added force moments due to pair- and three-particle interactions from all atoms. Given that many atoms are part of a bound pair, one may ask whether the molecular method [92] is more convenient. Both methods are discussed in detail by Ciccotti and Ryckaert [92]. In the appendix of their article, they reproduce an unpublished proof given by Berendsen, showing

that both definitions give the same pressure. As we calculate the forces, positions and velocities of all atoms in the MD simulation, it is natural to use the atomic method here.

The molar density, c_k, of component k is:

$$c_k = \frac{N_k}{N_A V} \tag{4.9}$$

where N_k is the number of particles of component k (H or H_2). Furthermore N_A is Avogadro's number. The mass density of the system can be found from

$$\rho = \frac{N_p m_0}{V} \tag{4.10}$$

The thermodynamic equilibrium constant, K_{th}, can be found from the dissociation constant, K_x, and the activity coefficients according to

$$K_{th} = \frac{x_{\mathrm{H}}^2}{x_{\mathrm{H}_2}} \frac{\gamma_{\mathrm{H}}^2}{\gamma_{\mathrm{H}_2}} \equiv K_x \frac{\gamma_{\mathrm{H}}^2}{\gamma_{\mathrm{H}_2}} \tag{4.11}$$

The equilibrium constant can then be used to find Gibbs energy of the reaction

$$\Delta_r G = \Delta_r G^\circ + RT \ln K_{th} \tag{4.12}$$

The standard reaction enthalpy can then be found from the van't Hoff equation at constant pressure

$$\left[\frac{\mathrm{d} \ln K_{th}}{\mathrm{d}(1/T)} \right]_P = -\frac{\Delta_r H^\circ}{R} \tag{4.13}$$

At chemical equilibrium, $\Delta_r G = 0$ and hence $\Delta_r G^\circ = -RT \ln K_{th}$. For an ideal mixture $\gamma_{\mathrm{H}}^2/\gamma_{\mathrm{H}}$ is unity and $K_x = K_{th}$. When the ratio of the activity coefficients at constant pressure is constant, we can find $\Delta_r H^\circ$ from the van't Hoff equation using K_x. We shall seek to find such conditions.

4.4 Results and Discussion

4.4.1 Pair correlation functions

The atom-atom pair correlation function, $g(r)$, for the hydrogen atoms, including atoms that are part of a molecule, describes the correlation of two atoms as a function of the distance. A deviation in the pair correlation function from unity indicates correlations between particles due to intermolecular interactions. Hence, the pair correlation function gives information about the number of chemically bonded atoms and the distance between bonded atoms, and their neighboring atoms [3, 31].

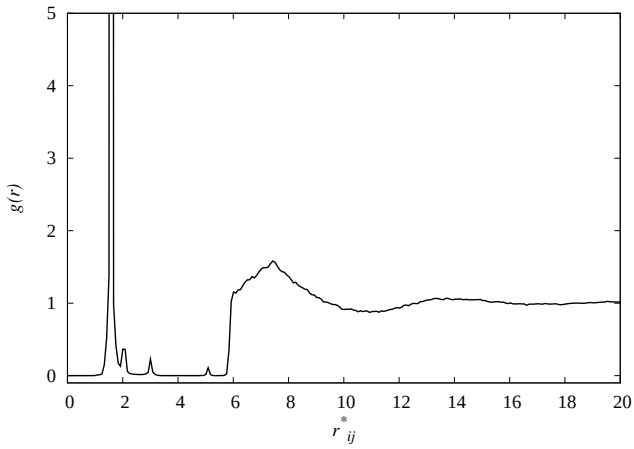

Figure 4.3: Pair correlation function near the triple point of the molecular fluid. T^*= 0.000268 ($T = 14$ K), ρ^*=0.004 ($\rho_H = 0.0695$ g cm^{-3}).

The pair correlation function near the triple point of the molecular fluid, $\rho^* = 0.004$ and $T^* = 0.000268$, is given in Figure 4.3. The figure shows a very high peak around $r^*_{ij} = 1.6$ and several minor peaks before a plateau is reached.

The high peak represents chemically bonded pairs and its area reflects the fact that there are 500 molecules in the system (no dissociation at this low temperature). The first three peaks in Figure 4.3 can be directly related to Figure 4.1, the potential energy of linear arrays of 3 hydrogen atoms. We see here that the distance $r^*_{ij} = 1.6$ corresponds to the arrangement with the lowest energy, $U^*_1 = -0.999$. Two atoms are bound at this distance while the third atom is found at a distance $r^*_{ik} = 6$. This is compatible with the first high peak. This part is similar to the results of Stillinger and Weber for fluorine [3]. They observed no additional peaks in their pair correlation functions for fluorine however; in agreement with one single minimum in their total potential.

The second minimum $U^*_2 = -0.941$ in Figure 4.1 leads to two small peaks in the pair correlation function in Figure 4.3 at reduced distances $r^*_{ij} = 2.2$ and 3.0. The third minimum $U^*_3 = -0.906$ in Figure 4.1 has no clear impact on the pair correlation function in Figure 4.3. The small peak around $r^*_{ij} \approx 5$ cannot be traced to a minimum in the energy landscape. For a temperature of 14 K, the de Broglie wavelength for H is 10.15 in reduced units ($\Lambda = h/\sqrt{2\pi m_0 k_B T}$, where h is Planck's constant, and m_0 the mass of one hydrogen atom). For this temperature the classical calculation is therefore not adequate. The triplet structure is an artefact of this. In the simulations these linear formations of triplets, when they appear,

are stable over the whole simulations, as the kinetic energy of the particles is to low to move to another minimum. We therefore interpret the peaks beyond $r_{ij}^* = 4$ as due to intermolecular short-range order of chemically bonded pairs. The reason to do the classical calculation for this low temperature is to compare the results with the results for fluorine in the paper by Stillinger and Weber [3]. The similarity of the results validates our analysis.

It is interesting to observe that the system develops an effective excluded volume diameter. The pair potential is zero at a distance 1 in reduced units. When three-particle interactions are included, the molecule obtains an effective excluded volume diameter of about 6, as seen from Figure 4.3, where the pair correlation function is approximately zero in the region $2.2 < r_{ij}^* < 6$, but rises sharply at 6. This value in real units is 2.748 Å, a value in good agreement with the value 2.7 Å given by Labet et al. [84] for the second shortest H-H separation at 1 GPa. Moreover, it compares well with the value 2.81 Å given by Allen and Tildesley [28] for a Lennard-Jones potential of molecular hydrogen. This means that our model for the chemical reaction at a meso-level is consistent with a coarser level fluid model of the molecular system, making this part of the model realistic.

Figure 4.4 shows the pair correlation function at $T^* = 0.003$, for both $\rho^* = 0.004$ (Figure 4.4(a)) and $\rho^* = 0.0011$ (Figure 4.4(b)). When we compare the two pair correlation functions for the two densities in Figure 4.4 we see that they have the same general trend. A large and narrow peak can be seen at $r_{ij}^* = 1.6$ in both cases. This peak is broadest at the lower density ($\rho^* = 0.0011$, Figure 4.4(b)). At the higher density ($\rho^* = 0.004$) it is just slightly broader than in Figure 4.3. A broadening is also observed in the rest of the structure, when we compare Figures 4.4(a) and 4.4(b) to the counterpart in Figure 4.3. In the high density results, $\rho^* = 0.004$ in Figure 4.4(a), the peak at $r_{ij}^* = 3$ has been incorporated into the small peak at $r_{ij}^* = 2.2$ as a shoulder. For the low density, $\rho^* = 0.0011$ in Figure 4.4(b), no distinct extra peak is observed, but a broad shoulder remains. A broadening of peaks take place, due to increase in the temperature as well as to the reduction in density. For a temperature of 156 K, the de Broglie wavelength for H is 3.03 in reduced units. For this temperature the classical calculation is therefore also not adequate. We refer to the discussion for 14 K above. The pair correlation function goes smoothly to unity as expected at about $r_{ij}^* = 10$ for the high density, and at about 8 for the low density. For neither density, dissociation was observed, cf. Tables 6.4 and 6.3.

The pair correlation function at $T^* = 0.03$ is given in Figure 4.5, for the high density, $\rho^* = 0.004$ in Figure 4.5(a), and the low density, $\rho^* = 0.0011$ in Figure 4.5(b). No dissociation was observed for either density, see Tables 6.4 and 6.3. The main peak at $r_{ij}^* = 1.6$, corresponding to the chemically bonded atoms, has further broadened for both densities compared to Figures 4.4(a) and 4.4(b). The two peaks due to the second potential minimum have disappeared. This is clearly due to the increase in the temperature. The area under the pair correlation function from $2.4 \leq r_{ij}^* \leq 5$ is zero for both densities. From r_{ij}^* around 9 the correlation function is roughly equal to one for both densities.

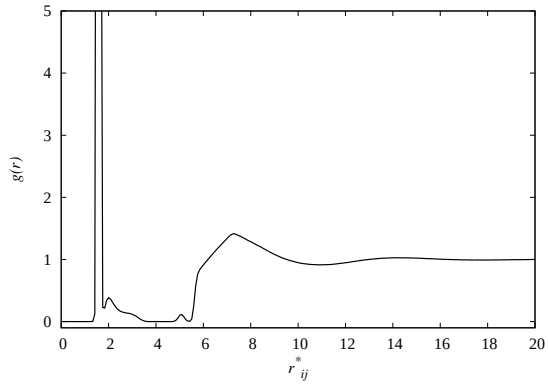

(a) $\rho^* = 0.004$ ($\rho = 0.0695$ g cm^{-3})

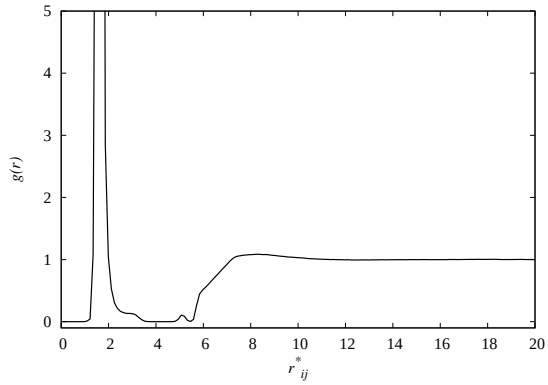

(b) $\rho^* = 0.0011$ ($\rho = 0.0191$ g cm^{-3})

Figure 4.4: Pair correlation functions at T^*= 0.003 (T = 156 K). The high density, $\rho^* = 0.004$ is shown to the left (4.4(a)) and the low density, $\rho^* = 0.0011$ to the right (4.4(b)).

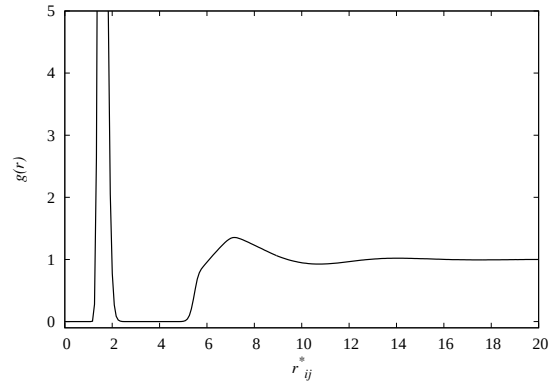

(a) $\rho^* = 0.004$ ($\rho = 0.0695$ g cm^{-3})

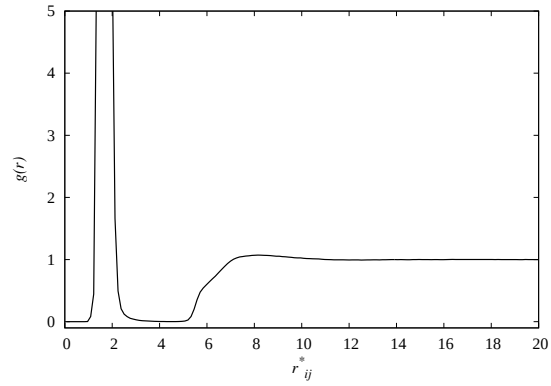

(b) $\rho^* = 0.0011$ ($\rho = 0.0191$ g cm^{-3})

Figure 4.5: Pair correlation functions at T^*= 0.03 (T = 1560 K). The high density, $\rho^* = 0.004$ is shown to the left (4.5(a)) and the low density, $\rho^* = 0.0011$ to the right (4.5(b)).

Figure 4.6 shows the pair correlation functions for both the high density, $\rho^* = 0.004$ (Figure 4.6(a)), and the low density, $\rho^* = 0.0011$ (Figure 4.6(b)), at $T^* = 0.3$. The correlation function is near unity for $r_{ij}^* > 6$, as one should expect for this temperature. But the pair correlation is no longer zero when $2.2 < r_{ij}^* < 5$. This is a sign of the reaction taking place. If we compare the high- and low density figures, we see that the main difference is the intensity and broadness of the first peak, as the main peak in Figure 4.6(b) is both broader and has a lower intensity than it's high density counterpart. Compatible with this we find that more particles are bound at the low density. For the high density in Figure 4.6(a), we observe 23 % dissociation (232.4 atoms), while for the low density, in Figure 4.6(b), a dissociation of 47 % (468.7 atoms) is observed, cf. Tables 6.4 and 6.3.

In the counting procedure used, we label all particles as either atoms or molecules. If, during the simulation, the distance between two atoms is less than 4, they are labelled as molecules. At the end of every 20 time steps, we count the number of atoms. The rest is then counted as molecules. At higher temperatures, bonds are continuously formed and broken, and as Stillinger and Weber [2] say, this counting procedure will give a reasonable, but still approximate value of the number of molecules. We estimate the accuracy to be within $\pm$ 1 %.

In summary, from Figures 4.3 – 4.6, we conclude that the three-particle potential has a large ordering effect on the molecules, in agreement with earlier observations [3]. The effective excluded volume diameter of the molecule becomes 6 in reduced units as a result of the three particle interaction, a value in agreement with the interparticle distance of the Lennard-Jones potential for molecular hydrogen [28]. The ordering effect was observed to decrease with increasing temperature.

At very low temperature (14 K and 156 K) quantum effects becomes important and for this reason our classical description leads to triplets which is an artefact of this. At very high temperatures, above 20 000 K, we see from the phase diagrams that we might be entering the plasma region of hydrogen [95–97]. At the highest temperature and density considered here (15 600 K and $\rho = 0.0695$ g cm^{-3}), we are however well within the region of the atomic fluid, and thus we expect that our model is able to predict the properties of hydrogen.

For all conditions, bound particles were be determined for a set distance $r_{ij}^* \leq 4$. For temperatures showing the behaviour illustrated by Figure 4.6 we are dealing with a chemical reaction, and can find the fraction of molecules by counting the particles which obey this inequality. The role of the two- and three particle interactions will be examined further below.

4.4.2 The Contributions to the Pressure in a Reacting Mixture

The overall pressure, P_{tot}, in the calculation is a sum of the kinetic (or ideal) pressure, P_{ideal}, and the contributions from the two- and three particle potentials,

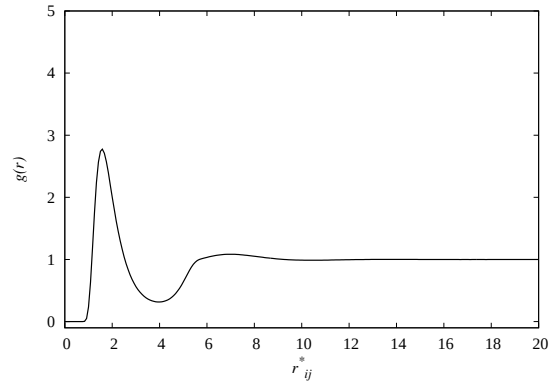

(a) $\rho^* = 0.004$ ($\rho = 0.0695$ g cm^{-3})

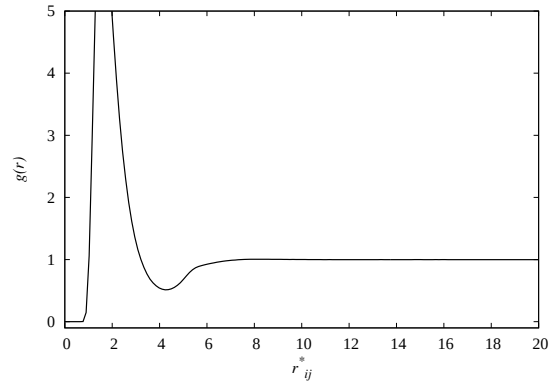

(b) $\rho^* = 0.0011$ ($\rho = 0.0191$ g cm^{-3})

Figure 4.6: Pair correlation functions at T^*= 0.3 (T = 15600 K). The high density, $\rho^* = 0.004$ is shown to the left (4.6(a)) and the low density, $\rho^* = 0.0011$ to the right (4.6(b)).

$P_{2\text{part}}$ and $P_{3\text{part}}$, see Eq. (4.8). The relative magnitude of these contributions to the overall pressure at $T^* = 0.03$ was calculated and is given in Figure 4.7 for densities in the range $0.00001 \leq \rho^* \leq 0.004$. The different contributions, P_i, to the pressure have been divided by the ideal pressure (P_i/P_{ideal}) to be able to compare the contributions at different densities relative to each other. As a consequence the ideal contribution, P_{ideal} (from the first part of Eq. (4.8)) in Figure 4.7 is equal to 1 for all densities. Important in Berendsen's proof of the equality of the atomic and

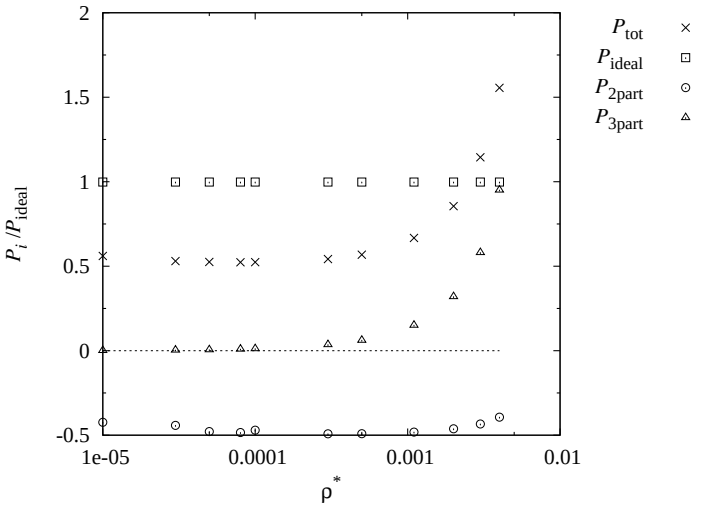

Figure 4.7: The total pressure, P_{tot}, and the contribution from the ideal part, P_{ideal}, and two- and three particle interactions, $P_{2\text{part}}$ and $P_{3\text{part}}$ at $T^* = 0.03$ as a function of the density of the system, $0.00001 \leq \rho^* \leq 0.004$. The densities are plotted using log scale. All pressures have been normalized with respect to the ideal pressure, giving $P_{\text{ideal}} = 1$ for all densities.

molecular method for pressure calculations (see Ciccotti and Ryckaert [92]), is that the intramolecular two particle forces give a negative contribution to the pressure. In good approximation, it replaces the kinetic pressure of two atoms $2k_BT/V$ by the kinetic pressure of one molecule k_BT/V. It follows that the contribution to the pressure due to pair interaction is negative, and in essence reduces the kinetic pressure from $(N_{\text{H}} + 2N_{\text{H}_2})k_BT/V$ to $(N_{\text{H}} + N_{\text{H}_2})k_BT/V$. The contribution from the pair potential to the pressure in Figure 4.7 is negative and approximately half the size of the ideal contribution, cf. [92]. So it is playing an important role to lower the overall pressure.

The role of the three-particle interaction is very different. As we have seen from the pair correlation functions (see Section 4.4.1), no particles aside from the bound

particles, approach each other closer than almost a diameter of 6 in reduced units. This means that the effective excluded volume is almost $6^3 = 216$ times larger than what one would expect on the basis of the pair potential alone. This results in a large positive contribution to the pressure for a reduced density of the order of $1/216 \approx 0.005$ and above. For lower densities the contribution from the three particle interaction to the total pressure becomes less important, as can be seen in Figure 4.7. In Figure 4.7 we see that for densities less than $\rho^* = 0.0001$ the 3-particle interaction does not contribute significantly to the pressure. For the higher densities, the pressure increases with the density due to an increased contribution from the three-particle interactions. As for the pair potential contribution, it deviates significantly above $\rho^* = 0.005$ where molecules are on average in close contact. The three-particle interaction can therefore contribute significantly to the non-ideality of the mixture, even if a reaction does not take place to any significant degree as is the case in this plot. The contribution from the three-particle interaction under these conditions for our systems, reflects that the higher the density becomes, the higher is the resulting repulsion without bond disruptions.

The influence of the temperature on the pressure at the densities $\rho^* = 0.004$ and $\rho^* = 0.0011$ was also investigated. The range of temperatures covers the range where we can expect a significant degree of reaction, cf. next subsection. The results for the high density case, $\rho^* = 0.004$, where we can expect an impact of the reaction from $T^* = 0.07$ and upwards, are given in Table 4.2. For $T^* \geq 0.03$ the results are plotted in Figure 4.8. All pressures have been normalized with respect to the ideal pressure (P_i/P_{ideal}), as before. This gives a normalized ideal pressure of 1 for all temperatures, which for this reason is left out of the table. The statistical

Table 4.2: The total pressure, P_{tot}, and the contributions to the pressure from the two- and three-particle interactions, $P_{2\text{part}}$ and $P_{3\text{part}}$, as a function of temperature for $\rho^* = 0.004$. All data are normalized with respect to the ideal pressure, P_{ideal}, is 1 per definition for all cases, and is left out of the table. The accuracy was estimated to be 10 % for $T^* < 0.03$ and a few percent for $T^* \geq 0.03$.

T^*	0.000268	0.002	0.003	0.004	0.03	0.05	0.07	0.09
P_{tot}	1.92	1.77	1.73	1.72	1.55	1.50	1.46	1.43
$P_{2\text{part}}$	-5.7	-9.8	-5.6	-4.2	-0.39	-0.40	-0.41	-0.43
$P_{3\text{part}}$	6.6	10.5	6.3	4.9	0.95	0.90	0.88	0.87
T^*	0.15	0.17	0.2	0.23	0.25	0.3	0.4	
P_{tot}	1.41	1.41	1.41	1.41	1.40	1.39	1.37	
$P_{2\text{part}}$	-0.49	-0.51	-0.52	-0.52	-0.51	-0.48	-0.41	
$P_{3\text{part}}$	0.91	0.92	0.93	0.92	0.91	0.87	0.78	

error of the various pressures are in the order of a few percent, for $T^* < 0.03$ we estimate the statistical error of the two- and three-particle pressures (but not their sum) be in the order of 10 %.

In Table 4.2 we see that the normalized total pressure increases about 11% when the temperature is reduced by an order of magnitude. The sum of the normalized $P_{2\text{part}}$

and $P_{3\text{part}}$, which equals the normalized total pressure minus 1, similarly increases when the temperature decreases. For T^* between 0.03 and 0.4 the change of the values of the normalized $P_{2\text{part}}$ and $P_{3\text{part}}$ is similarly rather small. The absolute value of these contributions is between zero and one for these temperatures. For lower temperatures the normalized $P_{2\text{part}}$ and $P_{3\text{part}}$ both increase by up to an order of magnitude without a similar increase in their sum. For these low temperatures, all hydrogen atoms are bound in molecules.

At low temperatures a particular property of this system affects the results. At these temperatures, there are no atoms in the system, and no reaction is going on. Most of the atoms, once they are bound to each other in a molecule, remain bound during the whole simulation. Concurrent with this is that also 3 atoms can arrive in the second or third minimum, see Figure 4.1. The occurrence of such triplets was observed in Figures 4.3 and 4.4 as small side peaks (shoulders) at reduced distances 2.2 and 3. The number of triplets is small, but they can remain stuck to each other during the whole simulation at low temperatures. The existence of some permanent triplets can explain the enormous decrease of the 2 particle contribution and roughly the same increase of the 3 particle contributions, while their sum is only slightly increased above the higher temperature value. The existence of triplets is a consequence of the potential we have used. The potential was an analytical representation of an energy surface generated from quantum mechanics [3], but it may not represent reality under these extreme conditions. In Figure 4.8, we only plot the normalized pressures for the high temperature domain, T^* between 0.03 and 0.4. The statistical error was estimated to be in the order of a few percent for $T^* \geq 0.03$. For lower temperatures the statistical error of the two- and three-particle pressures (but not their sum) was estimated to be in the order of 10 %.

For the low density case, $\rho^* = 0.0011$, the total pressure and the different contributions to the pressure as a function of temperature is given in Table 4.3 below, and plotted in Figure 4.9 for $T^* \geq 0.03$. Also here we can expect an impact of the reaction from $T^* = 0.07$ and up. From Table 4.3 we see that the normalized

Table 4.3: The total pressure, P_{tot} and the contributions to the pressure from the two- and three-particle interactions, $P_{2\text{part}}$ and $P_{3\text{part}}$, as a function of temperature for $\rho^* = 0.0011$. All data are normalized with respect to the ideal pressure, P_{ideal}. The normalized ideal pressure, P_{ideal}, is 1 per definition for all cases, and is left out of the table. The accuracy was estimated to be 10 % for $T^* < 0.03$ and a few percent for $T^* \geq 0.03$.

T^*	0.002	0.003	0.004	0.03	0.05	0.07	0.09	
P_{tot}	0.69	0.69	0.68	0.67	0.66	0.66	0.67	
$P_{2\text{part}}$	-2.6	-1.9	-2.9	-0.48	-0.48	-0.48	-0.48	
$P_{3\text{part}}$	2.3	1.6	2.6	0.15	0.15	0.15	0.15	
T^*	0.11	0.13	0.15	0.17	0.2	0.25	0.3	0.4
P_{tot}	0.68	0.70	0.73	0.76	0.80	0.85	0.88	0.92
$P_{2\text{part}}$	-0.47	-0.44	-0.44	-0.42	-0.38	-0.32	-0.27	-0.20
$P_{3\text{part}}$	0.16	0.17	0.17	0.18	0.18	0.17	0.15	0.12

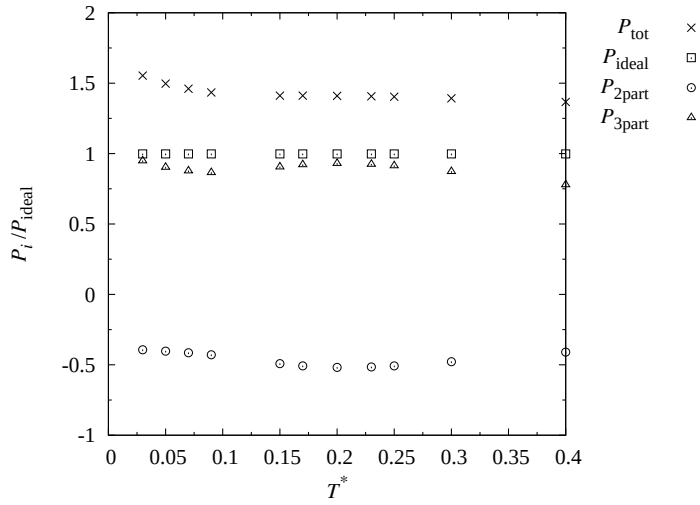

Figure 4.8: The total pressure, P_{tot}, and the different contributions to the pressure, P_{ideal} and from the two- and three-particle interactions, $P_{2\text{part}}$ and $P_{3\text{part}}$ as a function of temperatures for the high density case, $\rho^* = 0.004$. All data have been normalized with respect to the ideal pressure, giving $P_{\text{ideal}} = 1$.

total pressure is essentially constant at low temperatures (between $T^* = 0.002$ and $T^* = 0.13$) and increases by about 20% when the reduced temperature increases to $T^* = 0.4$. This behavior is different from the result for the higher density, where the normalized total pressure decreased when the temperature increased. The sum of the normalized $P_{2\text{part}}$ and $P_{3\text{part}}$, which equals the normalized total pressure minus 1, behaves similarly. The value of the normalized $P_{2\text{part}}$ is reduced about 60% from $T^* = 0.03$ to $T^* = 0.4$, while the value of the normalized $P_{3\text{part}}$ remains essentially constant in this temperature domain. For lower temperatures the normalized $P_{2\text{part}}$ and $P_{3\text{part}}$ both increase by up to an order of magnitude without a similar increase in their sum. The reason for this is the same as the one given for the higher density. In Figure 4.9, we only plot the normalized pressures for the high temperature domain, T^* between 0.03 and 0.4.

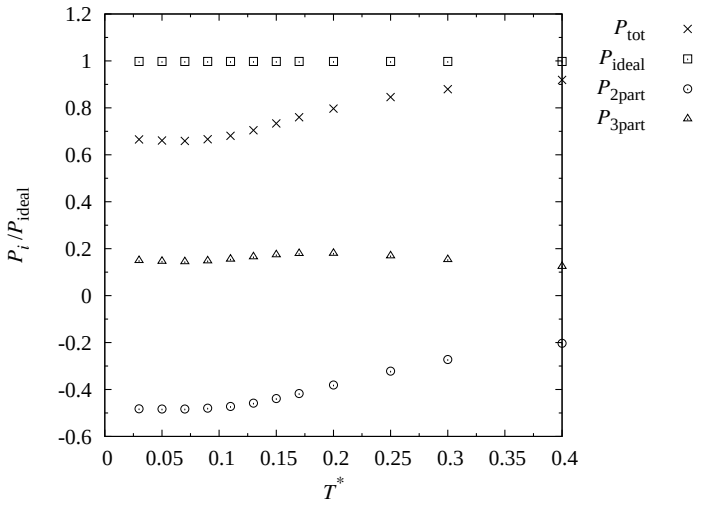

Figure 4.9: The total pressure, P_{tot}, and the different contributions to the pressure, P_{ideal} and from the two- and three-particle interactions, $P_{2\text{part}}$ and $P_{3\text{part}}$ as a function of temperatures for the low density case, $\rho^* = 0.0011$. All data have been normalized with respect to the ideal pressure, giving $P_{\text{ideal}} = 1$.

For the high density, we see that the relative contributions to the normalized pressure are constant, up or down 10%, for $T^* = 0.03 - 0.4$, indicating that γ_H^2/γ_{H_2} is approximately constant in this range. This indicates that we can use the van't Hoff equation, Eq.(4.13), with K_x, to determine the standard enthalpy of the reaction, and we shall do so below. For the low density, we see the same trend in the normalized overall pressure for a lower temperature range, $0.03 \leq T^* \leq 0.13$, indicating that γ_H^2/γ_{H_2} is constant also there.

For all temperatures, the effect of the three-particle potential is smaller in the low density case, compared to the ideal contribution and the contribution from two-particle interactions.

4.4.3 Dissociation constants and the enthalpy of reaction

The dissociation of hydrogen was studied as a function of temperature for two different densities, $\rho^* = 0.004$ and $\rho^* = 0.0011$, by counting the number of atoms every 20 steps. At the end, an average over the last 2000 steps was taken.

For the liquid like density, $\rho^* = 0.004$, the total pressure, the dissociation (number of H), mole fraction along with the calculated the dissociation constants, K_x, are given in Table 6.4 below. From Table 6.4, we see that no dissociation is observed

Table 4.4: Dissociation (N_{H}), mole fraction (x_i), total pressure (P^*) and the dissociation constant (K_x) for the high density, $\rho^* = 0.004$.

T^*	0.000268	0.002	0.003	0.004	0.03
N_{H}	0.00	0.00	0.00	0.00	0.00
$N_{\mathrm{H_2}}$	500.00	500.00	500.00	500.00	500.00
$x_{\mathrm{H_2}}$	1.000	1.000	1.000	1.000	1.000
K_x	-	-	-	-	-
P^*	$3 \cdot 10^{-6}$	$1 \cdot 10^{-5}$	$2 \cdot 10^{-5}$	$3 \cdot 10^{-5}$	$2 \cdot 10^{-4}$
T^*	0.05	0.07	0.09	0.15	0.17
N_{H}	0.00	1.98	5.54	66.90	91.42
$N_{\mathrm{H_2}}$	500.00	499.01	497.23	466.55	454.29
$x_{\mathrm{H_2}}$	1.000	0.996	0.989	0.875	0.832
K_x	-	0.000	0.000	0.018	0.034
P^*	$3 \cdot 10^{-4}$	$4 \cdot 10^{-4}$	$5 \cdot 10^{-4}$	$8 \cdot 10^{-4}$	$9 \cdot 10^{-4}$
T^*	0.2	0.23	0.25	0.3	0.4
N_{H}	137.61	172.42	192.39	232.42	288.50
$N_{\mathrm{H_2}}$	431.19	413.79	403.81	383.79	355.75
$x_{\mathrm{H_2}}$	0.758	0.706	0.677	0.623	0.552
K_x	0.077	0.123	0.154	0.228	0.363
P^*	$1.1 \cdot 10^{-3}$	$1.3 \cdot 10^{-3}$	$1.4 \cdot 10^{-3}$	$1.7 \cdot 10^{-3}$	$2.2 \cdot 10^{-3}$

for $T^* \leq 0.05$ at $\rho^* = 0.004$. When we increase the temperature from $T^* = 0.05$ to $T^* = 0.4$, we see a large increase in the dissociation to 29 %. As expected, since the main contribution to the pressure is the ideal pressure, the overall pressure increases with temperature.

The results for the dissociation, mole fraction, total pressure and the dissociation constant is given in Table 6.3 below for the low density, $\rho^* = 0.0011$. From Table 6.3 we see that for $T^* \leq 0.05$ no dissociation is observed, while at $T^* = 0.09$ we observe almost 2 % dissociation. Increasing the temperature further increases the

Table 4.5: Dissociation (N_H), mole fraction (x_i), total pressure (P^*) and the dissociation constant (K_x) for the low density, $\rho^* = 0.0011$.

T^*	0.002	0.003	0.004	0.03	0.05
N_H	0.00	0.00	0.00	0.00	0.00
N_{H_2}	500.00	500.00	500.00	500.00	500.00
x_{H_2}	1.000	1.000	1.000	1.000	1.000
K_x	-	-	-	-	-
P^*	$1 \cdot 10^{-6}$	$2 \cdot 10^{-6}$	$3 \cdot 10^{-6}$	$2 \cdot 10^{-5}$	$4 \cdot 10^{-5}$
T^*	0.07	0.09	0.11	0.13	0.15
N_H	5.92	15.77	53.05	98.20	147.71
N_{H_2}	497.04	492.11	473.48	450.90	426.14
x_{H_2}	0.988	0.969	0.899	0.821	0.743
K_x	0.000	0.001	0.011	0.039	0.089
P^*	$5 \cdot 10^{-5}$	$7 \cdot 10^{-5}$	$8 \cdot 10^{-5}$	$1 \cdot 10^{-4}$	$1 \cdot 10^{-4}$
T^*	0.17	0.2	0.25	0.3	0.4
N_H	212.97	285.00	396.19	468.74	554.88
N_{H_2}	393.51	357.50	301.91	265.63	227.56
x_{H_2}	0.649	0.556	0.432	0.362	0.295
K_x	0.190	0.354	0.745	1.126	1.689
P^*	$1 \cdot 10^{-4}$	$2 \cdot 10^{-4}$	$2 \cdot 10^{-4}$	$3 \cdot 10^{-4}$	$4 \cdot 10^{-4}$

dissociation up to 55 % at $T^* = 0.4$. As expected the pressure increases with temperature. Comparing the dissociation for the high and low density a larger dissociation was observed for the low density for $T^* \geq 0.07$. As expected, the observed overall pressure is higher for the higher density.

Assuming that the ratio γ_H^2/γ_{H_2} is constant, the logarithm of the dissociation constant, $\ln K_x$, as a function of $1/T$ was used to calculate the standard enthalpy of reaction, $\Delta_r H^\circ$, for temperatures where the reaction is significant, $0.09 \leq T^* \leq 0.4$. The results are plotted in Figure 4.10 for both densities. An approximate linear trend is observed for both densities. For both densities a deviation can be observed from the linear trend. This deviation is caused by a pressure effect, as the pressure is not the same in all the simulations. This effect is however expected to be small and to not have a big effect on the calculation of the enthalpy. From the linear fit made to the Figure 4.10, we have estimated the standard enthalpy of reaction to be $\Delta_r H^\circ = 430$ kJ mol^{-1} and $\Delta_r H^\circ = 380$ kJ mol^{-1} for the high- and low density, respectively. The standard enthalpy of reaction can be compared to the binding energy of H_2 (436 kJ/mol at 298 K and 1 bar) [8, 29]. At the moment, we are not able to determine the standard enthalpy of the reaction independently for each temperature, as we have no knowledge about the ratio of the activity constants.

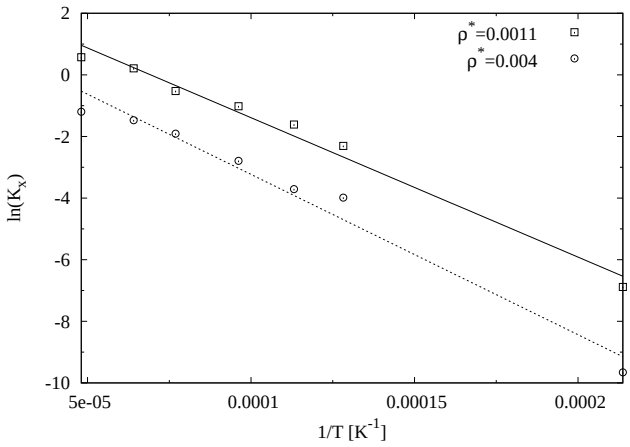

Figure 4.10: The natural logarithm of the dissociation constant, $\ln K_x$, plotted as a function of the inverse temperature ($T^* = 0.09 - 0.3$)

4.5 Conclusion

We have seen in the preceding sections that a classical MD model is able to capture the essential properties of a chemical reaction at equilibrium; namely its dissociation, enthalpy of reaction, and pressure and temperature variations. This was made possible by adding to the pair potential a three-particle interaction potential. The system behaviour on the meso-scale, characterized here by pair correlation functions, was found to be compatible with a coarser scale description, where the pair potential is the sole potential needed. In particular, the effective excluded volume diameter of the molecule was in agreement with the Lennard-Jones diameter used by others [28,84] to model fluid hydrogen. For low temperatures (14 K and 156 K) the de Broglie wavelength was large compared to the binding distance. For these temperatures the classical calculation is not appropriate. The triplet state found in the calculation at these temperatures is an artefact of this.

For two densities, $\rho^* = 0.0011$ and $\rho^* = 0.004$, and a series of temperatures, the three-particle interaction was found to have a large positive impact on the overall pressure. Assuming that the activity coefficient ratio was constant, the standard enthalpy of the reaction was estimated from van't Hoff equation to be 430 kJ/mol ($\rho^* = 0.004$) and 380 kJ/mol ($\rho^* = 0.0011$).

We have thus seen that a reacting mixture can be well modelled in a classical way, if the temperature is not to low. This opens up the possibility for dealing with problems related to reaction, diffusion, heat conduction, even thermal diffusion, and

interface transport, in problems which are central to chemical reactor (combustion) technology. This is in complete accordance with the view of Stillinger and coworkers [3,29]. To the best of our knowledge the idea of these authors have not been taken to the next steps yet. Neither has the impact of a three-particle interaction potential been discussed in the literature, see however [31]. A simple model for the chemical reaction as presented here for hydrogen, will allow its introduction in fluid modelling at large. The model may facilitate simultaneous studies of reaction and diffusion under various non-equilibrium conditions, and serve as a benchmark for quantum mechanical calculations of reactions.

Acknowledgement

P. O. Åstrand is thanked for clarifying discussions concerning the potential and the resulting triplet structures. The authors are grateful to the Storforsk Project Transport no 167336 from NFR and the Department of Chemistry, NTNU, for financial support.

Chapter 5

Partial Molar Enthalpies and Reaction Enthalpies From Equilibrium Molecular Dynamics Simulation

Sondre K. Schnell[1,2,3], Ragnhild Skorpa[3], Dick Bedeaux[1], Signe Kjelstrup[1,3] Thijs J. H. Vlugt[1] and Jean-Marc Simon[4],

1. Process & Energy Laboratory, Delft University of Technology, Leeghwaterstraat 39, 2628CB Delft, The Netherlands

2. Department of Chemical and Biomolecular Engineering, University of California, Berkeley, Berkeley, California 94720, United States

3. Department of Chemistry, Norwegian University of Science and Technology, NO-7491 Trondheim, Norway

4. Laboratorie Interdisciplinaire Carnot de Bourgogne, UMR, CNRS-Université de Bourgogne, Dijon, France.

This chapter was published in *J. Chem. Phys* (2014) 141:144501

Abstract

We present a new molecular simulation technique for determining partial molar enthalpies in mixtures of gases and liquids from single simulations, without relying on particle insertions, deletions, or identity changes. The method can also be applied to systems with chemical reactions. We demonstrate our method for binary mixtures of WCA particles by comparing with conventional simulation techniques, as well as for a simple model that mimics a chemical reaction. The method considers small subsystems inside a large reservoir (*i.e.* the simulation box), and uses the construction of Hill to compute properties in the thermodynamic limit from small-scale fluctuations. Results obtained with the new method are in excellent agreement with those from previous methods. Especially for modeling chemical reactions, our method can be a valuable tool for determining reaction enthalpies directly from a single MD simulation.

5.1 Introduction

The state-function enthalpy, H, is an important thermodynamic property in a wide variety of applications, ranging from chemical engineering to biology [98–100]. From knowledge of the enthalpy as a function of composition, one can determine the partial molar enthalpy of a component in a mixture. This quantity is central to understand thermodynamics of mixtures and chemical reactions under equilibrium and non-equilibrium conditions [12, 100]. In most applications, the temperature T and pressure p are constant, meaning that it is convenient to express the total differential of the enthalpy $H(T, p, N_i)$ like:

$$\mathrm{d}\,H = \left(\frac{\partial H}{\partial T}\right)_{p,N_i} \mathrm{d}\,T + \left(\frac{\partial H}{\partial p}\right)_{T,N_i} \mathrm{d}\,p + \sum_{i=1}^{n} \left(\frac{\partial H}{\partial N_i}\right)_{T,p,N_{j\neq i}} \mathrm{d}\,N_i, \tag{5.1}$$

where N_i is the number of particles of component i and n the number of different species. Only component contributions remain at constant temperature and pressure, leading to the integrated version

$$H = \sum_{i=1}^{n} N_i H_i, \tag{5.2}$$

with $H_i = \left(\frac{\partial H}{\partial N_i}\right)_{T,p,N_{j\neq i}}$ being the partial enthalpy per particle of component i at constant T, p, $N_{j\neq i}$, the partial molar enthalpy is obtained by multiplying H_i with the Avogadro number. In the following, in particular in the Chapter 5.4, we will transform partial enthalpies at constant T, V, $\mu_{j\neq i}$ to constant T, V, $N_{j\neq i}$ finally to constant T, p, $N_{j\neq i}$, μ_j being the chemical potential of component j. We shall use the name "partial enthalpy" for all these properties and reserve the name "partial molar enthalpy" of component i for derivatives of H that refer to T, p and

$N_{j\neq i}$ constant, whatever it is per particle or per mole of particle.
Partial molar enthalpies are normally obtained using numerical derivation of the total enthalpy H with respect to one component [14]. For species that take part in a chemical reaction at equilibrium, such a procedure is not straightforward, as it is difficult, if not impossible, to keep the number of particles of one component constant, while varying the other.

Molecular simulations are helpful in building of reliable databases of thermodynamic data. Several methods have been developed for calculating H_i in systems without chemical reactions. These methods rely on differentiating the total enthalpy H with respect to composition, or particle insertions or identity changes [19,21]. To the best of our knowledge, there are no techniques available to directly obtain partial molar enthalpies of reacting species, or reaction enthalpies.

Most classical molecular dynamics (MD) simulations do not allow for the formation and breaking of chemical bonds. Nevertheless, a few force fields mimic chemical reactions using classical interaction potentials, like ReaxFF [38], REBO [39], and AIREBO [40]. A classical three-body interaction potential [3, 29, 32, 48] was also used to model chemical reactions $2F \rightleftharpoons F_2$ [3, 31] and $2H \rightleftharpoons H_2$ [48]. As the reaction enthalpy is needed to calculate how the equilibrium constant changes with temperature, it would be very useful to compute it from a single simulation.

The aim of this paper is to present a new molecular simulation technique for determining partial molar enthalpies. The method presented in this paper can also be applied to systems with chemical reactions. We will demonstrate our method for binary mixtures of WCA particles [101], as well as for a simple model that mimics a chemical reaction. The method considers small subsystems in a large reservoir (*i.e.* the simulation box), and uses the construction of Hill [50] to compute thermodynamic properties in the thermodynamic limit from small-scale fluctuations. The method largely expands the work on small systems by Schnell *et al.* [22–24,56,102].

The subsystem refers to an open volume (or area element) with a linear size of the order of 1 to 10 molecular diameters, inside a much larger simulation box (a reservoir). We will derive how energy and particle fluctuations inside the subsystem can be used to obtain thermodynamic properties in the grand-canonical ensemble. This ensemble differs from the ensemble specified above (constant T, p, N_j) in which partial molar enthalpies are defined. The total differential of the enthalpy in the grand-canonical ensemble equals

$$\mathrm{d}\,H = \left(\frac{\partial H}{\partial T}\right)_{V,\mu_i} \mathrm{d}\,T + \left(\frac{\partial H}{\partial V}\right)_{T,\mu_i} \mathrm{d}\,V + \sum_{i=1}^{n} \left(\frac{\partial H}{\partial \mu_i}\right)_{T,V,\mu_{j\neq i}} \mathrm{d}\,\mu_i. \tag{5.3}$$

The partial derivatives with respect to chemical potentials of component i, μ_i, are obtained for conditions T and V constant. To find the partial molar enthalpies defined in Eq. (5.1), we need to relate them to the partial derivatives in Eq. (5.3). We will show how Legendre transformations can be used to convert the partial derivatives in Eq. (5.3) to partial molar enthalpies.

This paper is organized as follows: we start by briefly recapitulating the theory of thermodynamics of small systems as derived by Hill [50], *cf.* Section 5.2. In Section 5.3, we discuss the relation of small-scale properties to fluctuating variables. In Section 5.4, we derive expressions for the partial enthalpies of the components in the thermodynamic limit as a function of the temperature T, the volume V, and chemical potentials μ_j. We explain how one can obtain the partial molar enthalpies as function of temperature T, pressure p, and composition of other components, N_j. We proceed by simulating and analyzing binary mixtures of Weeks-Chandler-Anderson (WCA) particles. We use this mixture to document and evaluate the method. We also make a first simulation of a reacting mixture, an isomerisation reaction $A \rightleftharpoons B$. Simulation details are described in Section 5.5 and results are presented and discussed in Section 5.6. Our findings are summarized in Section 5.7.

5.2 Small system properties for controlled variables T, V and μ_j

Hill [50] considered $\mathcal{N}$ replicas of a small system, constructing thereby an ensemble (the total system), which is large enough to follow the laws of classical thermodynamics. The Gibbs equation for this new ensemble equals [50]:

$$\mathrm{d}\, U_t^{\mathrm{GC}} = T\,\mathrm{d}\, S_t^{\mathrm{GC}} - p^{\mathrm{GC}}\mathcal{N}\,\mathrm{d}\, V + \sum_{i=1}^{n} \mu_i\,\mathrm{d}\, N_{i,t}^{\mathrm{GC}} + X^{\mathrm{GC}}\,\mathrm{d}\,\mathcal{N}, \tag{5.4}$$

and the replica energy is defined by

$$X^{\mathrm{GC}}(T,V,\mu_j) = \left(\frac{\partial U_t^{\mathrm{GC}}}{\partial \mathcal{N}}\right)_{S_t,V,N_i} \equiv -\hat{p}(T,V,\mu_j)V. \tag{5.5}$$

The subscript t refers to the total system (the whole ensemble of replicas), the symbol U is used for internal energy, and S for entropy. The superscript GC means grand-canonical and indicates that the variable should be calculated as a function of the controlled variables T, V, μ_j, and $\mathcal{N}$. We need to indicate this explicitly because, for instance, the pressure is different if one controls other variables in a small system. We call X^{GC} the replica energy. The replica energy can be interpreted as the reversible work needed to add one replica of the small system at constant S_t^{GC}, V and $N_{i,t}^{\mathrm{GC}}$. The addition of one replica of the small system at constant S_t^{GC}, V and $N_{i,t}^{\mathrm{GC}}$, implies that S_t^{GC} and $N_{i,t}^{\mathrm{GC}}$ have to be redistributed over one more replica, while the total volume $\mathcal{N}V$ increases. This is the reason to alternatively call this derivative $-\hat{p}V$, see Ref. [50] for a detailed discussion.

By integrating Eq. (5.4) at constant T, V, μ_j and X^{GC} , using linear homogeneity in the number of replicas, we obtain:

$$U_t^{\mathrm{GC}}(T,V,\mu_j,\mathcal{N}) = TS_t^{\mathrm{GC}}(T,V,\mu_j,\mathcal{N}) + \sum_{i=1}^{n} \mu_i N_{i,t}^{\mathrm{GC}}(T,V,\mu_j,\mathcal{N}) - \hat{p}(T,V,\mu_j)V\mathcal{N}. \tag{5.6}$$

Average values of grand-canonical variables in a small system are thus related to the variables of the total system by:

$$\begin{aligned} U_t^{\mathrm{GC}}(T,V,\mu_j,\mathcal{N}) &\equiv \mathcal{N}\overline{U}^{\mathrm{GC}}(T,V,\mu_j), \\ S_t^{\mathrm{GC}}(T,V,\mu_j,\mathcal{N}) &\equiv \mathcal{N}S^{\mathrm{GC}}(T,V,\mu_j), \\ N_{i,t}^{\mathrm{GC}}(T,V,\mu_j,\mathcal{N}) &\equiv \mathcal{N}\overline{N}_i^{\mathrm{GC}}(T,V,\mu_j). \end{aligned} \tag{5.7}$$

We have used a bar to denote an average value of a single replica property. As explained by Hill, the entropy S^{GC} is the same for all replicas and therefore the bar is omitted [50]. By introducing the average variables of the small system into Eq. (5.6), we obtain:

$$\overline{U}^{\mathrm{GC}} = TS^{\mathrm{GC}} + \sum_{i=1}^{n} \mu_i \overline{N}_i^{\mathrm{GC}} - \hat{p}V. \tag{5.8}$$

This equation pinpoints that $\overline{U}^{\mathrm{GC}}$ is not a linear homogeneous function of S^{GC}, V and $\overline{N}_i^{\mathrm{GC}}$, due to the term $\hat{p}$ which depends on the system size. Eq. (5.8) reduces to its well-known classical form if $\hat{p} = p^{\mathrm{GC}}$. The quantity $\hat{p}$, called p-hat by Hill was essentially defined in Eq. (5.5) but has no special name in thermodynamics so far. The system can be considered small when $\hat{p}$ significantly differs from p^{GC} [50]. By substituting Eq. (5.7) into Eq. (5.4) and using Eq. (5.8), we obtain the Gibbs relation for the small system

$$\mathrm{d}\,\overline{U}^{\mathrm{GC}} = T\,\mathrm{d}\,S^{\mathrm{GC}} - p^{\mathrm{GC}}dV + \sum_{i=1}^{n} \mu_i\,\mathrm{d}\,\overline{N}_i^{\mathrm{GC}}. \tag{5.9}$$

The corresponding Gibbs-Duhem-type equation is

$$\mathrm{d}\,(\hat{p}V) = S^{\mathrm{GC}}\,\mathrm{d}\,T + p^{\mathrm{GC}}\,\mathrm{d}\,V + \sum_{i=1}^{n} \overline{N}_i^{\mathrm{GC}}\,\mathrm{d}\,\mu_i. \tag{5.10}$$

We can then obtain expressions for S^{GC}, p^{GC} and $\overline{N}_i^{\mathrm{GC}}$:

$$\begin{aligned} S^{\mathrm{GC}} &= \left(\frac{\partial \hat{p}V}{\partial T}\right)_{V,\mu_j}, \\ p^{\mathrm{GC}} &= \left(\frac{\partial \hat{p}V}{\partial V}\right)_{T,\mu_j} = \hat{p} + V\left(\frac{\partial \hat{p}}{\partial V}\right)_{T,\mu_j}, \\ \overline{N}_i^{\mathrm{GC}} &= \left(\frac{\partial \hat{p}V}{\partial \mu_i}\right)_{T,V,\mu_{j\neq i}}. \end{aligned} \tag{5.11}$$

These equations are special for small systems considered here, as they require partial derivatives of $\hat{p}$. It follows from Eq. (5.11) that p^{GC} and $\hat{p}$ differ when $\hat{p}$ depends on V.

The elements of the so-called matrix of thermodynamic factors [55, 103, 104] are here defined by

$$\frac{1}{\Gamma_{ik}^{\mathrm{GC}}} \equiv \frac{k_{\mathrm{B}}T}{\overline{N}_i^{\mathrm{GC}}} \left(\frac{\partial \overline{N}_i^{\mathrm{GC}}}{\partial \mu_k} \right)_{T,V,\mu_{j\neq k}} = k_{\mathrm{B}}T \left(\frac{\partial \ln \overline{N}_i^{\mathrm{GC}}}{\partial \mu_k} \right)_{T,V,\mu_{j\neq k}}, \tag{5.12}$$

where k_{B} is the Boltzmann constant. These quantities are defined for a small grand-canonical system. To avoid Legendre transformations for small systems, the transformation of the elements $\Gamma_{ik}^{\mathrm{GC}}$ to other control variables (*e.g.* at constant pressure) will only be performed in the thermodynamic limit. Using the Maxwell relations following from Eq. (5.9) we obtain the symmetry relation

$$\Gamma_{ik}^{\mathrm{GC}} \overline{N}_k^{\mathrm{GC}} = \Gamma_{ki}^{\mathrm{GC}} \overline{N}_i^{\mathrm{GC}}. \tag{5.13}$$

The enthalpy $\widehat{H}$ of a small system can now be defined for controlled variables T, V, μ_j by:

$$\widehat{H} \equiv \overline{U}^{\mathrm{GC}} + \hat{p}V. \tag{5.14}$$

It is important to note that $\widehat{H}$ and $\overline{H}^{\mathrm{GC}}$ differ, as the latter is defined by $\overline{H}^{\mathrm{GC}} \equiv \overline{U}^{\mathrm{GC}} + p^{\mathrm{GC}}V$. It turns out that the use of $\widehat{H}$ is more practical, see below.

5.3 Relations to fluctuating variables and system size dependence

As shown in the previous section, in a small grand-canonical system the number of particles and the internal energy fluctuate. For any grand-canonical system, from fluctuation theory it directly follows that [22]

$$\left(\frac{\partial \overline{U}}{\partial \overline{N_i}} \right)_{V,T,\mu_{j\neq i}} = \frac{\overline{UN_i} - \overline{U}\ \overline{N_i}}{\overline{N_i^2} - \overline{N_i}^2}. \tag{5.15}$$

The thermodynamic factors defined in Eq. (5.12) follow in a similar way

$$\frac{1}{\Gamma_{ij}} = \frac{\overline{N_i N_j} - \overline{N_i}\ \overline{N_j}}{\overline{N_i}}. \tag{5.16}$$

For convenience, we have dropped the superscript GC. From the partial derivative of the $\widehat{p}V$ term,

$$\left(\frac{\partial \widehat{p}V}{\partial \mu_i} \right)_{T,V,\mu_{j\neq i}} = \overline{N_i} = \left(\frac{\partial \widehat{p}V}{\partial \overline{N_i}} \right)_{T,V,\mu_{j\neq i}} \left(\frac{\partial \overline{N_i}}{\partial \mu_i} \right)_{T,V,\mu_{j\neq i}}, \tag{5.17}$$

we obtain an expression in terms of averages of fluctuating particle variables:

$$\left(\frac{\partial \widehat{p}V}{\partial \overline{N_i}} \right)_{T,V,\mu_{j\neq i}} = \left(\frac{\partial \mu_i}{\partial \ln \overline{N_i}} \right)_{T,V,\mu_{j\neq i}} = k_{\mathrm{B}}T\Gamma_{ii} = k_{\mathrm{B}}T \frac{\overline{N_i}}{\overline{N_i^2} - \overline{N_i}^2}. \tag{5.18}$$

From $\widehat{H} \equiv \overline{U} + \widehat{p}V$, we find

$$\left(\frac{\partial \widehat{H}}{\partial \overline{N}_i}\right)_{T,V,\mu_{j\neq i}} = \frac{\overline{UN_i} - \overline{U}\ \overline{N_i} + \overline{N_i}\, k_B T}{\overline{N_i^2} - \overline{N_i}^2}. \tag{5.19}$$

This partial enthalpy is obtained for conditions constant V, T, and $\mu_{j\neq i}$. In MD simulations, it can be computed using the "small system method" developed by Schnell and co-workers by calculating energy and particle number fluctuations in randomly positioned subsystems inside the simulation box [22, 23].

At this stage it is important to note that fluctuations inside small subsystems strongly depend on the size of the subsystem. There is a general theorem [105, 106] due to Hadwiger that implies that every extensive thermodynamic variable (*e.g.* X) in a system where the interaction potentials have a finite range has the following form

$$X = A_b V + A_s L^2 + A_e L + A_c. \tag{5.20}$$

where $V \equiv L^3$ equals the system size (assuming 3D systems). This means that X has contributions proportional to the volume (A_b), the surface area (A_s), the linear diameter (A_e), and a constant (A_c). There are no other contributions. The term proportional to the linear diameter is due to the edges for polyhedra and to the Tolman length for curved surfaces (or a combination of the two). The term proportional to a constant is due to the corners for polyhedra and to the rigidities for curved surfaces (or a combination of the two). In terms of the density of X one has

$$\frac{X}{V} = A_b + A_s L^{-1} + A_e L^{-2} + A_c L^{-3}. \tag{5.21}$$

It should be noted that there is some dispute about the validity of Hadwiger's theorem, see the paper by Blokhuis [107]. This dispute does not affect the validity of Eq. (5.21).

In MD simulations, interaction potentials have a finite range so that the theorem applies. Our previous MD simulations of small systems [22–24, 56, 102] confirm this behavior. In practice, extrapolation to $1/L \to 0$ can easily be performed as the scaling in $1/L$ is usually leading. This enables us to obtain the thermodynamic limit value of property $X/V = A_b$ [22–24, 102]. More specifically, for the enthalpy we can write

$$\lim_{1/L\to 0} (\partial \widehat{H}/\partial N_i)_{T,V,\mu_{j\neq i}} = (\partial H/\partial N_i)_{T,V,\mu_{j\neq i}}. \tag{5.22}$$

As it was found that the required system size is surprisingly small, this approach was of great practical use in applications *e.g.* calculating Fick diffusion coefficients from Maxwell-Stefan diffusivities [54, 55].

The transformation between the partial enthalpy as a function of T, V, $\mu_{j\neq i}$ and the corresponding partial molar enthalpy of Eq. (5.1) as a function of T, p, $N_{j\neq i}$ must be performed in the thermodynamic limit and is discussed in the next Section.

5.4 Transformation between ensembles T, V, μ_j and T, p, N_j

We are interested in $(\partial H/\partial N_i)_{T,P,N_{j\neq i}}$ rather than $(\partial H/\partial N_i)_{T,V,\mu_{j\neq i}}$ for a two-component system in the thermodynamic limit. This transformation can be obtained as follows (see also Refs. [54,108,109]). The total differential of $H(V,T,N_1,N_2)$ equals

$$\mathrm{d}\,H = \left(\frac{\partial H}{\partial T}\right)_{V,N_1,N_2} \mathrm{d}\,T + \left(\frac{\partial H}{\partial V}\right)_{T,N_1,N_2} \mathrm{d}\,V + \left(\frac{\partial H}{\partial N_1}\right)_{T,V,N_2} \mathrm{d}\,N_1 + \left(\frac{\partial H}{\partial N_2}\right)_{T,V,N_1} \mathrm{d}\,N_2, \tag{5.23}$$

and from this we have

$$\left(\frac{\partial H}{\partial N_1}\right)_{T,V,\mu_2} = \left(\frac{\partial H}{\partial N_1}\right)_{T,V,N_2} + \left(\frac{\partial H}{\partial N_2}\right)_{T,V,N_1} \left(\frac{\partial N_2}{\partial N_1}\right)_{T,V,\mu_2}, \tag{5.24}$$

$$\left(\frac{\partial H}{\partial N_2}\right)_{T,V,\mu_1} = \left(\frac{\partial H}{\partial N_1}\right)_{T,V,N_2} \left(\frac{\partial N_1}{\partial N_2}\right)_{T,V,\mu_1} + \left(\frac{\partial H}{\partial N_2}\right)_{T,V,N_1}. \tag{5.25}$$

Using the identity A.20 in Appendix A of Ben-Naim's book [109] leads to

$$\left(\frac{\partial N_2}{\partial N_1}\right)_{T,V,\mu_2} = -\left(\frac{\partial \mu_2}{\partial N_2}\right)^{-1}_{T,V,N_1} \left(\frac{\partial \mu_2}{\partial N_1}\right)_{T,V,N_2} = -\left(\frac{\partial \mu_2}{\partial c_2}\right)^{-1}_{T,V,c_1} \left(\frac{\partial \mu_2}{\partial c_1}\right)_{T,V,c_2}, \tag{5.26}$$

$$\left(\frac{\partial N_1}{\partial N_2}\right)_{T,V,\mu_1} = -\left(\frac{\partial \mu_1}{\partial N_1}\right)^{-1}_{T,V,N_2} \left(\frac{\partial \mu_1}{\partial N_2}\right)_{T,V,N_1} = -\left(\frac{\partial \mu_1}{\partial c_1}\right)^{-1}_{T,V,c_2} \left(\frac{\partial \mu_1}{\partial c_2}\right)_{T,V,c_1}, \tag{5.27}$$

where $c_i \equiv N_i/V$. Following Kirkwood and Buff [108] or more transparently Ben-Naim [109] (Eqs. (4.23) and (4.24)), we have

$$\begin{aligned} B_{ik} &= \frac{k_\mathrm{B}T}{V}\left(\frac{\partial N_i}{\partial \mu_k}\right)_{T,V,\mu_{j\neq k}} = k_\mathrm{B}T\left(\frac{\partial c_i}{\partial \mu_k}\right)_{T,V,\mu_{j\neq k}} \\ &= c_i c_k G_{ik} + c_i\delta_{ik} = \frac{\overline{N_iN_k} - \overline{N_i}\;\overline{N_k}}{V} = B_{ki}, \end{aligned} \tag{5.28}$$

where G_{ik} are the so-called Kirkwood-Buff integrals [56, 102, 108]. The averages, indicated by a bar, are in the grand-canonical ensemble. Furthermore, we have

$$A_{ik} = \beta V\left(\frac{\partial \mu_i}{\partial N_k}\right)_{T,V,N_{j\neq k}} = \beta\left(\frac{\partial \mu_i}{\partial c_k}\right)_{T,V,c_{j\neq k}} = A_{ki}. \tag{5.29}$$

The B and the A matrices are each other's inverse:

$$\sum_j B_{ij}A_{jk} = \delta_{ik}. \tag{5.30}$$

We can now introduce Eq. (5.29) into Eqs. (5.26), (5.27) and obtain

$$\left(\frac{\partial N_2}{\partial N_1}\right)_{T,V,\mu_2} = -\frac{A_{12}}{A_{22}} \quad \text{and} \quad \left(\frac{\partial N_1}{\partial N_2}\right)_{T,V,\mu_1} = -\frac{A_{12}}{A_{11}}. \tag{5.31}$$

Using Eq. (5.31), we can write Eqs. (5.24), (5.25) in the form

$$\left(\frac{\partial H}{\partial N_1}\right)_{T,V,\mu_2} = \left(\frac{\partial H}{\partial N_1}\right)_{T,V,N_2} - \left(\frac{\partial H}{\partial N_2}\right)_{T,V,N_1} \frac{A_{12}}{A_{22}}, \tag{5.32}$$

$$\left(\frac{\partial H}{\partial N_2}\right)_{T,V,\mu_1} = -\left(\frac{\partial H}{\partial N_1}\right)_{T,V,N_2} \frac{A_{12}}{A_{11}} + \left(\frac{\partial H}{\partial N_2}\right)_{T,V,N_1}. \tag{5.33}$$

By inverting this equation, we obtain using Eq. (6.12):

$$\left(\frac{\partial H}{\partial N_1}\right)_{T,V,N_2} = B_{22}\left[A_{22}\left(\frac{\partial H}{\partial N_1}\right)_{T,V,\mu_2} + A_{12}\left(\frac{\partial H}{\partial N_2}\right)_{T,V,\mu_1}\right], \tag{5.34}$$

$$\left(\frac{\partial H}{\partial N_2}\right)_{T,V,N_1} = B_{11}\left[A_{11}\left(\frac{\partial H}{\partial N_2}\right)_{T,V,\mu_1} + A_{12}\left(\frac{\partial H}{\partial N_1}\right)_{T,V,\mu_2}\right]. \tag{5.35}$$

The above equations provide explicit expressions for $(\partial H/\partial N_1)_{T,V,N_2}$ and $(\partial H/\partial N_2)_{T,V,N_1}$.

In the following, we use the partial molar volume (Eq. (4.30) of Ben-Naim [109]) that can be calculated from fluctuations in the grand-canonical ensemble or from the Kirkwood-Buff coefficients (see Eq. (17) of Ref. [108])

$$V_i = \left(\frac{\partial V}{\partial N_i}\right)_{T,P,N_{j\neq i}} = \left(\frac{\partial \mu_i}{\partial P}\right)_{T,N_j}. \tag{5.36}$$

Using Eq. (5.23), we can write

$$\left(\frac{\partial H}{\partial N_i}\right)_{T,P,N_{j\neq i}} = \left(\frac{\partial H}{\partial N_i}\right)_{T,V,N_{j\neq i}} + \left(\frac{\partial H}{\partial V}\right)_{T,N_j} V_i. \tag{5.37}$$

We use the extensive property of the total enthalpy from Eq. (5.23):

$$H = N_1\left(\frac{\partial H}{\partial N_1}\right)_{T,V,N_2} + N_2\left(\frac{\partial H}{\partial N_2}\right)_{T,V,N_1} + V\left(\frac{\partial H}{\partial V}\right)_{T,N_1,N_2}. \tag{5.38}$$

It follows that:

$$\left(\frac{\partial H}{\partial V}\right)_{T,N_1,N_2} = \frac{H}{V} - \frac{N_1}{V}\left(\frac{\partial H}{\partial N_1}\right)_{T,V,N_2} - \frac{N_2}{V}\left(\frac{\partial H}{\partial N_2}\right)_{T,V,N_1}. \tag{5.39}$$

By introducing Eq. (5.37) we finally obtain the required transformation

$$V\left(\frac{\partial H}{\partial N_1}\right)_{T,P,N_2} = V_1 H + N_2\left[V_2\left(\frac{\partial H}{\partial N_1}\right)_{T,V,N_2} - V_1\left(\frac{\partial H}{\partial N_2}\right)_{T,V,N_1}\right], \tag{5.40}$$

$$V\left(\frac{\partial H}{\partial N_2}\right)_{T,P,N_1} = V_2 H + N_1\left[V_1\left(\frac{\partial H}{\partial N_2}\right)_{T,V,N_1} - V_2\left(\frac{\partial H}{\partial N_1}\right)_{T,V,N_2}\right]. \tag{5.41}$$

One can easily verify that Eqs. (5.40) and (5.41) agree with

$$H = N_1 \left(\frac{\partial H}{\partial N_1} \right)_{T,p,N_2} + N_2 \left(\frac{\partial H}{\partial N_2} \right)_{T,p,N_1} = N_1 H_1 + N_2 H_2. \tag{5.42}$$

The partial molar enthalpy can be calculated from Eqs. (5.19), (5.40), and (5.41) when we know sets of corresponding values of H, V, V_1, V_2, N_1, N_2.

5.5 Simulations

Series of MD simulations were performed to validate the small system method for the calculation of partial enthalpies and partial molar enthalpies. The method was also applied to a model system for a chemical reaction and the reaction enthalpy was computed. For binary systems of interacting particles we compared the following methods to compute partial molar enthalpies ((a),(b),(c)):

(a) The small system method as outlined above, using Eqs. (5.34) and (5.35), followed by Eqs. (5.40) and (5.41) to transform between different ensembles. In the remainder of the paper this method is denoted by the abbreviation SSM.

(b) The particle insertion method of Frenkel and co-workers [19, 21], the so-called *difference method*, in the isobaric-isothermal ensemble (denoted by DM).

(c) Numerical differentiation of the enthalpy as function of composition for constant pressure and temperature systems (denoted by ND).

Partial enthalpies in the canonical (i) and grand-canonical (ii) ensembles were determined to verify the validity of SSM and transformation of enthalpy from the grand-canonical ensemble to the canonical ensemble. This was done using two different methods:

(i) A direct evaluation of $(\partial H/\partial N_i)_{T,V,N_{j\neq i}}$ by simulating systems in the canonical ensemble with different particle numbers N_i at constant volume.

(ii) A direct evaluation of the rhs. of Eq. (5.19) by simulating systems in the grand-canonical ensemble.

The partial molar volume, see Eq. 5.36, needed for the transformation between ensembles has been calculated using the SSM method but can alternatively be computed using methods (b) or (c).

5.5.1 Binary mixture simulations

Simulations were performed for a binary mixture of particles interacting with the WCA interaction potential. The WCA interaction potential is a shifted Lennard-Jones (LJ) potential with the attractive tail cut-off [20,28,101]. For all simulations,

we have used reduced units in with the mass m of particle is used as unit of mass, the LJ size parameter σ (essentially the particle diameter) is used as unit of length, and the LJ energy parameter ϵ is used as unit of energy [20]. In the remainder of the text and in the figures and tables, reduced units will be used. For convenience, the σ parameter was set to 1 for both component 1 and 2. The interaction distance of the WCA-particles thus equals $2^{1/6}$. The energy parameters were set to $\epsilon_{11} = 1.0$, $\epsilon_{22} = 5.0$, and $\epsilon_{12} = \epsilon_{21} = 0.1$ for 1–1, 2–2, and 1–2 interactions, respectively.

The total number of particles in the simulation box was 480 in the isothermal-isobaric ensemble (method (b), DM); 40,000 particles in the NVT ensemble (method (a), SSM). The composition was varied from pure component 1 to pure component 2. The temperature of the system was fixed at 2.0 for all simulations in this work. Simulations in the isothermal-isobaric ensemble were performed at a pressure of 6.5 in reduced units. For the NVT simulations, the size of the simulation box were adjusted to have the same pressure (6.5 in reduced units) and density as in the isothermal-isobaric ensemble. The isothermal-isobaric simulations were run with five independent simulations for each composition. Each simulation consisted of 10 million cycles, where one cycle involves an attempt to modify the system 480 times (equal to the number of particles in the system). The first 100,000 cycles in each simulation were used to equilibrate the systems, and not for the analysis. The simulations in the NVT ensemble were run for 1 million time steps, whereof the first 100,000 time steps were taken for equilibration.

The small system procedure (a) was performed by embedding small systems in a simulation box of 40,000 particles in the NVT ensemble. Fluctuations in energy and density inside the small system were then sampled [22]. The small systems are spherical with a diameter ranging from the size of a particle $R = 1$ to half the size of the simulation box. Increments in the sphere diameter were made to be linear in the reciprocal sphere diameter $1/R$. In addition, Kirkwood-Buff integrals, G_{ik}, see Eq. (5.28), were calculated for different spherical volumes of radius R using the finite-size-method presented by Krüger *et al.* [102]:

$$G_{ik}^{R} = \int_0^{2R} \left[g_{ik}(r) - 1\right] w(r,x) dr, \tag{5.43}$$

$$w(r,x) = 4\pi r^2 \left(1 - 3x/2 + x^3/2\right), \tag{5.44}$$

where g_{ik} are the pair correlation functions (PCFs) and $x = r/2R$. It is important that the finite-size effects of the Kirkwood-Buff integrals are accounted for, see Ref. [102].

The small system method provides the thermodynamic limit of the partial enthalpies $(\partial H/\partial N_1)_{T,V,\mu_2}$ and $(\partial H/\partial N_2)_{T,V,\mu_1}$. As explained in the previous Section, conversion to partial molar enthalpies can be performed using Eqs. (5.34) and (5.35) then Eqs. (5.40) and (5.41).

Monte Carlo simulations with methods (b, DM) and (c, ND) were performed in the isobaric-isothermal ensemble [20]. The pressure was kept constant at 6.5 in reduced units. In method (b) the difference in partial molar enthalpies between

the components was calculated from [19, 21]

$$\begin{aligned}\Delta H &= H_1 - H_2, \\ &= \frac{\langle \left[\Delta U^{1+2-} + U + pV\right] \exp\left[-\beta \Delta U^{1+2-}\right]\rangle}{\langle \exp\left[-\beta \Delta U^{1+2-}\right]\rangle_{N_1,N_2}} - \langle U + pV\rangle, \\ &= -\frac{\langle \left[\Delta U^{2+1-} + U + PV\right] \exp\left[-\beta \Delta U^{2+1-}\right]\rangle}{\langle \exp\left[-\beta \Delta U^{2+1-}\right]\rangle_{N_1,N_2}} + \langle U + pV\rangle,\end{aligned} \tag{5.45}$$

in which the brackets $\langle \cdots \rangle$ denote averages in the isothermal-isobaric ensemble and ΔU^{i+j-} is the change in internal energy when a random particle of type j is transformed into a particle of type i.

The partial molar enthalpies follow directly from the total enthalpy of the system:

$$H_1 = \frac{H}{N} + (1 - x_1)\Delta H, \tag{5.46}$$

$$H_2 = \frac{H}{N} - x_1 \Delta H, \tag{5.47}$$

In method (c, ND), partial molar enthalpies were determined by numerical differentiation of the total enthalpy according to [14]

$$\left(\frac{\partial H}{\partial N_1}\right)_{T,P,N_2} = \frac{H}{N} + (1 - x_1)\left(\frac{\partial \left(\frac{H}{N}\right)}{\partial x_1}\right)_{T,P} \tag{5.48}$$

$$\left(\frac{\partial H}{\partial N_2}\right)_{T,P,N_1} = \frac{H}{N} - x_1\left(\frac{\partial \left(\frac{H}{N}\right)}{\partial x_1}\right)_{T,P}, \tag{5.49}$$

where the molar enthalpy, H/N, of the system can be fitted with a polynomial in terms of powers of x_1.

To evaluate the small system method further (method (a)), the partial enthalpies at constant volumes, $(\partial H/\partial N_1)_{T,V,N_2}$ and $(\partial H/\partial N_2)_{T,V,N_1}$ were also calculated using method (i). To test the system size effect on the results using the method (i), a total of 200 and 500 particles were simulated at the same thermodynamic states as for the other simulations. By adding two to five particles of type 1 or type 2 (to create altogether 8 new compositions), the enthalpy was found as a function of particle numbers added while keeping the volume and temperature constant. The values of $(\partial H/\partial N_i)_{T,V,N_{j\neq i}}$ were estimated by taking the limit of $\Delta N_i \to 0$.

Simulations in the grand-canonical ensemble were used to verify the extrapolation of the partial enthalpies extrapolated to the thermodynamic limit using the small system method. The fluctuations in energy and density (see Eq. (5.19)) were sampled directly. The density and composition were set close to the density and composition from the canonical simulations, by changing the chemical potential of the two components. The box used had sides of length 15 in reduced units, and for each composition the system were simulated for 1.5 million cycles.

5.5.2 Reaction enthalpies

As our new method (a) to compute partial molar enthalpies only requires local density and energy fluctuations inside small subsystems, the method is not hindered by the presence of chemical reactions between the components in the mixture. To test this, we considered the following reaction in the binary system A, B:

$$\mathrm{A} \rightleftharpoons \mathrm{B} \tag{5.50}$$

The enthalpy of reaction then follows from the difference in partial molar enthalpies

$$\Delta_r H = H_\mathrm{B} - H_\mathrm{A}. \tag{5.51}$$

Different approaches to the molecular-level modeling of chemical reaction equilibrium exist [110]. The equilibrium reaction of Eq. (5.50) can be modeled in an MD simulation by considering a reactive force field that gives rise to a system of monomers and dimers of WCA particles. The two atoms of the dimer interact with a double-well spring that has two well-defined minima, corresponding to state A and B. The reaction can be thought of as a transition between the two minima in a double-well potential. Here, we used the following double-well spring potential between the two atoms of a dimer [111]:

$$u(r) = h\left[1 - \frac{(r - w - r_\mathrm{WCA})^2}{w^2}\right]^2 + \frac{h_{min,2}}{2w}\,(r - r_\mathrm{WCA}) \tag{5.52}$$

where $u(r)$ is the interaction energy between the two atoms of the dimer which are at distance r, h is the height of the potential energy barrier when $h_{min,2}$ is zero, r_WCA is the cut-off distance of the WCA potential ($2^{1/6}$ in reduced units), and the constant w was set to 0.25 in reduced units. $h_{min,2}$ is the energy minimum for the second well. The maximum of $u(r)$ was used to distinguish between states A and B. In Fig. 5.1, the double-well spring potential is illustrated. All simulations with this interaction potential were performed in a box with 2800 and 1850 pairs, in boxes of size 20.0 and 17.42 in reduced units. The temperature were kept to 2 in reduced units for all simulations. The small systems method was applied to the largest box, while the smaller box was used as a reference to improve the calculation of the KB integrals, see Krüger et al. for more details [102].

5.6 Results and Discussion

5.6.1 Results for binary WCA systems

We discuss first the intermediate results from the small system method (method (a)), see Figs. 5.2–5.4, before the main results are presented in Fig. 5.5. All computed data were obtained with statistical uncertainties lower than 5%.

The first step in the small system method provides values for $(\partial H/\partial N_i)_{T,V,\mu_j}$. The thermodynamic limit is obtained from linear extrapolation of the quantity calculated from Eq. (5.19) in small systems, see Fig. 5.2. As $1/\Gamma_{ij}$, scales linearly with $1/L$ [22], we calculated $(\partial N_i/\partial H)_{T,V,\mu_j}$, and inverted its value in the thermodynamic limit. The results are plotted as a function of the composition in Fig. 5.3, and compared to the simulation results directly obtained in the grand-canonical ensemble. Clearly, the SSM (method (a)) yield results that are identical to grand-canonical simulations.

Fig. 5.4 shows the values of $(\partial H/\partial N_i)_{T,V,N_j}$ for $i = 1, 2$, calculated from Eqs. (5.34) and (5.35), where the values of $(\partial H/\partial N_i)_{T,V,\mu_j}$ were taken from Fig. 5.3, and A_{ij} and B_{ij} were calculated from the Kirkwood-Buff integrals. In addition, the values of $(\partial H/\partial N_i)_{T,V,N_j}$ were calculated directly from simulations in the canonical ensemble following method (i). The systems with 200 and 500 particles resulted in nearly identical results indicating that no significant size effect was found varying the system size in method (i).

The partial molar enthalpies, $(\partial H/\partial N_i)_{T,p,N_j} = H_i$, as a function of composition are shown in Fig. 5.5. The results of the different methods described in the Simulation section are plotted, namely results from (a) the small system method, (b) the difference method (DM), and (c) the numerical differentiation (ND) method. Methods (a) and (c) provide, within the accuracy of a few percent, the same values. The difference method (b) deviate strongly from the two other methods. This is expected, as the difference method often suffers from poor sampling. This is a well-known disadvantage of this method [19] and strongly depends on differences in size and interaction strength of the components. For the simulated binary systems the methods (a) and (c) were both very efficient numerically, the method (c), because smaller systems can potentially be used, could be more advantageous, however increasing the number of components the method (a) becomes more efficient compared to method (c).

As a general comment to this part it is important to underline that H_i is the full partial molar enthalpy of the simulated components, it contains both ideal and excess or residual terms which values depend on the chosen molecular model. In order to compare with other molecular models, the variation of the different ground state energies of the different models should be taken into account, the comparison with experimental results is more tricky and is out of the scope of this manuscript. In practice (both for simulations and experiments), we compare the difference of the H_i values between the studied system and an "equivalent" known reference state. Because H_i is a mixture property, it is common in thermodynamics to give excess partial molar enthalpies, i.e. to use the pure components under the same pressure and temperature as the reference state. From a molecular simulation point of view it implies to compute pure components separately. Despite this restriction, the knowledge of H_i is particularly useful to quantify directly the heat effects during chemical or physical transformation as we will see in the following for chemical reactions.

5.6.2 Results for the reaction enthalpy

Just as for the SSM, method (b) requires one single simulation to compute partial molar enthalpies. This is a clear advantage over method (c), which needs three or more simulations in order to determine the enthalpy as a function of composition. A drawback of method (b), mentioned already, is however the fact that the method is unsuitable for particles which vary largely in size. Already for a system with WCA particles, this becomes evident. The small system method (a) can be used to obtain partial molar enthalpies in a single simulation too. In the following, we will apply the SSM to a reactive force field model for the reaction A $\rightleftharpoons$ B.

By keeping the parameters h and w in Eq. (5.52) constant, and by varying the parameter $h_{min,2}$, the effect of a difference in energy between the wells of the dumbbells was obtained. Based on Van't Hoff equation and using the property that the number of A or B molecules are proportional to their potential energy, the mole fraction of A and B can be written, in first approximation, as a function of the potential energy $h_{min,2}$:

$$x_A = \frac{1}{1 + J \exp\left(-\frac{h_{min,2}}{k_B T}\right)}, \tag{5.53}$$

$$x_B = \frac{1}{1 + \left[J \exp\left(-\frac{h_{min,2}}{k_B T}\right)\right]^{-1}}, \tag{5.54}$$

where J is a constant which can be fitted to equilibrium results at a single temperature.

In Table 5.1, we present simulation results for the equilibrium mole fraction of components A, the threshold value (the maximum of the function $u(r)$), and the reaction enthalpy ($\Delta_r h$). The results of x_A calculated with Eq. (5.54) are in excellent agreement with the values of the simulation under equilibrium chemical conditions.

In Fig. 5.6, the computed reaction enthalpy, using our new method (a), is plotted as a function of the energy difference between the two wells in the dumbbell-potential, $h_{min,2}$. It is worth to note that $\Delta_r S = \Delta_r H/T$ because the system obeys chemical equilibrium. As expected for this simple system, the reaction enthalpy is linearly proportional to the energy difference between components A and B, $h_{min,2}$, $\Delta_r H = 0.703 + 0.912 h_{min,2}$, the slope constant, 0.912, being close to one. As can be seen from Table 5.1, the composition of the system changes significantly with the value of $h_{min,2}$ following Eq. (5.54).

5.7 Conclusions

We have presented a computational method for calculation of partial molar enthalpies and reaction enthalpies for systems of interacting particles. The method requires simulations in the canonical ensemble or alternatively in the microcanonical or grand-canonical ensemble, and the sampling of energy and particle fluctuations inside small sub-systems. Using Kirkwood-Buff integrals, partial enthalpies in the grand-canonical ensemble can be converted into partial enthalpies in the canonical ensemble, as well as partial molar enthalpies in isobaric-isothermal ensemble.

The results of our method lead to the same results as obtained by differentiation of the enthalpy with respect to the composition. It can in addition be used to determine partial molar enthalpies directly from a single canonical simulation.

The small system method has the significant advantage above the other methods in its ability to handle the electroneutrality condition for ionic systems [56]. We have shown that the method can also be conveniently used to calculate reaction enthalpies in the context of a reactive force field model from a single MD simulation.

Acknowledgments

Computational resources were supported by NWO Exacte Wetenschappen (Physical Sciences) for the use of supercomputer facilities, with financial support from the Nederlandse Organisatie voor Wetenschappelijk Onderzoek (Netherlands Organization for Scientific Research, NWO). SK, SKS, and TJHV acknowledge financial support through NWO-CW, through an ECHO grant. RS and SK acknowledge the Storforsk grant no. 167336 from the Norwegian Research Council and the Department of Chemistry at the Norwegian University of Science and Technology for financing the PhD of RS. SKS also acknowledges financial support from the Research Council of Norway through a Post-Doc. Fellowship, grant no. 230534.

System	$h_{min,2}$	x_A	Threshold	$\Delta_r h$	x_A Eq. (5.54)
1	0.0	0.518	1.372	0.695	0.518
2	0.75	0.611	1.388	1.378	0.610
3	1.0	0.640	1.393	1.589	0.639
4	1.5	0.697	1.404	2.102	0.695
5	2.0	0.749	1.415	2.546	0.745
6	2.5	0.795	1.427	3.103	0.790

Table 5.1: Values of the computed mole fraction of species A, the maximum of $u(r)$ (the threshold to distinguish between A and B), and the computed molar reaction enthalpy for the model reaction $A \rightleftharpoons B$ as a function of $h_{min,2}$. In this table the last column was calculated from Eq. (5.54) and calculating the constant J from the first system. The temperature is 2.0 in reduced units.

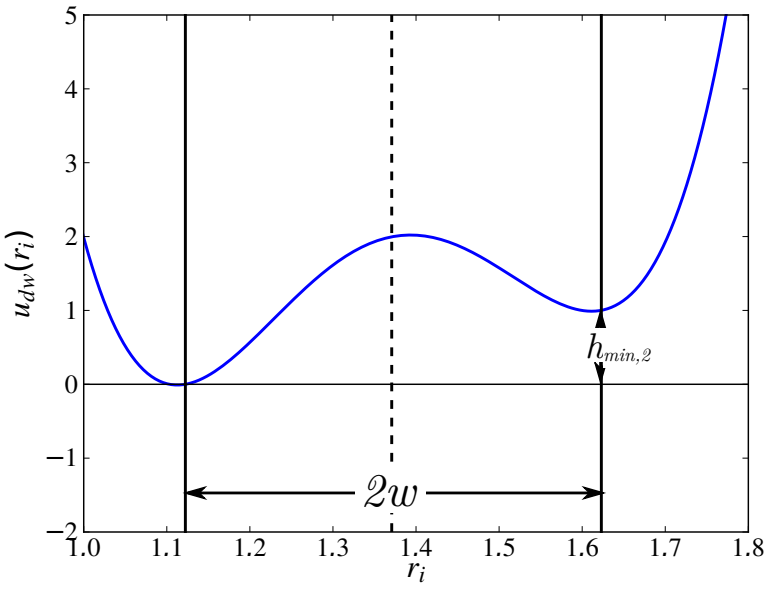

Figure 5.1: Double-well spring potential (Eq. (5.52)) used for the model reaction $A \rightleftharpoons B$. The distance between the potential wells is $2w$, and $h_{min,2}$ is the height of the second well. The height of the barrier between the two wells changes with $h_{min,2}$.

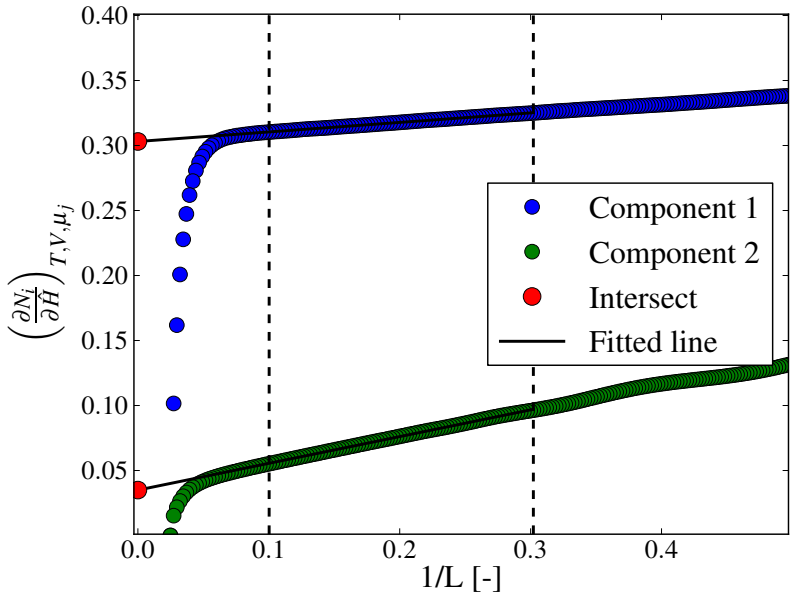

Figure 5.2: $\left(\partial N_i/\partial \hat{H}\right)_{T,V,\mu_j}$ as a function of the small system size $1/L$ for $x_1 = 0.2$. In agreement with Eq. (5.21), the trend is linear until it deviates for small $1/L$ when the small system size is close to the simulation box size. The thermodynamic limit was obtained from a linear extrapolation (black lines and red points) between the two dashed lines.

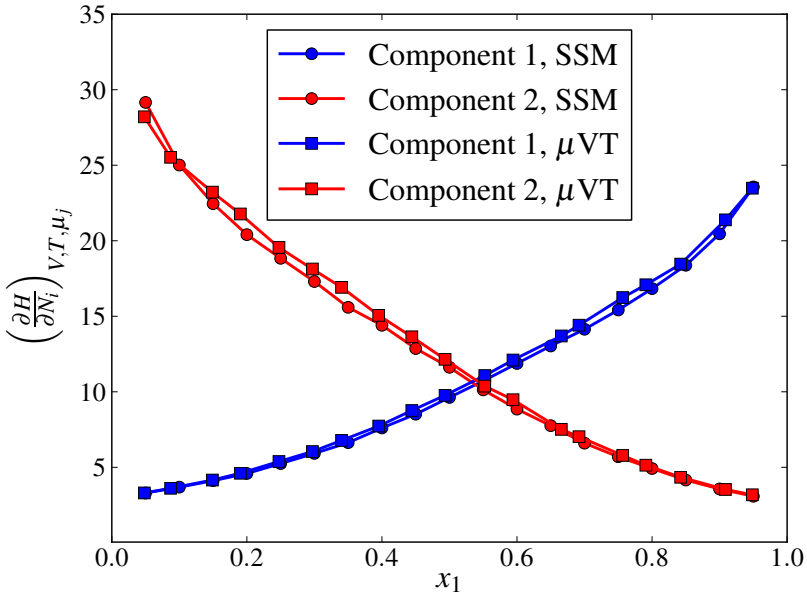

Figure 5.3: Partial enthalpies in the grand-canonical ensemble. Data was sampled for small systems embedded in a larger simulation box, maintained in the canonical ensemble. These values were extrapolated to the thermodynamic limit (see also Fig. 5.2). For comparison, partial enthalpies were computed directly in grand-canonical simulations. The chemical potential was adjusted to approximate the density and composition used in the canonical ensemble. Clearly both approaches yield identical results.

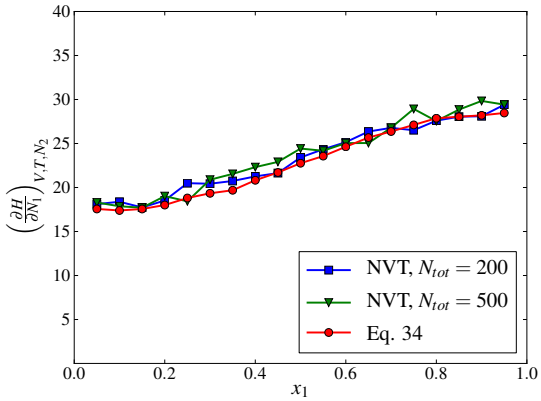

(a)

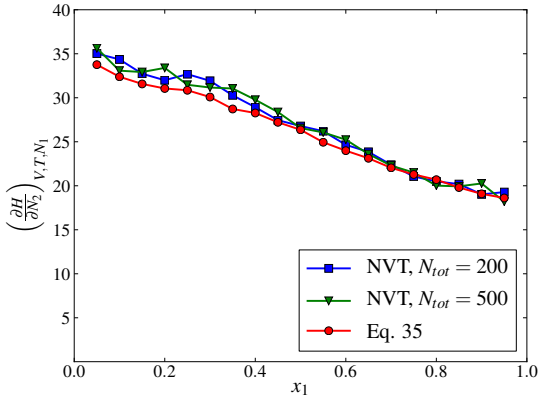

(b)

Figure 5.4: Partial enthalpies in the NVT ensemble. A series of NVT simulations with different particle numbers were carried out (method (i)). The red line is obtained by converting the molar enthalpies from Fig. 5.3, using the Kirkwood-Buff coefficients needed to calculate **A** and **B**.

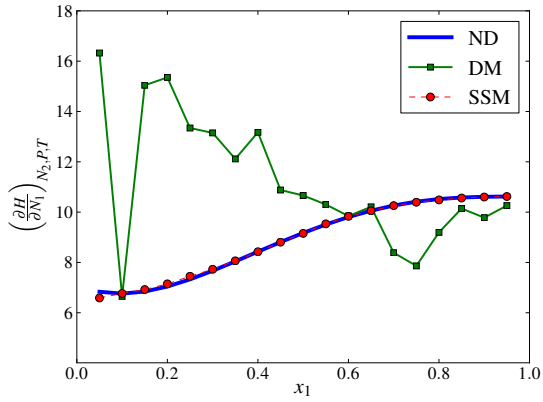

(a)

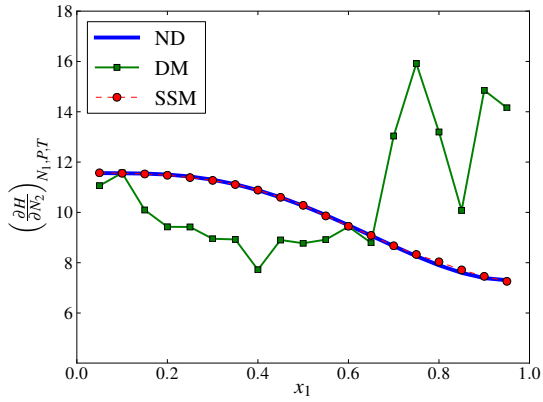

(b)

Figure 5.5: The partial molar enthalpies of component 1 and component 2, calculated using numerical differentiation (ND), the difference method (DM), and the small system method (a), SSM. The results from the difference method is however not in agreement with the two other methods. This is caused by the poor sampling when changing the identity of particles.

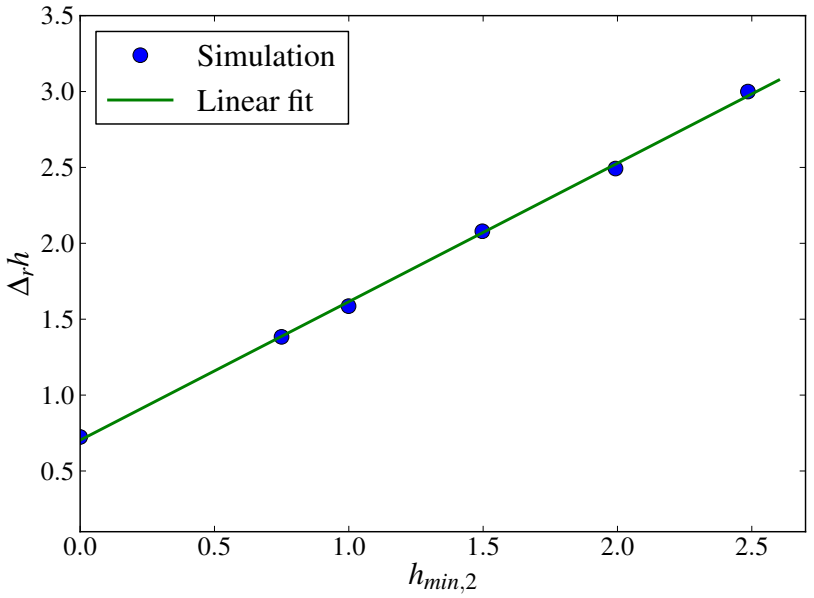

Figure 5.6: Partial molar reaction enthalpies as a function of the difference in energy between the two minima. The slope of the fitted curve is 0.912.

Chapter 6

The reaction enthalpy of hydrogen dissociation calculated with the Small System Method from simulation of molecular fluctuations

Ragnhild Skorpa[1], Jean-Marc Simon[2], Dick Bedeaux[1] and Signe Kjelstrup[1,3]

1. Department of Chemistry,
Norwegian University of Science and Technology,
NO-7491 Trondheim, Norway

2. Laboratorie Interdisciplinaire Carnot de Bourgogne,
UMR, CNRS-Université de Bourgogne, Dijon, France.

3. Process & Energy Laboratory, Delft University of Technology,
Leeghwaterstraat 39, 2628CB Delft, The Netherlands

This chapter was published in *PCCP* (2014) 16:19681–19693

Abstract

We show how we can find the enthalpy of a chemical reaction under non-ideal conditions using the Small System Method to sample molecular dynamics simulation data on fluctuating variables. This method, created with Hill's thermodynamic analysis, is used to find properties in the thermodynamic limit, such as thermodynamic correction factors, partial enthalpies, volumes, heat capacities and compressibility. The values in the thermodynamic limit at (T, V, μ_j), are then easily transformed to other ensembles, (T, V, N_j) and (T, P, N_j), where the last ensemble gives the partial molar properties which are of interest to chemists. The dissociation of hydrogen from molecule to atoms was used as a convenient model system. Molecular dynamics simulations were preformed with three densities; $\rho = 0.0052$ g cm^{-3} (gas), $\rho = 0.0191$ g cm^{-3} (compressed gas) and $\rho = 0.0695$ g cm^{-3} (liquid), and temperatures in the range; $T = 3640 - 20800$ K. The enthalpy of the reaction was observed to follow a quadratic trend as a function of temperature for all densities. The enthalpy of reaction was observed to only have a small pressure dependence. With a reference point close to an ideal stateÂ ($T = 3640$ K and $\rho = 0.0052$ g cm^{-3}), we where able to calculate the thermodynamic equilibrium constant, and thus the distance from ideal conditions for the lowest density. We found the thermodynamic equilibrium constant to increase with increasing temperature, and with a negligible pressure dependence. Taking the enthalpy variation into account in the calculation of the thermodynamic equilibrium constant, we found the ratio of activity coefficients to be in the order of 0.7–1.0 for the lowest density, indicating repulsive forces between H and H_2. The study shows that the compressed gas- and liquid density at higher temperatures are far from ideal conditions. It is important to have a method that can give access to partial molar properties, independent of the ideality of the reacting mixture. Our results shows how this can be achieved with the use of the Small System Method.

6.1 Introduction

It is cumbersome to obtain reliable values for enthalpies, in the laboratory as well as by computations [13]. Thanks to progress with a new molecular simulation method, the so-called Small System Method for prediction of thermodynamic data [22–24], one can now find precise values for partial molar enthalpies is a single simulation, from systematic studies of fluctuations in a small volume element [25]. The Small System Method uses ideas first described by Hill [50], and the small system is embedded in a reservoir to examine the fluctuations in a small part under controlled conditions.

Molecular dynamics simulation have over the years been important for studies of partial molar properties, such as enthalpy and volume as they determine the equilibrium properties of a multicomponent system. Kirkwood and Buff established

already in 1951, a first fluctuation-based method for calculation of partial molar properties from pair correlation functions [108]. Sindzingre et al. calculated the partial molar enthalpy and -volume in terms of time averages [19, 112]. Shing and Chung [113] calculated the partial molar volume and internal energy for an infinitely dilute system in 1988, and found them to be strongly dependent on the isothermal compressibility. Debendetti used a fluctuation-based method to determine partial molar volumes, energies and enthalpies [114–116]. Most of these methods do not give the connection between the thermodynamic limit values for several ensembles, however, and the Small System Method may therefore offer an advantage.

Liu et al. have successfully used the method to find matrices of thermodynamic factors, needed to relate Fick's diffusion coefficients to Maxwell-Stefan diffusivities [54, 55]. The method was also used to find Kirkwood-Buff integrals, which are central for determination of thermodynamic properties in general (see e.g. Ben Naim, [109]). Kirkwood-Buff integrals for closed systems are unable to deal with linearly dependent variables [25], while this restriction is lifted in the Small System Method, where the sampling takes place in a small, but open system. This is a great advantage of the Small System Method [56], and it is therefore thought to be particularly well suited for chemical reactions, as demonstrated by us for a toy reaction studied in [25]. This has given us the motivation to apply the method to a more realistic reaction.

The aim of this work is to determine the reaction enthalpy and related thermodynamic properties for a more realistic reaction, namely the hydrogen dissociation reaction. In earlier work [48] we established that the system of atoms and molecules could be well modeled if the temperature was not too low (above 156 K). Using the dissociation constant based on mole fractions, K_x, and the van't Hoff equation, we found an enthalpy of reaction equal to 430 kJ/mol in a dense fluid of the reacting mixture. We shall now find the reaction enthalpy from a direct calculation of partial molar enthalpies and compare with that value.

The present work can be seen as an extension of the work by Xu and coworkers on chemical reactions [26, 31], but also of the Small System Method by Schnell et al. [22–24]. We shall present results for the compressibility, partial molar volumes, thermodynamic correction factors, and partial molar enthalpies of components of the hydrogen dissociation reaction. From this we find the reaction enthalpy and the true thermodynamic equilibrium constant. A classical description of the hydrogen dissociation reaction has been established [48], producing a convenient basis for the work. The hydrogen dissociation reaction is interesting e.g. in the physics of plasma modeling [88, 117, 118]. In the chemical world it is relevant for separation of hydrogen gas from a gas mixture (e.g. from the water gas shift reaction) using a palladium membrane [11, 64, 72]. At the surface of this membrane, molecular hydrogen dissociates and atomic hydrogen diffuses through the membrane and is recombined to molecular hydrogen at the opposite surface [11, 68, 72].

The paper is structured as follows. In Section 6.2 we give a short recapitulation of the Small System Method. A description of the interaction potential and the

simulation- and calculation procedures follow. Section 6.3 gives results, and finally we give conclusions in Section 6.4.

6.2 Methods

6.2.1 The Small System Method

The Small System Method is used here to give access to partial enthalpies in the thermodynamic limit for a binary system, but the method can also be generalized. The enthalpies were first calculated for small systems at constant (T, V, μ_j). After going to the thermodynamic limit, the Small System Method, by Schnell et al. [25] gives the procedure to transform the variables to other ensembles. The expressions for these transformations between sets of partial enthalpies for two components i and j from (T, V, μ_j) to (T, V, N_j) is given in Eqs. (6.1) and (6.2)

$$\left(\frac{\partial H}{\partial N_i}\right)_{T,V,N_{j\neq i}} = B_{jj}\left[A_{jj}\left(\frac{\partial H}{\partial N_i}\right)_{T,V,\mu_{j\neq i}} + A_{ij}\left(\frac{\partial H}{\partial N_j}\right)_{T,V,\mu_{i\neq j}}\right] \tag{6.1}$$

$$\left(\frac{\partial H}{\partial N_j}\right)_{T,V,N_{i\neq j}} = B_{ii}\left[A_{ii}\left(\frac{\partial H}{\partial N_j}\right)_{T,V,\mu_{i\neq j}} + A_{ij}\left(\frac{\partial H}{\partial N_i}\right)_{T,V,\mu_{j\neq i}}\right] \tag{6.2}$$

and then to (T, P, N_j)

$$\left(\frac{\partial H}{\partial N_i}\right)_{T,P,N_{j\neq i}} = \frac{V_i H}{V} + \frac{N_j}{V}\left[V_j\left(\frac{\partial H}{\partial N_i}\right)_{T,V,N_{j\neq i}} - V_i\left(\frac{\partial H}{\partial N_j}\right)_{T,V,N_{i\neq j}}\right] \tag{6.3}$$

with the last expression as the present target. In Eqs. (6.1) and (6.2) a summation is performed over all double appearing indices.The expressions requires the thermodynamic limit value of:

- Partial enthalpies at constant T, V, μ
- Thermodynamic correction factors, Γ_{ij} at T, V, μ (see Eq.(6.4))
- Partial molar volumes, V_i at constant T, V, μ
- Matrices A_{ij} and B_{ij} as defined by Kirkwood and Buff [108]

The input quantities are defined and briefly explained in the following subsections for a binary mixture. For further details, see [25].

Partial enthalpies

The partial enthalpy of component i, h_i, at constant T, V, μ_j is determined from following formula for fluctuations of the total energy and density in the small system

[25]

$$h_i(L) = \left(\frac{\partial H}{\partial N_i}\right)_{T,V,\mu_{j\neq i}} = -\frac{\langle UN_i\rangle - \langle U\rangle\langle N_i\rangle + k_BT\langle N_i\rangle}{\langle N_i^2\rangle - \langle N_i\rangle^2} \tag{6.4}$$

Brackets denote time averages. The Small System Method gives the enthalpy as a (predominantly) linear function of the inverse of the radius of the small system used in the sampling of fluctuation [22–24], L. The derivative of H (in the thermodynamic limit) is found by extrapolation.

$$h_i(L) = h_{i,\infty} + \frac{A'_i}{L} + ... \tag{6.5}$$

Here, $h_{i,\infty}$ is the derivative of H at constant (T, V, μ_j) in the thermodynamic limit (needed in Eqs.(6.1) – (6.3)). For a spherical sampling volume, the scaling law only has the linear term, as the non linear terms can be neglected [22].

Thermodynamic correction factor

The thermodynamic correction factor, Γ_{ij}, is defined as

$$\Gamma_{ij}^{-1} = \frac{1}{\beta}\left(\frac{\partial \ln\langle N_i\rangle}{\partial \mu_j}\right)_{T,V,\mu_{k\neq i}} = \frac{1}{\beta\langle N_i\rangle}\left(\frac{\partial\langle N_i\rangle}{\partial \mu_j}\right)_{T,V,\mu_{k\neq i}} \tag{6.6}$$

where $\beta = 1/k_BT$, k_B is Boltzmann's constant, μ is the chemical potential and subscript i or j denote H or H_2. At constant (T, V, μ_j) we determine Γ_{ij} from the fluctuation theory formula derived by Reed and Ehrlich [119].

$$\Gamma_{ij}^{-1}(L) = \frac{\langle N_iN_j\rangle - \langle N_i\rangle\langle N_j\rangle}{\langle N_j\rangle} \tag{6.7}$$

The Small System Method gives the inverse of the thermodynamic correction factor as a (predominantly) linear function of the inverse of L [22–24] for constant (T, V, μ_j):

$$\Gamma_{ij}^{-1}(L) = \Gamma_{ij,\infty}^{-1} + \frac{A_{ij}}{L} + ... \tag{6.8}$$

We use this to obtain $\Gamma_{ij,\infty}^{-1}$ in the thermodynamic limit as a function of T, V, μ_j. In the following sections the values in the thermodynamic limit is used.

Kirkwood-Buff integrals and the matrices A_{ij}, B_{ij}

The integral over the pair correlation function g_{ij} of the particle fluctuations, is called the Kirkwood-Buff integral after the groundbreaking work of Kirkwood and Buff [108]

$$G_{ij} = \int [g_{ij}(r) - 1]dV = V\frac{\langle N_iN_j\rangle - \langle N_i\rangle\langle N_j\rangle}{\langle N_i\rangle\langle N_j\rangle} - \frac{\delta_{ij}}{c_i} = \frac{1}{c_i}\Gamma_{ij}^{-1} - \frac{\delta_{ij}}{c_i} \tag{6.9}$$

where G_{ij} is the Kirkwood-Buff integral at constant T, V, μ_j, δ is the Kroenecker delta, and c_i is the concentration of i ($c_i = N_i/V$). The last equality in Eq.(6.9) was obtained by introducing Eq.(6.7) in the middle equality of Eq (6.9). Note that G_{ij} and $(1/c_i)\Gamma^{-1}_{ij}$ are symmetric. Several properties can be expressed by these integrals, such as partial molar volume and isothermal compressibility. Both the thermodynamic limit value of G_{ij} and $\Gamma^{-1}_{ij,\infty}$ are as a function of (T, V, μ_j).

Following Kirkwood and Buff [108] or more transparently Ben Naim [109] (Eqs. 4.23 and 4.24), we have for the symmetric B_{ij} matrix, at constant (T, V, μ_j)

$$B_{ij} = B_{ji} = \frac{k_{\mathrm{B}}T}{V}\left(\frac{\partial N_j}{\partial \mu_i}\right)_{T,V,\mu_{k\neq i}} = k_{\mathrm{B}}T\left(\frac{\partial c_j}{\partial \mu_i}\right)_{T,V,\mu_{k\neq i}} \tag{6.10}$$
$$= c_i c_j G_{ij} + c_i \delta_{ij} = \frac{1}{V}\left(\langle N_i N_j\rangle - \langle N_i\rangle\ \langle N_j\rangle\right)$$

where G_{ij} always are Kirkwood-Buff integrals which refer to the grand canonical ensemble. Furthermore we define the matrix A_{ij}, at constant T, V, N_j, by

$$A_{ij} = A_{ji} = \beta V\left(\frac{\partial \mu_j}{\partial N_i}\right)_{T,V,N_{k\neq i}} = \beta\left(\frac{\partial \mu_j}{\partial c_i}\right)_{T,V,c_{k\neq i}} \tag{6.11}$$

The A_{ij} and B_{ij} matrices are each other's inverse, so:

$$\sum_j B_{ij}A_{jk} = \delta_{ik} \tag{6.12}$$

These properties can be used to characterize a binary reacting mixture, as we shall see.

Properties from the Kirkwood-Buff integrals

Kirkwood and Buff gave the derivative of the chemical potential of one component with respect to its mole fraction in a binary mixture, at constant T and P

$$\frac{1}{k_B T}\left(\frac{\partial \mu_i}{\partial x_i}\right)_{T,P} = \frac{1}{x_i} + \frac{c_j\left(2G_{ij} - G_{ii} - G_{jj}\right)}{1 + x_i c_j\left(G_{ii} + G_{jj} - 2G_{ij}\right)} \tag{6.13}$$

where x_i is the mole fraction of i ($x_i = N_i/(N_{\mathrm{H}} + N_{\mathrm{H_2}})$; here $N_{\mathrm{H_2}}$ is the number of molecules so that $x_{\mathrm{H}} + x_{\mathrm{H_2}} = 1$). The relation between the thermodynamic correction factor and the activity coefficient, γ_i, was also given in terms of Kirkwood-Buff integrals [23]

$$\left(\frac{\partial \ln \gamma_i}{\partial \ln x_i}\right)_{T,P} = -\frac{x_i c_j (G_{ii} + G_{jj} - 2G_{ij})}{1 + c_j x_i (G_{ii} + G_{jj} - 2G_{ij}} \tag{6.14}$$

The partial molar volume (Eq.(6.15)) and the isothermal compressibility (Eq.(6.16)) for a binary mixture are

$$V_i = \frac{1 + (G_{jj} - G_{ij})c_j}{c_i + c_j + c_i c_j (G_{ii} + G_{jj} - 2G_{ij})} \tag{6.15}$$

and

$$\kappa k_B T = \frac{1 + G_{ii}c_i + G_{jj}c_j + \left(G_{ii}G_{jj} - G_{ij}^2\right) c_i c_j}{c_i + c_j + \left(G_{ii} + G_{jj} - 2G_{ij}\right) c_i c_j} \tag{6.16}$$

Thermodynamic properties of the chemical reaction

The enthalpy of a system is $H = U + PV$, where U is the internal energy, P is the pressure, and V is the volume. The enthalpy at constant T and P can be written as

$$H = \sum_{i=1}^{n} H_i N_i \tag{6.17}$$

where H_i is the partial molar enthalpy of component H or H_2. Thus, the partial molar enthalpy is the derivative of H with respect to the number of either H or H_2, N_i:

$$H_i = \left(\frac{\partial H}{\partial N_i}\right)_{T,P,N_j} \tag{6.18}$$

The enthalpy of a reaction is given by the partial molar enthalpies of the components

$$\Delta_r H = 2H_{\mathrm{H}} - H_{\mathrm{H_2}} \tag{6.19}$$

The equilibrium constant can be calculated from the van't Hoff equation, at constant pressure, if the enthalpy of reaction is known at standard conditions.

$$\left[\frac{\mathrm{d}(\ln K_{th})}{\mathrm{d}(1/T)}\right]_P = -\frac{\Delta_r H^{\ominus}}{R} \tag{6.20}$$

Superscript $^{\ominus}$ denotes the standard state (1 bar). In the presence of a varying pressure, there is an additional term in this equation:

$$\mathrm{d}\ln K_{th} = -\frac{\Delta_r H^{\ominus}}{R}\mathrm{d}\left(\frac{1}{T}\right) - \frac{\Delta_r V^{\ominus}}{RT}\mathrm{d}P \tag{6.21}$$

where the last term gives the pressure dependence, and $\Delta_r V^{\ominus}$ is the reaction volume.

With ideal gas and pure component as standard state at 1 bar pressure, the chemical potential is

$$\mu_i = \mu_i^{\ominus} + RT\ln f_i/P^{\ominus} = \mu^{\ominus} + RT\ln(x_i P\gamma_i)/P^{\ominus} \tag{6.22}$$

The fugacity of the gas component, f_i, is equal to the partial pressure of the gas, which is $x_i P$, times the activity coefficient γ_i. By introducing this into the condition $\Delta G = 0$ for the reaction in question we obtain the equilibrium constant in terms of the dissociation constant, K_x, total pressure, and the activity coefficient ratio:

$$K_{th} = \frac{x_{\mathrm{H}}^2}{x_{\mathrm{H_2}}}\frac{P}{P^{\ominus}}\frac{\gamma_{\mathrm{H}}^2}{\gamma_{\mathrm{H_2}}} = K_x\frac{P}{P^{\ominus}}\frac{\gamma_{\mathrm{H}}^2}{\gamma_{\mathrm{H_2}}} = K_P\frac{\gamma_{\mathrm{H}}^2}{\gamma_{\mathrm{H_2}}} \tag{6.23}$$

where $K_P = K_x P/P^{\ominus}$ is the pressure based dissociation constant. The partial molar heat capacities of the components and the reaction and the isothermal compressibility of the mixture are found from standard expressions:

$$C_P = \left(\frac{\partial H}{\partial T}\right)_P \tag{6.24}$$

$$\kappa_T = -\frac{1}{V}\left[\frac{\partial V}{\partial P}\right]_T \tag{6.25}$$

The ideal value of the heat capacity of the reaction is $3R/2$, when vibrational modes are not excited. For an ideal gas, $\kappa_T = 1/P$.

The temperature T is calculated from the average kinetic energy per degree of freedom of all particles:

$$T = \frac{1}{3k_B N_p}\sum_{i=1}^{N_p} m_i \mathrm{v}_i^2 \tag{6.26}$$

where $\mathrm{v}_i^2 = \mathrm{v}_{x,i}^2 + \mathrm{v}_{y,i}^2 + \mathrm{v}_{z,i}^2$ and $N_p = N_{\mathrm{H}} + 2N_{\mathrm{H}_2}$ is the total number of atoms.

From the virial theorem, the expression for the pressure in the presence of two- and three-particle interactions is:

$$\begin{aligned} P = \frac{k_B T N_p}{V} - \frac{1}{3V}\sum_{i=1}^{N_p}\Bigg[&\frac{1}{2}\sum_{j \text{ pair with } i}\frac{\partial u_2(r_{ij})}{\partial r_{ij}} r_{ij} \\ &+ \sum_{j<k \text{ triplet with } i}\Bigg(\frac{\partial h_{j,i,k}(r_{ji}, r_{ik}, \theta_{j,i,k})}{\partial r_{ji}} r_{ji} \\ &+ \frac{\partial h_{j,i,k}(r_{ji}, r_{ik}, \theta_{j,i,k})}{\partial r_{ik}} r_{ik} + \frac{\partial h_{j,i,k}(r_{ji}, r_{ik}, \theta_{j,i,k})}{\partial r_{jk}} r_{jk}\Bigg)\Bigg] \end{aligned} \tag{6.27}$$

The first term in Eq. (6.27) gives the ideal contribution to the pressure, while the second term gives the contribution from the two- and three particle potentials, respectively. For a discussion regarding the pressure calculations, see [48].

6.2.2 Interaction Potentials

The chemical reaction was modeled accurately with molecular dynamics simulations using anaytical potentials derived from quantum mechanical results, in the same manner as [3,26,29,31]. Stillinger and Weber [3] showed that it was sufficient to use an interaction potential, U, which is the sum of two- and three-particle interaction contributions, to describe the essentials of a chemical reaction:

$$U(\mathbf{r}_1, ..., \mathbf{r}_N) = \sum_{i<j} u_{(2)}(r_{ij}) + \sum_{i<j<k} u_{(3)}(\mathbf{r}_i, \mathbf{r}_j, \mathbf{r}_k) \tag{6.28}$$

here $u_{(2)}$ and $u_{(3)}$ are the two- and three-particle potentials, given in Eqs. (6.29) and (6.30), respectively. Based on the quantum mechanical results of Diedrich and Anderson [46, 47], Kohen et al derived expressions for two- and three-particle potentials [29] for hydrogen.

$$u_{(2)}(r) = \begin{cases} \alpha\left(\beta_2 r^{-p} - 1\right)\exp\left[\frac{\gamma_2}{r-r_c}\right] & \text{if } r < r_c \\ 0 & \text{if } r > r_c \end{cases} \tag{6.29}$$

here $\alpha = 5.59 \cdot 10^{-21}$ kJ, $\beta_2 = 0.044067$ Å^p, $\gamma_2 = 3.902767$ Å, $r_c = 2.8$ Å and $p = 4$ are constants [29]. α is chosen such that the minimum of the potential gives the binding energy of hydrogen (432.065 kJ mol^{-1}) [29] at the bond distance between two hydrogen atoms, $r_e = 0.74$ Å [47]. When the distance between two atoms is larger than the cut-off distance, $r \geq r_c$, the potential is zero. Reduced units, based on the pair potential, are used throughout the paper. σ is defined at $u_2(\sigma) = 0$, giving $\sigma = \sqrt[p]{\beta_2} = 0.458$Å, and ϵ is based on the binding energy of hydrogen, so that $-\epsilon$ is the minimum of the pair potential, giving $\epsilon/k_B = 51991$ K.

The three particle-potential is given as a sum over the contribution from each particle, and it's role is to prevent formation of more than one bond to each hydrogen atom.

$$u_{(3)} = h_{i,j,k}(r_{ij}, r_{jk}, \theta_{i,j,k}) + h_{j,i,k}(r_{ji}, r_{ik}, \theta_{j,i,k}) + h_{i,k,j}(r_{ik}, r_{kj}, \theta_{i,k,j}) \tag{6.30}$$

Where the h-functions are given by

$$h_{j,i,k}(r_{ji}, r_{ik}, \theta_{j,i,k}) = \begin{cases} \lambda a \exp\left[\frac{\gamma_3}{(r_{ji}-r_c)} + \frac{\gamma_3}{(r_{ik}-r_c)}\right] & \text{if } r_{ji} < r_c \text{ and } r_{ik} < r_c \\ 0 & \text{otherwise} \end{cases} \tag{6.31}$$

and

$$a = \left[1 + \mu\cos(\theta_{j,i,k}) + \nu\cos^2(\theta_{j,i,k})\right] \tag{6.32}$$

$\lambda = 2.80 \cdot 10^{-21}$ kJ, $\mu = 0.132587$, $\nu = -0.2997$ and $\gamma_3 = 1.5$ Å are constants [29]. The cut-off distance, r_c, is the same for both the two- and three-particle interactions (2.8 Å). The interaction potential we use has a finite range (has no long range dispersion attraction). A potential tail plays no role for the chemical reaction.

In the triad subscript j, i, k the middle letter i refers to the atom at the subtended angle vertex. A full description and analysis of the interaction potential was given earlier [48]. The total potential was used to determine the distance of chemically bonded particles. When the distance between two particles was shorter than $r^*_{ji} \leq 4.0$, they were labeled as part of a molecule, in agreement with the procedure used by Stillinger and Weber [3].

6.2.3 Calculation details

The simulation procedure was given earlier [48], and for this reason only the main details are given here. The simulation box contained 1000 particles ($N_p = N_{\mathrm{H}} +$

$2N_{H_2} = 1000$), with dimensions $V = L_x L_y L_z$, where $L_y = L_z = L_x/2$. The mass of one hydrogen atom, $m_0 = 1.67 \cdot 10^{-27}$ kg, was used to define the reduced total mass density $\rho^* = \rho\sigma^3/m_0$. This implies that the reduced total mass density equals the reduced total molar density in terms of ($N_p = N_H + 2N_{H_2}$). Reduced units are used throughout the paper, and are indicated by superscript *. The relations between real and reduced units is given in Table 6.1, $\epsilon/k_B = 51991$ K and $\sigma = 0.458$ Å [48].

Table 6.1: Relations between reduced and real units, $\epsilon/k_B = 51991$ K, σ=0.458 Å and $m_0 = 1.67 \cdot 10^{-27}$ kg.

Reduced variables	Formula
Mass	$m^* = m/m_0$
Distance	$r^* = r/\sigma$
Energy	$u^* = u/\epsilon$
Time	$t^* = (t/\sigma)\sqrt{\epsilon/m_0}$
Temperature	$T^* = k_B T/\epsilon$
Density	$\rho^* = \rho\sigma^3/m_0$
Pressure	$P^* = P\sigma^3/\epsilon$
Velocity	$v^* = v\sqrt{m_0/\epsilon}$

Dissociation of H_2

The degree of dissociation, mole fraction and pressure for the two higher densities was studied by us in a previous paper [48]. These results are repeated here for ease of reading, and supplemented with similar results for the low density $\rho^* = 0.0003$, see Tables 6.2–6.4.

For the lowest gas-like density, $\rho^* = 0.0003$ in Table 6.2, we have almost 1 % dissociation at the lowest temperature ($T^* = 0.07$), while for the highest temperature ($T^* = 0.4$) we have almost 80 % dissociation.

Table 6.2: Number of H atoms (N_H), mole fraction (x_i), total pressure (P^*) and the dissociation constant (K_x) for the density, $\rho^* = 0.0003$.

T^*	0.07	0.15	0.2	0.25	0.3	0.4
N_H	8	254.17	477.81	574.69	710.95	760.95
N_{H_2}	496	372.92	261.09	212.65	144.52	119.52
x_{H_2}	0.984	0.595	0.353	0.270	0.169	0.136
K_x	-	0.276	1.183	1.973	4.088	5.502
$10^5 P^*$	1.138	3.045	4.672	6.347	7.983	11.148

By increasing the density to that of a denser gas, to $\rho^* = 0.0011$ in Table 6.3, the dissociation degree decreases as expected. It is less than 1 % at $T^* = 0.07$, and

about 55 % at $T^* = 0.4$.

Table 6.3: Number of H atoms (N_{H}), mole fraction (x_i), total pressure (P^*) and the dissociation constant (K_x) for the density, $\rho^* = 0.0011$.

T^*	0.07	0.15	0.2	0.25	0.3	0.4
N_{H}	5.92	147.71	285.00	396.19	468.74	554.88
$N_{\mathrm{H_2}}$	497.04	426.14	357.50	301.91	265.63	227.56
$x_{\mathrm{H_2}}$	0.988	0.743	0.556	0.432	0.362	0.295
K_x	-	0.089	0.354	0.745	1.126	1.689
$10^5 P^*$	5.082	12.119	17.554	23.287	29.054	40.492

At the highest (liquid-like) density, $\rho^* = 0.004$ in Table 6.4, a further decrease is seen in the degree of dissociation. For the lowest temperature, $T^* = 0.07$, we now have 0.2 % dissociation, while there is an increase to 29 % for $T^* = 0.4$.

Table 6.4: Number of H atoms (N_{H}), mole fraction (x_i), total pressure (P^*) and the dissociation constant (K_x) for the density, $\rho^* = 0.004$.

T^*	0.07	0.15	0.2	0.25	0.3	0.4
N_{H}	1.98	66.90	137.61	192.39	232.42	288.50
$N_{\mathrm{H_2}}$	499.01	466.55	431.19	403.81	383.79	355.75
$x_{\mathrm{H_2}}$	0.996	0.875	0.758	0.677	0.623	0.552
K_x	-	0.018	0.077	0.154	0.228	0.363
$10^4 P^*$	4.094	8.478	11.292	14.051	16.729	21.892

Simulations were carried out for the series of composition and temperature listed in these tables, and thermodynamic data were computed according to this and the equations given in Section 2.1.

Simulation details

The Small System Method was applied according to procedures described by Schnell et al. [22–25], using the formulas given in Section 2.1. The sampling volume was a sphere with radius, L, varying from $L = \sigma$ to $L = 0.5\mathrm{L}_y$, where L_y is the length of the simulation box in the y-direction. The sampling was done at random positions in the simulation box. The number of particles and the energy were then computed for each sphere (50 spheres per sampling) and the time average gave the fluctuation of particle numbers and energy. The fluctuations were sampled every 100 time step, and time averages were calculated every 10 000 time step, after equilibration of the system. Data was plotted as a function of $1/L$. In order to test reservoir size dependence, we repeated some of the equilibrium simulations for the same density with 4096 particles, no significant size dependence was observed.

To check that the method performed in the expected way, we plotted the thermodynamic correction factors, obtained from particle fluctuations, versus the inverse sphere size ($1/L$). The plots are given in Figure 6.1 for $T^* = 0.07$, for all densities ($\rho^* = 0.0003$, $\rho^* = 0.0011$ and $\rho^* = 0.004$).

For the lowest density $\rho^* = 0.0003$ in Figure 6.1(a), we see that $\Gamma^{-1}_{\mathrm{HH}}$ as well as $\Gamma^{-1}_{\mathrm{HH_2}}$ vary linearly with $1/L$. The linear regression was in all cases done for points in the region $0.125 \leq 1/L^* \leq 0.16$, a range where such a dependence was observed. The range corresponded to spheres that included from 12 to 16 particles. It was chosen after observing that the inverse thermodynamic correction factor for systems with 4096 and 1000 particles coincide in this range.

The values reported are as expected. When the radius of the small system approaches zero, the value of Γ^{-1}_{ii} approaches 1, as a volume with one particle is ideal. The value of $\Gamma^{-1}_{\mathrm{HH}} = 1$ obeys this already for a wide range of values, while $\Gamma^{-1}_{\mathrm{H_2H_2}}$ increases from approximately 0.9 for the biggest sphere to 1 for $1/L = 0.4$ The correlation between H and H_2 is approximately zero, as the system mainly contains H_2, explaining $\Gamma^{-1}_{\mathrm{HH2}} = 0$.

The results for the higher densities followed the same trend. By increasing the density to $\rho^* = 0.0011$, see Figure 6.1(b), we find again that $\Gamma^{-1}_{\mathrm{HH}}$ and $\Gamma^{-1}_{\mathrm{H_2H_2}}$ are constant, while the $\Gamma^{-1}_{\mathrm{H_2H_2}}$ increases with decreasing size of the sphere, and at $1/L = 0.5$ we see that it is approximately 1. For the highest density, $\rho^* = 0.004$ in Figure 6.1(c), we again see that $\Gamma^{-1}_{\mathrm{HH}}$ is approximately 1 and independent of the sizes of the spheres, while $\Gamma^{-1}_{\mathrm{H_2H_2}}$ increases towards 1 for small spheres as expected.

For all three densities, there is only a variation in the value of $\Gamma^{-1}_{\mathrm{H_2H_2}}$. For all densities the factor increases with decreasing size of the sphere, and we also see that by increasing the density (and the number of H_2) we decrease the value in the thermodynamic limit. The limiting value of 1 for infinitely small spheres is reached for all densities, the approach being faster for the lowest density. $\Gamma^{-1}_{\mathrm{HH}}$ and $\Gamma^{-1}_{\mathrm{HH_2}}$ are constant at 1 and 0, respectively, for all densities.

All these results on $\Gamma^{-1}_{ij}(L)$ taken together confirm that the method works in a manner expected for the thermodynamic correction factor for the range of the variables chosen. This range is well above the limit where quantum mechanical effects take over [48], and away from boundaries where singularities can be expected [25]. We are therefore confident about the results.

No further results will be shown for $\Gamma_{ij}(L)$, as the smallness of the system is not a topic per se. We present results which all have been extrapolated to the thermodynamic limit.

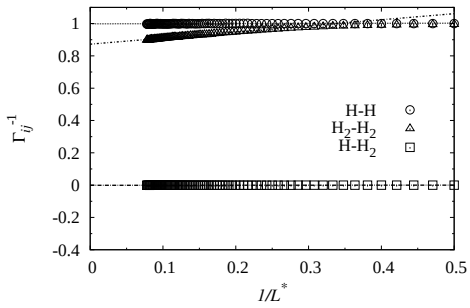

(a) $\rho^* = 0.0003,\ x_{\mathrm{H}_2} = 0.984$

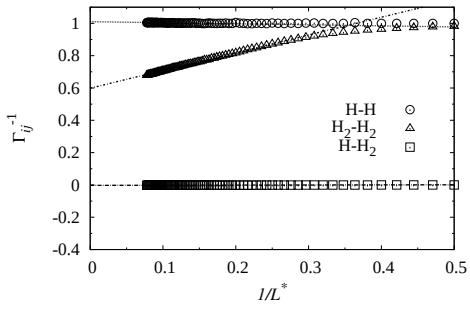

(b) $\rho^* = 0.0011,\ x_{\mathrm{H}_2} = 0.988$

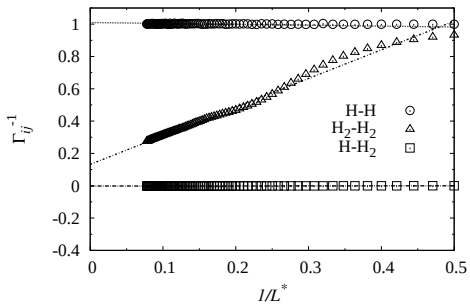

(c) $\rho^* = 0.004,\ x_{\mathrm{H}_2} = 0.996$

Figure 6.1: The inverse thermodynamic correction factor, Γ_{ij}^{-1}, for densities $\rho^* = 0.0003, \rho^* = 0.0011$ and $\rho^* = 0.004$ at $T^* = 0.07$. At this temperature it was observed that the degree of dissociation was independent of density, within the numerical accuracy. Linear regression was done in the region $0.125 \leq 1/L^* \leq 0.16$

6.3 Results

The main outcome of the calculations are the sets of enthalpies at constant (T, V, μ_j), (T, V, N_j) and (T, P, N_j), and the results derived from them. We present first the enthalpies obtained for the thermodynamic limit in the ensemble (T, V, μ_j), the original data from the sampling of fluctuations in the small system, and the corresponding sets for other ensembles, obtained by Lagrange transformations, see Eqs.(6.1) and (6.2).

The matrices A_{ij} and B_{ij} are not directly reported, instead we give Γ_{ij}^{-1} which is equivalent to B_{ij}, and which gives A_{ij}. The temperature interval $T^* = 0.07 - 0.4$ was used. We proceed to present results for the partial enthalpies in the different ensembles, the thermodynamic correction factors, the partial molar volumes, and the isothermal compressibility, to elucidate system properties, before we determine the enthalpy of reaction and the equilibrium constant as a function of temperature.

6.3.1 Partial molar enthalpy

The partial enthalpy at constant (T, V, μ_j), h, was found using the fluctuation method described in Section 6.2.3 for $T^* = 0.7 - 0.4$. The results for h for H and H_2 (for the small system) are shown as a function of the inverse radius of the small system in Figure 6.2 for $T^* = 0.2$. At this temperature, the mole fraction of H_2 varies from $x_{H_2} = 0.353$ ($\rho^* = 0.0003$) to $x_{H_2} = 0.758$ ($\rho^* = 0.004$) between the lowest and highest densities. The linear regression was preformed in the range $0.15 \leq 1/L^* \leq 0.3$. The range was chosen after comparing results for systems with with 1000 and 4096 particles. No size effect was found in this range. At the other temperatures, the plots looked like Figures 6.2(a) and 6.2(b), and are for this reason not shown.

The extrapolated partial enthalpies in the thermodynamic limit are given in Table 6.5 for all temperatures, $T^* = 0.07 - 0.4$, and all densities; $\rho^* = 0.0003$, $\rho^* = 0.0011$ and $\rho^* = 0.004$. All results showed a linear dependence and the linear regression was done for $0.15 \leq 1/L^* \geq 0.3$ in all cases.

From Table 6.5 we see that the partial enthalpy increases with increasing temperature, for H as well as H_2, for all densities. Using the method by Schnell et al. [25] we transformed the partial enthalpies at $(\partial H^*/\partial N_i)_{T,V,\mu_{j\neq i}}$ to $(\partial H^*/\partial N_i)_{T,V,N_{j\neq i}}$ and finally to the partial molar enthalpies, $(\partial H^*/\partial N_i)_{T,P,N_{j\neq i}}$. Where the partial molar enthalpies gives us access to the reaction enthalpy of the system as a function of the temperature, independent of the ideality of the mixture.

A plot of the data in Table 6.5 partial enthalpies in the different ensembles; (T, V, μ_j), (T, V, N_j) and (T, P, N_j) is given in Figure 6.3. The results for the different conditions may be interesting for a set of application purposes. Additional data are added in the plot for the highest densities, $\rho^* = 0.0011$ and $\rho^* = 0.004$. The

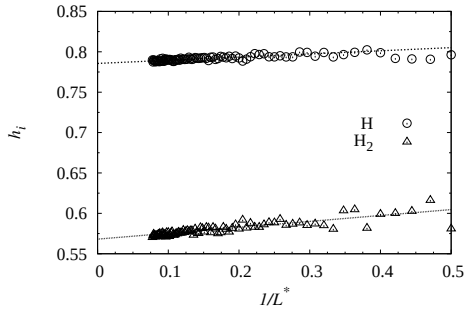

(a) $\rho^* = 0.0003,\ x_{\mathrm{H}_2} = 0.353$

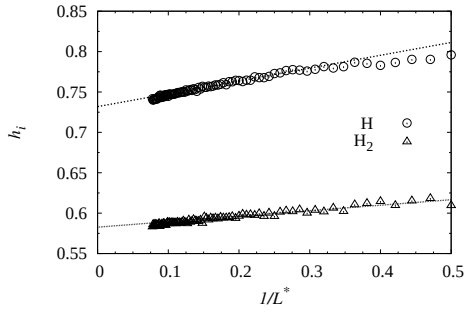

(b) $\rho^* = 0.0011,\ x_{\mathrm{H}_2} = 0.556$

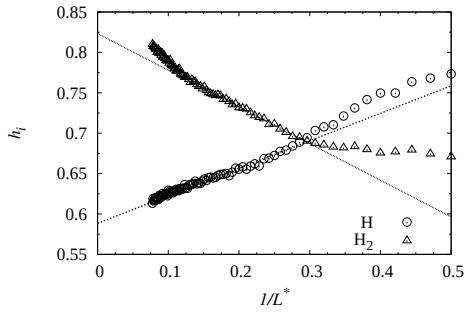

(c) $\rho^* = 0.004,\ x_{\mathrm{H}_2} = 0.758$

Figure 6.2: Partial enthalpies determined from fluctuation at (T, V, μ_j), h_i, as a function of the size of the sphere $(1/L^*)$ at $T^* = 0.2$. The linear regression was done in the region $0.15 \leq 1/L^* \leq 0.3$.

Table 6.5: Partial enthalpies, $h_{i,\infty}$ ($(\partial H^*/\partial N_i)_{T,V,\mu_j\neq i}$), in the thermodynamic limit. All values are given in reduced units.

	$\rho^* = 0.0003$		$\rho^* = 0.0011$		$\rho^* = 0.004$	
T^*	$h_{\mathrm{H},\infty}$	$h_{\mathrm{H_2},\infty}$	$h_{\mathrm{H},\infty}$	$h_{\mathrm{H_2},\infty}$	$h_{\mathrm{H},\infty}$	$h_{\mathrm{H_2},\infty}$
0.07	0.34	-0.46	0.44	-0.42	0.59	-0.27
0.15	0.60	0.18	0.59	0.21	0.59	0.46
0.2	0.79	0.57	0.73	0.58	0.59	0.86
0.25	0.98	0.95	0.89	0.93	0.61	1.15
0.3	1.19	1.31	1.07	1.27	0.66	1.47
0.4	1.59	2.04	1.44	1.92	0.78	2.08

difference is small for low gas-like densities, as expected, and becomes substantial at liquid-like densities. At the lowest density, $\rho^* = 0.0003$ in Figure 6.3(a), we see for the lowest temperatures, $T^* \leq 0.15$, that the values for (T, V, μ_j) and (T, V, N_j) are the same, for both H (open symbols) and H_2 (closed symbols). The mixtures at these conditions are then ideal.

At a higher temperature, the values for H_2 become more different, while they are approximately constant for H. This is in agreement with the results observed for the inverse thermodynamic correction factor, cf. Table 6.6. Increasing the density to $\rho^* = 0.0011$ in Figure 6.3(b) we see a deviation for H_2 (closed symbols) at high temperatures, $T^* \geq 0.15$; while for H (open symbols) we see deviations with increasing temperature. For the highest density, $\rho^* = 0.04$, we see that partial enthalpies of H_2 is constant for low temperature, but becomes significantly different at high temperature. For H a deviation is seen over the whole temperature range, but increases with increasing temperature.

The results for the ensemble (T, P, N_j) in these figures were used to construct the enthalpy of reaction. Before we show the outcome of that, we consider the other thermodynamic results.

6.3.2 Thermodynamic correction factor

The inverse thermodynamic correction factor in the thermodynamic limit, $\Gamma^{-1}_{ij,\infty}$, for all temperatures ($T^* = 0.07 - 0.4$) and densities ($\rho^* = 0.0003$, $\rho^* = 0.0011$ and $\rho^* = 0.004$) are given in Table 6.6. The values at infinity was found from linear extrapolation of the curve between $0.125 \leq 1/L \leq 0.16$, according to plots shown in Section 6.2.3

The inverse thermodynamic correction factors are also plotted in Figure 6.4 as a function of temperature for all densities. Red open symbols corresponds to $\Gamma^{-1}_{\mathrm{HH},\infty}$, blue filled symbols to $\Gamma^{-1}_{\mathrm{H_2H_2},\infty}$ and black cross shaped symbols to $\Gamma^{-1}_{\mathrm{HH_2},\infty}$. The figure shows that $\Gamma^{-1}_{\mathrm{HH},\infty}$ (red open symbols) is approximately constant independent

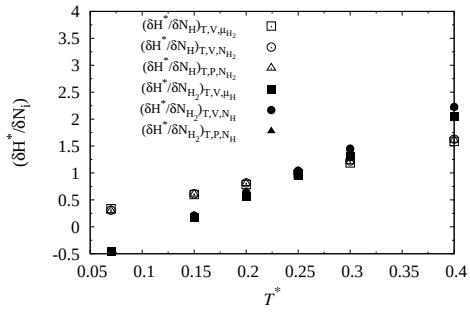

(a) $\rho^* = 0.0003$

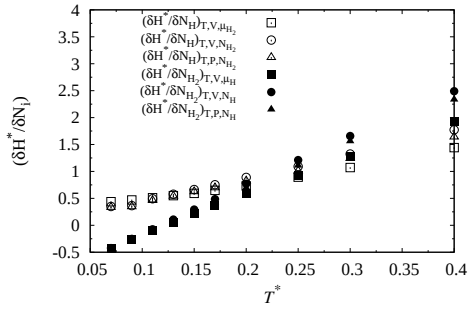

(b) $\rho^* = 0.0011$

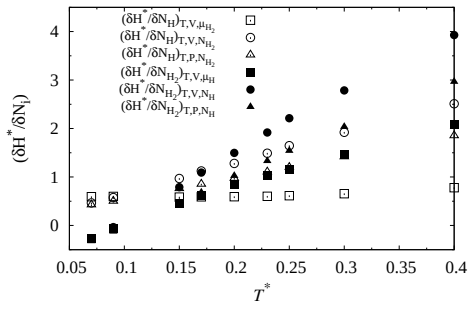

(c) $\rho^* = 0.004$

Figure 6.3: Partial enthalpies for all densities at the different ensembles; T, V, μ_j ($\square$), T, V, N_j ($\circ$) and T, P, N_j ($\triangle$). Open symbols corresponds to values for H while closed symbols represent H_2.

Table 6.6: The inverse thermodynamic correction factors, $\Gamma^{-1}_{ij,\infty}$, at constant μ, V, T in the thermodynamic limit.

	$\rho^* = 0.0003$			$\rho^* = 0.0011$		
T^*	$\Gamma^{-1}_{\mathrm{HH},\infty}$	$\Gamma^{-1}_{\mathrm{HH_2},\infty}$	$\Gamma^{-1}_{\mathrm{H_2H_2},\infty}$	$\Gamma^{-1}_{\mathrm{HH},\infty}$	$\Gamma^{-1}_{\mathrm{HH_2},\infty}$	$\Gamma^{-1}_{\mathrm{H_2H_2},\infty}$
0.07	1.00	-0.00	0.87	1.01	-0.00	0.60
0.15	1.00	-0.04	0.91	0.98	-0.08	0.67
0.2	0.98	-0.08	0.94	0.97	-0.16	0.73
0.25	0.96	-0.09	0.97	0.93	-0.20	0.78
0.3	0.96	-0.12	0.97	0.91	-0.24	0.82
0.4	0.94	-0.11	0.99	0.88	-0.28	0.87

	$\rho^* = 0.004$		
T^*	$\Gamma^{-1}_{\mathrm{HH},\infty}$	$\Gamma^{-1}_{\mathrm{HH_2},\infty}$	$\Gamma^{-1}_{\mathrm{H_2H_2},\infty}$
0.07	1.01	-0.00	0.13
0.15	1.02	-0.07	0.21
0.2	0.97	-0.17	0.23
0.25	0.97	-0.22	0.34
0.3	0.95	-0.26	0.38
0.4	0.91	-0.33	0.44

of temperature and density. For all densities; $\rho^* = 0.0003$ (△), $\rho^* = 0.0011$ (○) and $\rho^* = 0.004$ (□), we see that $\Gamma^{-1}_{\mathrm{HH},\infty} \in [0.9 : 1]$. A small decrease is found from 1 at $T^* = 0.07$ with increasing temperature, but the value stays within the given interval. An increasing temperature leads to an increasing amount of H in the system, see Tables 6.2–6.4.

The value of $\Gamma^{-1}_{\mathrm{H_2H_2},\infty}$ (filled blue symbols) is seen to increase with temperature, as the amount of H_2 decreases. For the lowest density, $\rho^* = 0.0003$ (▲), we see that it increases from approximately 0.9 to 1 for the investigated temperature interval. Increasing the density to $\rho^* = 0.0011$ (●), a steeper increase is seen with temperature, and this is further enhanced by increasing the density to $\rho^* = 0.004$ (■). If we compare $\Gamma^{-1}_{\mathrm{HH_2},\infty}$ for the different densities we see the smallest temperature dependence for the lowest density, $\rho^* = 0.0003$ (∗). For the two higher densities, $\rho^* = 0.0011$ (×) and $\rho^* = 0.004$ (+), we see a bigger decrease with increasing temperature.

The value of the thermodynamic correction factor for one component interacting with itself is 1 if the system is ideal (pure component; ideal gas). The value is zero for interactions between different components in this state. We conclude that the gas-like fluid at the lowest temperature and density, $T^* = 0.07$, $\rho^* = 0.0003$, is close to an ideal mixture. This is not surprising since, only 0.8% of the hydrogen is dissociated at the temperature (8 H atoms out of a 1000 particles). This is supported by a very small contribution from the three-particle interaction on the pressure.

The conclusion is supported by the expression for the chemical potential given by

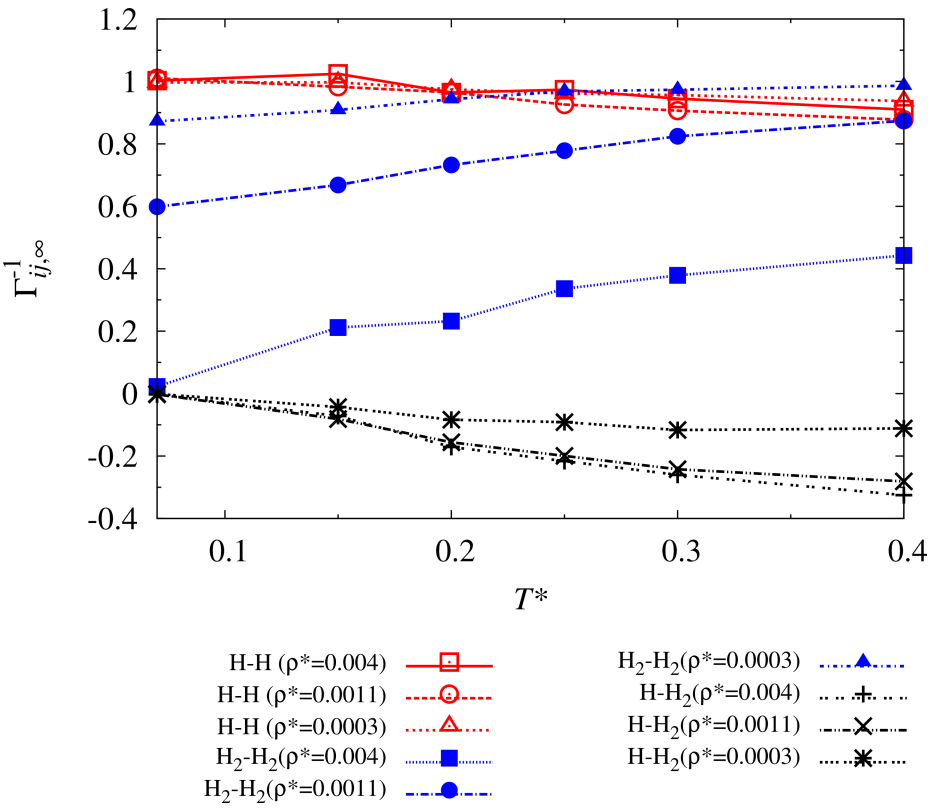

Figure 6.4: The inverse thermodynamic correction factor at the thermodynamic limit, $\Gamma^{-1}_{ij,\infty}$ for all three densities under consideration ($\rho^* = 0.0003$, $\rho^* = 0.0011$ and $\rho^* = 0.004$). The values are also given in Table 6.6. Red open symbols represent $\Gamma^{-1}_{\mathrm{HH},\infty}$, blue closed symbols $\Gamma^{-1}_{\mathrm{H_2H_2},\infty}$ and black cross symbols $\Gamma^{-1}_{\mathrm{HH_2},\infty}$.

Kirkwood and Buff [108]

$$\mu_1/k_BT = \log x_1 + f_2 x_2^2 + ... + \mu^\circ/k_BT \tag{6.33}$$

where

$$f_2 = \frac{G^\circ_{11} + G^\circ_{22} - 2G^\circ_{12}}{2v^\circ_1} \tag{6.34}$$

Here the superscript $^\circ$ indicates that the cluster integrals are evaluated in the infinitely dilute solvent (pure H_2). Here component 1 represent the solvent (H_2) and 2 the solute (H). We used the values at $T^* = 0.07$ for G°_{ii} and G°_{ij}. At this temperature we do not have a pure component (0.8 % dissociation), but we assume that the effect of this is negligible, and that the system still behaves approximately like a pure component system. f_2 in the above equation can then be directly linked to the activity coefficient for H, γ_{H}, via

$$f_2 x_2^2 = \ln \gamma_2 \tag{6.35}$$

From this we obtained $\gamma_2 = \gamma_H = 0.99$, indicating that we are indeed very close to ideal solution conditions.

6.3.3 Compressibility and reaction volume

The isothermal compressibility of the reacting mixture, κ_T, was calculated using Eq. (6.16). The results for all densities ($\rho^* = 0.0003$; $\rho^* = 0.0011$ and $\rho^* = 0.004$) are given in Figure 6.5. Studying Figure 6.5 we see that κ_T varies with density, and as expected, the lowest density, $\rho^* = 0.0003$, is easier to compress than the liquid, $\rho^* = 0.004$. The smaller the value of κ_T, the bigger the pressure needed to compress the mixture. This is also reflected in Figure 6.5, where we see that the compressibility of the high density mixture, $\rho^* = 0.004$, is constant, and approximately zero throughout the temperature interval. For the two lower densities, $\rho^* = 0.0011$ and $\rho^* = 0.0003$, we see a decrease in the compressibility with increasing temperature.

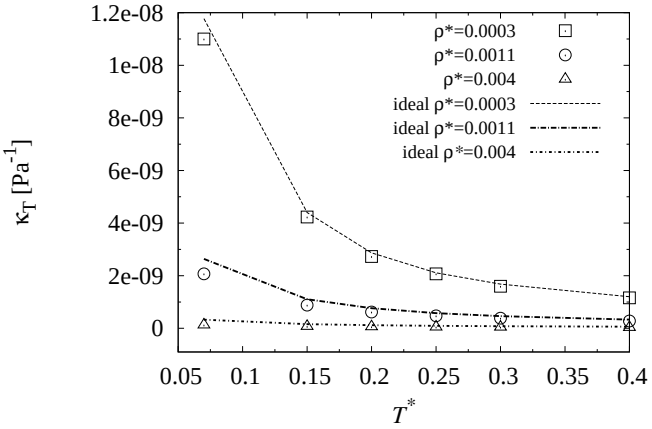

Figure 6.5: The compressibility of the solution, κ_T, as a function of temperature for all densities; $\rho^* = 0.0003$; (□), $\rho^* = 0.0011$; (○) and $\rho^* = 0.004$; (△). The ideal compressibility $(1/P)$ is given with lines for all densities.

The gas-like fluid with the lowest density, $\rho^* = 0.0003$, is the easiest mixture to compress. It is also possible to compress the moderate density, $\rho^* = 0.0011$, corresponding to a compressed gas mixture, though significantly less than the lowest density. For a moderate density, the molecules are sufficiently close enough to be affected by intermolecular forces, and is thus still compressible [113].

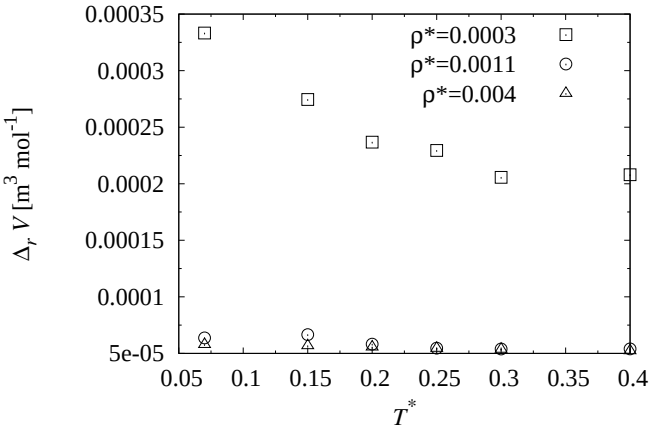

Figure 6.6: $\Delta_r V$ (m^3 mol^{-1}) for all densities. The low density $\Delta_r V$ has a significant temeperature variation.

The ideal compressibility $(1/P)$ is shown for comparison in Figure 6.5. It is fair to say that the low density mixture at low temperature has results that are relatively speaking, closest to ideal condition. Relatively speaking, the other fluids are further away from the ideal result.

The partial molar volumes of H and H_2 were calculated from Eq. (6.15) and used to compute $\Delta_r V$ for all densities, see Figure 6.6. As the difference between the partial molar volumes of H and H_2 increases with decreasing density and temperature, more curvature is seen for $\Delta_r V$ for the lowest density compared to the higher densities.

6.3.4 The reaction enthalpy and the thermodynamic equilibrium constant

In our previous work [48] we found a constant reaction enthalpy of 430 and 380 kJ mol^{-1}, assuming ideal conditions for the whole range of temperatures for $\rho^* = 0.004$ and $\rho^* = 0.0011$, respectively, from a plot of $\ln K_x$ vs $1/T$. We are now in a position to evaluate this calculation for the lowest density, $\rho^* = 0.0003$.

The standard state. Pressure variations of the reaction enthalpy.

In order to determine the thermodynamic equilibrium constant from the van't Hoff equation, Eq. (6.23), we need information on the standard state, in the present case defined by an ideal gas at 1 bar.

We have seen above, that the lowest density mixture of reactant and product are close to be an ideal solution, because the thermodynamic correction factors for the main components were close to unity at this condition, $\Gamma^{-1}_{\mathrm{HH},\infty} = 1.00$, $\Gamma^{-1}_{\mathrm{H_2H_2},\infty} = 0.87$, and $\Gamma^{-1}_{\mathrm{HH_2},\infty} \approx 0$. In addition, the compressibility was observed to follow and approximately equal to $1/P$.

With more simulation results, it is possible to find the ideal limit. The limit will be difficult to approach in this case, as the density must be much lower than the one used here to reach a overall pressure of 1 bar in the system. We will for this reason use the lowest density results at the lowest temperature, ($T^* = 0.07,\ \rho^* = 0.0003$), and use Eq.(6.21) to correct for the distance to 1 bar. At this temperature and density, the overall pressure of the system is approximately 850 bar. This gives a contribution of 7 units to K_{th} which must be added to the normal van't Hoff term (see Eq. (6.21)) for these conditions. For the whole range of pressures and densities used, the correction term varies from 3 - 24 units. We shall find that this gives a correction within the accuracy in the determination used otherwise.

The situation is illustrated in Figure 6.7. Studying this figure, we see that the reaction enthalpy, $\Delta_r H$, varies little with pressure compared to temperature. At $T^* = 0.07$ we therefore conclude that $\Delta_r H(T^* = 0.07) = \Delta_r H^{\ominus}$ is a good approximation.

Constant enthalpy

The enthalpy of reaction does not vary much for the lowest density, so a first estimate of K_{th} as a temperature function can be obtained using the approximation, $\Delta_r H(T^* = 0.07) = \Delta_r H^{\ominus} = 460$ kJ mol^{-1}.

With a constant enthalpy of reaction, the integrated van't Hoff equation gives

$$\ln\left(\frac{K_{th,2}}{K_{th,1}}\right) = -\frac{\Delta_r H^{\ominus}}{R}\left(\frac{1}{T_2} - \frac{1}{T_1}\right) \tag{6.36}$$

Evaluating the equation from $T_1 = 0.07$ (reference point) to $T_2 = 0.15,\ 0.2,\ 0.25,\ 0.3$ or 0.4, we can find $K_{th}(T_2)$. From the known value of the equilibrium constant, $K_{th,1}$, we find the ratio of the activity coefficients from Eq. (6.23). This ratio is given in Table 6.7 for the lowest density only.

Here, $K_P(T^* = 0.07) = K_{th}(T^* = 0.07)$ per definition as $T^* = 0.07$ was used as reference point. From Table 6.7 we see that K_{th} has the same order of magnitude as

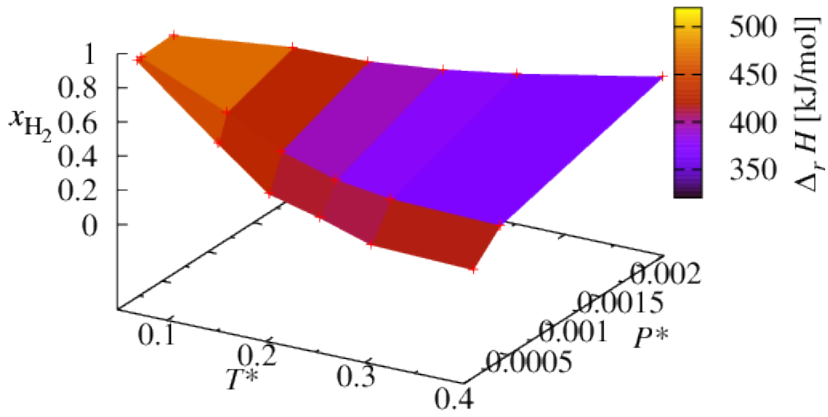

Figure 6.7: Reaction enthalpy, $\Delta_r H$ as a function of the reduced temperature (T^*) and pressure (P^*) and the fraction of H_2 in the system (x_{H_2}), for all densities.

Table 6.7: K_{th} and K_P and γ_H^2/γ_{H_2} as a function of the temperature, assuming that $\Delta_r H^\ominus = 460$ kJ/mol is constant, at $\rho^* = 0.0003$.

T^*	K_{th}	K_P	γ_H^2/γ_{H_2}
0.15	722	628	1.2
0.2	4256	4116	1.0
0.25	12335	9344	1.3
0.3	25075	24356	1.0
0.4	60867	45778	1.3

K_P and that the fraction of the activity coefficients varies from 1.0–1.3, indicating that we have attractive forces acting between H and H_2 (assuming $\gamma_H = 0.99$ (Eq. (6.35)) is constant over the temperature interval and $\gamma_{H_2} < 1$). This is so according to standard mixture theory when we compare with an ideal mixture of pure components. As one would expect H and H_2 to repel each other, this is unexpected.

Enthalpy varies with temperature

The temperature dependence on the enthalpy was next included in the van't Hoff equation.

The variation in $\Delta_r H$ as obtained from as a function of temperature, is given in Figure 6.8 in reduced units for all densities. The line in the bottom of the plot corresponds to the value found for the enthalpy by assuming the ideal condition used before (plot of $\ln K_x$ vs $1/T$) [48].

The reaction enthalpy (in J mol^{-1}) was now fitted to a quadratic function of the temperature, giving

$$\Delta_r H(\rho^* = 0.0003) = 0.0003T^2 - 8.9T + 4.9 \cdot 10^5 \tag{6.37}$$

$$\Delta_r H(\rho^* = 0.0011) = 0.0006T^2 - 19.5T + 5.5 \cdot 10^5 \tag{6.38}$$

$$\Delta_r H(\rho^* = 0.004) = 0.0007T^2 - 31.3T + 6.5 \cdot 10^5 \tag{6.39}$$

We rewrite the van't Hoff equation, using the identity $d(1/T) = -(1/T^2)dT$, and $\Delta_r H = aT^2 + bT + c$ and obtain after integration

$$\ln\left(\frac{K_{th,2}}{K_{th,1}}\right) = \frac{1}{R}\left[aT + b\ln T - \frac{c}{T}\right]\Bigg|_1^2 \tag{6.40}$$

The thermodynamic equilibrium constant and the ratio of the activity coefficients, calculated from this equation and Eq.6.23 are shown Table 6.8 for the lowest density. When we include the temperature dependence in $\Delta_r H$ we see from Table 6.8 that

Table 6.8: K_{th} and γ_H^2/γ_{H_2} as a function of the temperature at $\rho^* = 0.0003$ assuming the enthalpy of the reaction is described by a polynomial fit.

T^*	K_{th}	K_P	γ_H^2/γ_{H_2}
0.15	604	628	1.0
0.2	3208	4126	0.8
0.25	8606	9344	0.9
0.3	16564	24356	0.7
0.4	37932	45778	0.8

we get K_{th} in the same order of magnitude as K_P and K_{th} from Table 6.7 (where we used a constant $\Delta_r H$). The ratio of the activity coefficients are not constant

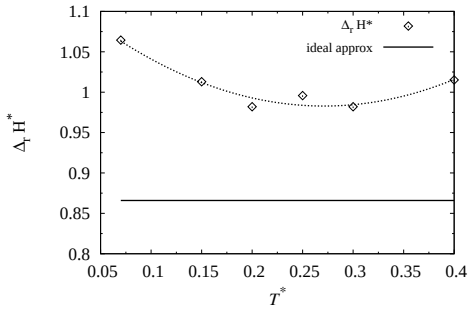

(a) $\rho^* = 0.0003$

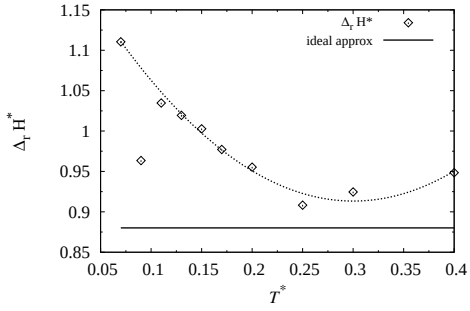

(b) $\rho^* = 0.0011$

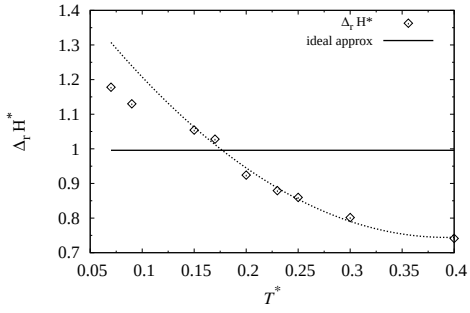

(c) $\rho^* = 0.004$

Figure 6.8: Reaction enthalpies, $\Delta_r H^*$, as a function of temperatures. The points ($\diamond$) represent results the simulation, $\Delta_r H = 2H_{\mathrm{H}} - H_{\mathrm{H_2}}$, the polynomial line represent the fit of the reaction enthalpy as a function of the temperature, while the line represent the ideal results, as found in previous paper [48] by plotting $\ln K_x$ as a function of temperature $(1/T)$.

and follow the same temperature dependence as we observe for $\Delta_r H$. The values indicates that we have repulsive forces (as expected) when $\gamma_{\mathrm{H}} \approx 1$ (Eq. (6.35)), at variance with the data in Table 6.7.

From the approximation $\Delta_r V(T^* = 0.07) = \Delta_r V^{\ominus}$ in the last term in Eq.(6.21) we calculate a correction due to pressure variation in K_{th} of 3–24, for the lowest to the highest temperature. Comparing these values to the calculated values of K_{th} in Tables 6.7 and 6.8 we see that they are negligible.

The results in Table 6.8 are therefore in agreement with results from the compressibility, and molar volume of the low density mixture, which all show essentially ideal behavior. We therefore conclude that the last method, where the temperature dependence on the enthalpy is included gives the most accurate results for K_{th}, as the repulsive forces between H and H_2 is captured.

The partial molar heat capacities of H and H_2, $C_{P,i}$ and the chemical reaction, are now readily available from Eq. (6.24). The partial molar enthalpies were linear functions of the temperature for all densities (not shown). This gave constant values for $C_{P,i}$ of H and H_2. The reaction heat capacity is shown in Figure 6.9.

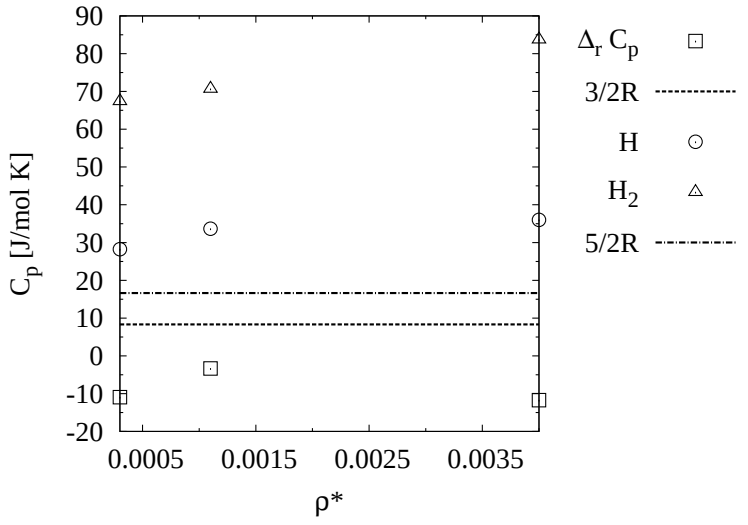

Figure 6.9: Partial molar heat capacity of H and H_2, $C_{P,i}$, and the reaction enthalpy, $\Delta_r C_P$, as a function of the density of the system. The ideal heat capacities, $3/2R$ and $5/2R$ have been included.

The value of C_{P,H_2} ($\triangle$) increases linearly with the density.No such trend was seen for $C_{P,\mathrm{H}}$ ($\circ$), where the partial molar heat capacity seems to go towards a constant

value. This is reasonable, as the atom has only kinetic degrees of freedom and a theoretical ideal heat capacity of $\frac{5}{2}R$. For the molecule, there are at least two more (rotational) degrees of freedom, and the possibility for activation of a vibrational degree of freedom.

6.3.5 The method

We have seen above that the Small System Method can be used to give accurate data for chemical reactions. Using the hydrogen dissociation reaction as example, we have calculated all relevant thermodynamic data for the reaction from one simulation at different temperatures and densities. The computations may seem cumbersome, by having to change between ensembles, but the transformation procedure is well established [25, 109]. The bonus is that information can be obtained about non-ideal behavior in mixtures and chemical reactions. This information is otherwise not easily accessible. This is promising for the future, as new force fields become available for calculation of chemical reactions using classical potentials, such as ReaxFF [38], REBO [39] and AIREBO [40].

The results elucidate that the normal assumption, to take the reaction enthalpy constant in the integration of van't Hofff's equation, can be much improved, see Figure 6.8. We see that the biggest error is observed for the low density, where the ideal value, assuming $K_{th} = K_x$, is far below the calculated value of the reaction enthalpy using the Small System Method. The calculated reaction enthalpy is for all densities in the same order of magnitude (350–460 kJ mol^{-1}) for $\rho^* = 0.0003 - -\rho^* = 0.004$ as the enthalpy of reaction at standard state conditions (436 kJ mol^{-1}) and the previous results obtained by us [48] 430 and 380 kJ mol^{-1} for $\rho^* = 0.004$ and $\rho^* = 0.0011$, respectively.

6.4 Conclusions

We have applied a new calculation method, the Small System Method, to sample data on particle and energy fluctuations, and find partial molar enthalpies and reaction enthalpies for the dissociation of hydrogen molecules to atoms. Data for the thermodynamic correction factor, compressibility, heat capacity and partial molar volumes were also obtained, all from the same set of simulations. The thermodynamic equilibrium constant was determined as a function of pressure and temperature for the lowest density studied, $\rho^* = 0.0003$. It was observed that the variation of the enthalpy with temperature was important to find the correct value of K_{th}.

We have earlier seen that the hydrogen dissociation reaction was far from ideal, as judged by contributions to i.e. the total pressure from the two-and three particle interaction potential, in spite of showing an apparently ideal behavior in terms of

pressure. In the present paper we see that even though we find the compressibility and the molar volume of the low density to give ideal behavior, non-ideality is observed in the heat capacity and the ratio of activity coefficients. From this we conclude that the method can provide information on the non-ideality of a system, which is information that is presently difficult to obtain, in a computationally effective way.

Acknowledgement

RS is grateful to Storforsk Project Transport nr. 167336 from NFR and the Department of Chemistry, NTNU, for financial support.

Chapter 7

Diffusion of heat and mass in a chemical reacting mixture

Ragnhild Skorpa[1], Thijs J. H. Vlugt[2], Dick Bedeaux[1] and Signe Kjelstrup[1]

1. Department of Chemistry,
Norwegian University of Science and Technology,
NO-7491 Trondheim, Norway

2. Process & Energy Laboratory, Delft University of Technology,
Leeghwaterstraat 39, 2628CB Delft, The Netherlands

This chapter is included as a manuscript draft

Is not included due to copyright

Chapter 8

Conclusions

The aim of this thesis project has been to model chemical reactions under both equilibrium and non-equilibrium conditions using classical molecular dynamics simulations. From this the aim was to improve and extend the existing methodology for describing chemical reactions, and gain knowledge about the nature of dissociative reactions. The dissociation of hydrogen $H_2 \rightleftharpoons 2H$ was used as a model system. This reaction is inevitable in producing hydrogen for fuel cells etc. using a palladium membrane reactor. Knowledge about the process is thus of great importance. This was illustrated by showing how a temperature gradient over a membrane could be used to enhance and control the flux of hydrogen through the membrane.

A temperature range where a significant degree of dissociation was present was determined using equilibrium molecular dynamics simulations. The Small System Method was extended to find partial molar enthalpies for both a non-reactive and a reactive system. From this the reaction enthalpy of the hydrogen dissociation reaction as a function of temperature, pressure and composition of the reacting mixture was found. Three different densities was studied, a gas (0.0052 g/cm^3), a compressed gas (0.0191 g/cm^3) and a liquid (0.0695 g/cm^3). Knowing the reaction enthalpy, it was possible to determine how far the system was from ideal conditions, and to find the thermodynamic equilibrium constant for a low density gas.

Knowing the equilibrium properties of the reaction, a temperature gradient was applied to the system. Based on analytical expressions for the mass flux and inverse temperature profiles the phenomenological coefficients and the transport properties of the system was determined, even though the reaction was observed to be far from chemical equilibrium, close to the thermostatted regions.

Thus, a model which can facilitate further studies of the impact of chemical reactions on transport systems has been made. The Small System Method makes it possible to determine e.g., reaction enthalpies for a linear dependent system, from

one simulation alone. The use of non-equilibrium thermodynamics makes it possible to describe and quantify the coupled heat and mass transport, which can in turn be used to e.g., enhance the hydrogen flux through a palladium membrane.

Chapter 9

Suggestions for further work

In this study classical molecular dynamics simulations have been used to study the dissociative hydrogen reaction under both equilibrium and non-equilibrium conditions. The newly developed extension to the Small System Method also made it possible to determine the reaction enthalpy as a function of temperature, pressure and composition. Based on the obtained results, some possibilities for further studies has been included below.

As the Small System Method has been incorporated into the familiar LAMMPS program, it is now easily accessible, for a variety of reactive and non-reactive force-fields. This means that partial molar enthalpies and reaction enthalpies can be calculated for a variety of systems. The method also gives access to the thermodynamic correction factor from which the chemical potential and activity coefficient can be found for a binary mixture. The thermodynamic correction factor can also be used to find Fick diffusion coefficients. These quantities are of interest for chemists and the chemical industry.

An interesting and natural extension of this thesis project would be to include a surface, e.g., palladium and study the reaction on a surface. The dissociative reaction of hydrogen on a palladium surface is important in a membrane reactor as discussed in this thesis. The Small System Method has already been extended to surfaces [59] and adding a temperature gradient would suite as a driving force for the chemical reaction. Non-equilibrium thermodynamics would also be a useful tool to study the temperature at the palladium surface.

In the last study, where non-equilibrium molecular dynamics was used to find transport coefficients, the thermal conductivity and heat of transfer in the presence of a chemical reaction was observed to be higher than expected. However, these quantities for a reactive system are scarcely reported in literature, and more studies could thus be beneficial to verify the observed results.

Bibliography

[1] F. H. Stillinger and T. A. Weber. Computer simulation of local order in condensed phases of silicon. *Phys. Rev. B*, 31:5262–5271, Apr 1985.

[2] F. H. Stillinger and T. A. Weber. Molecular dynamics study of chemical reactivity in liquid sulfur. *J. Phys. Chem.*, 91:4899–4907, 1987.

[3] F. H. Stillinger and T. A. Weber. Molecular dynamics simulation for chemically reactive substances. Fluorine. *J. Chem. Phys.*, 8:5123–5133, 1988.

[4] M. W. Finnis and J. E. Sinclair. A simple empirical n-body potential for transition metals. *Philosophical Magazine A*, 50(1):45–55, 1984.

[5] G. C. Abell. Empirical chemical pseudopotential theory of molecular and metallic bonding. *Phys. Rev. B*, 31:6184–6196, May 1985.

[6] L. Schlapbach and Züttel. Hydrogen-storage materials for mobile applications. *Nature*, 414:353–358, 2001.

[7] M. Momirlan and Veziroglu T. N. The properties of hydrogen as fuel tomorrow in sustainable energy system for a cleaner planet. *Int. J. of Hydrogen Energy*, 30(7):795 – 802, 2005.

[8] A. F. Holleman, E. Wiberg, and N. Wiberg. *Inorganic Chemistry*. Academic press, California, USA, 2001.

[9] D. Mendes, A. Mendes, L. M. Madeira, A. Iulianelli, J. M. Sousa, and A. Basile. The water-gas shift reaction: from conventional catalytic systems to Pd-based membrane reactors — a review. *Asia-Pac. J. Chem. Eng.*, 5:111–137, 2010.

[10] A. Basile. Hydrogen production using Pd-based membrane reactors for fuel cells. *Topics in Catalysis*, 51:107–122, 2008.

[11] S. Yun and S. T. Oyama. Correlations in palladium membranes for hydrogen separation: A review. *J. Mem. Sci.*, 375:28–45, 2011.

[12] S. Kjelstrup and D. Bedeaux. *Non-equilibrium thermodynamics of heterogeneous systems.* World Scientific, 2008.

[13] B. Hafskjold and T. Ikeshoji. Partial specific quantities computed by nonequilibrium molecular dynamics. *Fluid Phase Equilibria*, 104:173–184, 1995.

[14] S. I. Sandler. *Chemical, Biochemical, and Engineering Thermodynamics.* Wiley, 2006.

[15] P. Atkins and J. De Paula. *Atkins' Physical Chemisty.* Freeman, 8th edition, 2006.

[16] F. Daniels, J. W. Williams, P. Bender, R. A. Alberty, C. D. Cornwell, and J. E. Harriman. *Experimental Physical Chemistry.* McGraw-Hill, 7th edition, 1970.

[17] S. Sunner and M. Månsson. *Experimental Chemical Thermodynamics. Volume 1. Combustion Calorimetry.* Pergamon Press, 1979.

[18] F. A. Bettelheim. *Experimental Physical Chemistry.* W. B. Saunders Company, 1971.

[19] P. Sindzingre, G. Ciccotti, C. Massobrio, and D. Frenkel. Partial enthalpies and related quantities in mixtures from computer simulation. *Chem. Phys. Lett.*, 136:35–41, 1987.

[20] D. Frenkel and B. Smit. *Understanding Molecular Simulations. From Algorithms to Applications.* Academic Press, 2. edition, 2002.

[21] P. Sindzingre, C. Massobrio, G. Ciccotti, and D. Frenkel. Calculation of partial enthalpies of an Argon-Krypton mixture by NPT molecular dynamics. *Chem. Phys.*, 129:213–224, 1989.

[22] S. K. Schnell, T. J. H. Vlugt, J.-M. Simon, D. Bedeaux, and S. Kjelstrup. Thermodynamics of a small system in a μt reservoir. *Chem. Phys. Lett.*, 504:199–201, 2011.

[23] S. K. Schnell, X. Liu, J.-M. Simon, A. Bardow, D. Bedeaux, T. J. H. Vlugt, and S. Kjelstrup. Calculating Thermodynamic Properties from Fluctuations at Small Scales. *J. Phys. Chem. B*, 115:10911–10918, 2011.

[24] S. K. Schnell, T. J. H. Vlugt, J.-M. Simon, D. Bedeaux, and S. Kjelstrup. Thermodynamics of small systems embedded in a reservoir: a detailed analysus of finite size effects. *Mol. Phys.*, 110:1069–1079, 2012.

[25] S. K. Schnell, R. Skorpa, D. Bedeaux, S. Kjelstrup, T. J. H. Vlugt, and J.-M. Simon. Partial Molar Enthalpies and Reaction Enthalpies From Equilibrium Molecular Dynamics Simulation. *Submitted to JPC*, 2014.

[26] J. Xu, S. Kjelstrup, D. Bedeaux, and J.-M. Simon. Transport properties of $2F \rightleftharpoons F_2$ in a temperature gradient as studied by molecular dynamics simulations. *Phys. Chem. Chem. Phys.*, 9:969–981, 2007.

[27] D. C. Rapaport. *The Art of Molecular Dynamics Simulations.* Cambridge University Press, 2 edition, 2005.

[28] M. P. Allen and D. J. Tildesley. *Computer Simulation of Liquids.* Oxford University Press, New York, 1987.

[29] D. Kohen, J. C. Tully, and F. H. Stillinger. Modeling the interaction of hydrogen with silicon surfaces. *Surface Science*, 397:225–236, 1998.

[30] J. Xu, S. Kjelstrup, D. Bedeaux, A. Rœsjorde, and L. Rekvig. Verification of onsager's reciprocal relations for evaporation and condensation using non-equilibrium molecular dynamics. *J. Colloid Interf. Sci.*, 299:452–463, 2006.

[31] J. Xu, S. Kjelstrup, and D. Bedeaux. Molecular dynamics simulations of a chemical reaction; conditions for local equilibrium in a temperature gradient. *Phys. Chem. Chem. Phys.*, 8:2017–2027, 2006.

[32] J. Xu, S. Kjelstrup, D. Bedeaux, and J.-M. Simon. The heat of transfer in a chemical reaction at equilibrium. *J. Non-Equilib. Thermodyn.*, 32:341–349, 2007.

[33] B. M. Axilrod and E. Teller. Interaction of the van der Waals type between three atoms. *J. Chem. Phys.*, 11:299–300, 1943.

[34] R. J. Sadus. Exact calculation of the effect of three-body Axilrod-Teller interactions on vapour-liquid phase coexistence. *Fluid Phase Equilibria*, 144:351–359, 1998.

[35] R. J. Sadus. The effect of three-body interactions on the liquid-liquid phase coexistence of binary fluid mixtures. *Fluid Phase Equilibria*, 150:63–72, 1998.

[36] J. Tersoff. New empirical approach for the structure and energy of covalent systems. *Phys. Rev. B*, 37:6991–7000, Apr 1988.

[37] D. W Brenner. Empirical potential for hydrocarbons for use in simulating the chemical vapor deposition of diamond films. *Phys. Rev. B*, 42(15):9458–9471, 1990.

[38] A. C. T. van Duin, S. Dasgupta, F. Lorant, and W. A. Goddard III. ReaxFF: A reactive force field for hydrocarbons. *J. Phys. Chem. A*, 105:9396–9409, 2001.

[39] D. W. Brenner, O. A. Shenderova, J. A. Harrison, S. J. Stuart, B. Ni, and S. B. Sinnott. A second-generation reactive empirical bond order (rebo) potential energy expression for hydrocarbons. *J. Phys.: Condens. Matter*, 14:783–802, February 2002.

[40] S. J. Stuart, A. B. Tutein, and J. A. Harrison. A reactive potential for hydrocarbons with intermolecular interactions. *J. Phys. Chem.*, 112:6472–6486, April 2000.

[41] Kimberly Chenoweth, Adri C.T. van Duin, Petter Persson, Mu-Jeng Cheng, Jonas Oxgaard, and William A. Goddard, III. Development and application of a reaxff reactive force field for oxidative dehydrogenation on vanadium oxide catalysts. *J. Phys. Chem. C*, 112(37):14645–14654, 2008. PMID: 18652441.

[42] III Goddard, WilliamA., Adri Duin, Kimberly Chenoweth, Mu-Jeng Cheng, Sanja Pudar, Jonas Oxgaard, Boris Merinov, YunHee Jang, and Petter Persson. Development of the reaxff reactive force field for mechanistic studies of catalytic selective oxidation processes on bimoo x. *Topics in Catalysis*, 38(1-3):93–103, 2006.

[43] Kevin D. Nielson, Adri C. T. van Duin, Jonas Oxgaard, Wei-Qiao Deng, and William A. Goddard. Development of the reaxff reactive force field for describing transition metal catalyzed reactions, with application to the initial stages of the catalytic formation of carbon nanotubes. *J. Phys. Chem. A*, 109(3):493–499, 2005.

[44] Jeffery Ludwig, Dionisios G. Vlachos, Adri C. T. van Duin, and William A. Goddard. Dynamics of the dissociation of hydrogen on stepped platinum surfaces using the reaxff reactive force field. *J. Phys. Chem. B*, 110(9):4274–4282, 2006.

[45] F. H. Stillinger and T. A. Weber. Hidden structure in liquids. *Phys. Rev. A*, 25:978–989, Feb 1982.

[46] D. L. Diedrich and J. B. Anderson. Exact quantum Monte Carlo calculations of the potential energy surface for the reaction H $+H_2 \rightarrow H_2 +$ H. *J. Chem. Phys.*, 100:8089–8095, 1994.

[47] D. L. Diedrich and J. B. Anderson. An accurate quantum Monte Carlo calculation of the barrier height for the reaction H $+H_2 = H_2 +$ H. *Science*, 258:786–788, 1992.

[48] R. Skorpa, J.-M. Simon, D. Bedeaux, and K. Kjelstrup. Equilibrium properties of the reaction $H_2 \rightleftharpoons 2H$. *Phys. Chem. Chem. Phys.*, 6:1227–1237, 2014.

[49] P. Siegbahn and B. Liu. An accurate three-dimensional potential energy surface for H_3. *J. Chem. Phys.*, 68:2457–2465, 1978.

[50] T. L. Hill. *Thermodynamics of Small Systems, Part 1 and 2.* Benjamin, New York, 1963.

[51] T. L. Hill and R. V. Chamberlin. Extension of the thermodynamics of small systems to open metastable states: An example. *Proc. Natl. Acad. Sci.*, 95:12779–12782, 1998.

[52] T. L. Hill. Perspective: Nanothermodynamics. *Nano Letters*, 1:111–112, 2001.

[53] T. L. Hill. A Different Approach to Nanothermodynamics. *Nano Letters*, 1:273–275, 2001.

[54] X. Liu, S. K. Schnell, J.-M. Simon, D. Bedeaux, S. Kjelstrup, A. Bardow, and T. J. H. Vlugt. Fick Diffusion Coefficients of Liquid Mixtures Directly Obtained From Equilibrium Molecular Dynamics. *J. Phys. Chem. B*, 115:12921–12929, 2011.

[55] X. Liu, A. Martín-Calvo, E. McGarrity, S. K. Schnell, S. Calero, J.-M. Simon, D. Bedeaux, S. Kjelstrup, A. Bardow, and T. J. H. Vlugt. Fick Diffusion Coefficients in Ternary Liquid Systems from Equilibrium Molecular Dynamics Simulations. *Ind. Eng. Chem. Res.*, 51:10247–10258, 2012.

[56] S. K. Schnell, P. Englebienne, J.-M. Simon, P. Krüger, S. P. Balaji, S. Kjelstrup, D. Bedeaux, A. Bardow, and T. J. H Vlugt. How to apply the Kirkwood-Buff theory to individual species in salt solutions. *Chem. Phys. Lett.*, 582:154–157, 2013.

[57] J. Collell and G. Galliero. Determination of the thermodynamic correction factor of fluids confined in nano-metric slit pores from molecular simulation. *J. Chem. Phys.*, 140(19):–, 2014.

[58] M. M. Reif, M. Winger, and C. Oostenbrink. Testing of the GROMOS Force-Field Parameter Set 54A8: Structural Properties of Electrolyte Solutions, Lipid Bilayers, and Proteins. *J. Chem. Theory Comput.*, 9:1247–1264, 2013.

[59] T. T. Trinh, D. Bedeaux, J.-M. Simon, and S. Kjelstrup. Thermodynamic characterization of two layers of CO_2 on a graphite surface. *Chem. Phys. Lett.*, 612:214–218, 2014.

[60] S. Kjelstrup, D. Bedeaux, E. Johannesen, and J. Gross. *Non-Equilibrium Thermodynamics for Engineers*. World Scientific, 2010.

[61] S. R. Groot and P. Mazur. *Non-equilibrium thermodynamics*. Dover Publications, Inc., New York, 1984.

[62] L. Onsager. Reciprocal relations in irreversible processes. I. *Phys. Rev.*, 37:404–426, 1931.

[63] L. Onsager. Reciprocal relations in irreversible processes. II. *Phys. Rev.*, 38:2265–2279, 1931.

[64] R. Skorpa, M. Voldsund, M. Takla, S. K. Schnell, D. Bedeaux, and S. Kjelstrup. Assessing the coupled heat and mass transport of hydrogen through palladium membrane. *J. Mem. Sci.*, 394–395:131–139, 2012.

[65] J. W. Gibbs. *Scientific Papers: Thermodynamics.* Dover Publications, Inc., 1961.

[66] E. E. McLeary, J. C. Jansen, and F. Kapteijn. Zeolite based films, membranes and membrane reactors: Progress and prospects. *Micropor. Mesopor. Mater.*, 90:198–220, 2006.

[67] J. Coronas and J. Santamaria. State-of-the-art in zeolite membrane reactors. *Topics in Catalysis*, 29:29–44, 2004.

[68] T. P. Perng and J. K. Wu. A brief review note on mechanisms of hydrogen entry into metals. *Materials Letters*, 57:3437–3438, 2003.

[69] L. L. Jewell and B. H. Davis. Review of absorption and adsorption in the hydrogen-palladium system. *Applied Catalysis A:General*, 310:1–15, 2006.

[70] B. D. Morreale, M. V. Ciocco, R. M. Enick, B. I. Morsi, B. H. Howard, A. V. Cugini, and K. S. Rothenberger. The permeability of hydrogen in bulk palladium at elevated temperatures and pressures. *J. Mem. Sci.*, 212:87–97, 2003.

[71] S. K. Gade, P. M. Thoen, and D. J. Way. Unsupported palladium alloy foil membranes fabricated by electroless plating. *J. Mem. Sci.*, 316:112–118, 2008.

[72] T. L. Ward and T. Dao. Model of hydrogen permeation behavior in palladium membranes. *J. Mem. Sci.*, 153:211–231, 1999.

[73] I. J. Iwuchukwu and A. Sheth. Mathematical modeling of high temperature and high-pressure dense membrane separation of hydrogen from gasification. *Chemical Engineering and Processing*, 47:1292–1304, 2008.

[74] A. Caravella, G. Barbieri, and E. Drioli. Modelling and simulation of hydrogen permeation through supported Pd-alloy membranes with multicomponent approach. *Chem. Eng. Sci.*, 63:2149–2160, 2008.

[75] M. Coroneo, G. Montante, J. Catalano, and A. Paglianti. Modelling the effect of operating conditions on hydrodynamics and mass transfer in a Pd-Ag membrane module for H_2 purification. *J. Mem. Sci.*, 343:34–41, 2009.

[76] A. Bhargav and G. S. Jackson. Thermokinetic modeling and parameter estimation for hydrogen permeation through $Pd_{0.77}Ag_{0.23}$ membranes. *International Journal of Hydrogen Energy*, 34:5164–5173, 2009.

[77] J. Catalano, M. G. Baschetti, and G. C. Sarti. Hydrogen permeation in palladium-based membranes in the presence of carbon monoxide. *J. Mem. Sci.*, 362:221–233, 2010.

[78] E. Johannessen and K. Jordal. Study of a H_2 separating membrane reactor for methane steam reforming at conditions relevant for power processes with CO_2 capture. *Energy Conversion and Management*, 46:1059–1071, 2005.

[79] Y.-M. Lin, S.-L. Liu, C.-H. Chuang, and Y.-T. Chu. Effect of incipient removal of hydrogen through palladium membrane on the conversion of methane steam reforming. Experimantal and modeling. *Catalysis Today*, 82:127–139, 2003.

[80] J. Ge, S. Kjelstrup, D. Bedeaux, and J.-M. Simon. Transfer coefficients for evaporation of a system with a Lennard-Jones long-range spline potential. *Phys. Rev. E*, 75:061604, 2007.

[81] C. Y. Ho, R. W. Powell, and P. E. Liley. Thermal conductivity of the elements. *J. Phys. Chem. Ref. Data.*, 1:279–421, 1972.

[82] R. E. Buxbaum and T. L. Marker. Hydrogen transport through non-porous membranes of palladium- coated niobium, tantalum and vanadium. *J. Mem. Sci.*, 85:29–38, 1993.

[83] J.-M. Simon, O.-E. Haas, and S. Kjelstrup. Adsorption and desorption of H_2 on graphite by molecular dynamics simulations. *J. Phys. Chem. C*, 114:10212–10220, 2010.

[84] V. Labet, P. Gonzalez-Morelos, R. Hoffman, and N. W. Ashcroft. A fresh look at dense hydrogen under pressure.I. An introduction to the problem, amd an index probing equalization of H-H distances. *J. Chem. Phys.*, 136, 2012.

[85] C. E. Thomas. Fuel cell and battery electric vehicles compared. *Int. J. Hydrogen Energy*, 34:6005–6020, 2009.

[86] F. T. Wagner, B. Lakshmanan, and M. F Mathias. Electrochemistry and the Future of the Automobile. *J. Phys. Chem. Lett*, 1:2204–2219, 2010.

[87] P. T. Cummings and G. Stell. Statistical mechanical models of chemical reactions. *Mol. Phys.*, 51:253–287, 1984.

[88] W. R. Magro, D. M. Ceperley, C. Pierleoni, and B. Bernu. Molecular dissociation in hot, dense hydrogen. *Phys. Rev. Lett.*, 76:1240–1243, 1996.

[89] K. T. Delaney, C. Pierleoni, and D. M. Ceperley. Quantum Monte Carlo simulation of the high-pressure molecular-atomic crossover in fluid hydrogen. *Phys. Rev. Lett.*, 97:235702, 2006.

[90] H. Balamane, T. Halicioglu, and W. A. Tiller. Comparative study of silicon empirical interatomic potentials. *Phys. Rev. B*, 46:2250–2279, 1992.

[91] A. I. Boothroyd, P. G. Martin, W. J. Keogh, and M. J. Peterson. An accurate analytic H_4 potential energy surface. *J. Chem. Phys.*, 116:666–689, 2002.

[92] G. Ciccotti and J. P. Ryckaert. Molecular dynamics simulation of rigid molecules. *Computer Physics Reports*, 4:345–392, 1986.

[93] T. Ikeshoji and B. Hafskjold. Non-equilibrium molecular dynamics calculation of heat conduction in liquid and through liquid-gas interface. *Mol. Phys.*, 81:251–261, 1994.

[94] W. C. Swope, H. C. Andersen, P. H. Berens, and K. R. Wilson Wilson. A computer simulation method for the calculation of equilibrium constants for the formation of physical clusters of molecules: Application to small water clusters. *J. Chem. Phys.*, 76(1):637–649, 1982.

[95] B. Militzer, W. Margo, and D. Ceperley. Characterization of the state of hydrogen at high temperature and desity. *Contrib. Plasma. Phys.*, 39:151–154, 1999.

[96] D. Saumon and G. Chabrier. Fluid hydrogen at high density: Pressure dissociation. *Phys. Rev. A*, 44:5122–5141, 1991.

[97] B. Militzer and D. M. Ceperley. Path integral Monte Carlo simulation of the low-density hydrogen plasma. *Phys. Rev. E*, 63:066404, 2001.

[98] R. A. Alberty. *Thermodynamics of Biochemical Reactions.* Wiley-Interscience, 2003.

[99] T. Engell and P. Reid. *Physical Chemistry.* Prentice Hall, 2012.

[100] B. E. Poling, J. M. Prausnitz, and J. P. O. O'Connell. *The properties of gases and liquids.* McGraw-Hill, New York, 5th edition, 2004.

[101] J. D. Weeks, D. Chandler, and H. C. Andersen. Role of repulsive forces in determining the equilibrium structure of simple liquids. *J. Chem. Phys.*, 54:5237–5247, 1971.

[102] P. Krüger, S. K. Schnell, D. Bedeaux, S. Kjelstrup, T. J. H. Vlugt, and J.-M. Simon. Kirkwood-Buff integrals for finite volumes. *J. Phys. Chem. Lett.*, 4:235–238, 2013.

[103] R. Taylor and H. A. Kooijman. Composition derivatives of activity coefficient models (for the estimation of thermodynamic factors in diffusion). *Chem. Eng. Comm.*, 102:87–106, 1991.

[104] R. Krishna and J. A. Wesselingh. The Maxwell-Stefan approach to mass transfer. *Chem. Eng. Sci.*, 52(6):861–911, 1997.

[105] H. Hadwiger. *Vorlesungen über Inhalt, Oberfläche und Isoperimetrie*. Springer, 1957.

[106] K. R. Mecke. Integral geometry in statistical physics. *Int. J. Mod. Phys. B*, 12:861–899, 1998.

[107] E. M. Blokhuis. Existence of a bending rigidity for a hard-sphere liquid near a curved hard wall: Validity of the hadwiger theorem. *Phys. Rev. E*, 87(2):022401, February 2013.

[108] J. G. Kirkwood and F. P. Buff. The Statistical Mechanical Theory of Solutions. I. *J. Chem. Phys.*, 19:774–777, 1951.

[109] A. Ben-Naim. *A molecular theory of solutions*. Oxford University Press, 2006.

[110] C. H. Turner, J. K. Brennan, M. Lisal, W. R. Smith, J. K. Johnson, and K. E. Gubbins. Simulation of chemical reaction equilibria by the reaction ensemble monte carlo method: A review. *Mol. Sim.*, 34:119–146, 2008.

[111] T. J. H. Vlugt and B. Smit. On the efficient sampling of pathways in the transition path ensemble. *PhysChemComm*, 2:1–7, 2001.

[112] P. Sindzingre, G. Massobrio, C. Ciccotti, and D. Frenkel. Calculation of partial enthalpies of an argon-krypton mixture by NPT molecular dynamics. *Chemical Physics*, 129:213–224, 1989.

[113] K. S. Shing and S.-T. Chung. Calculation of Infinite-Dilution Partial Molar Properties by Computer Simulation. *AIChE J.*, 34:1973–1980, 1988.

[114] P. G. Debenedetti. Fluctuationbased computer calculation of partial molar properties. I. Molecular dynamics simulation of constant volume fluctuations. *J. Chem. Phys.*, 86:7126, 1987.

[115] P. G. Debenedetti. Fluctuationbased computer calculation of partial molar properties. II. A numerically accuarate method for the determination of partial molar energies and enthalpies. *J. Chem. Phys.*, 88:2681, 1988.

[116] P. G. Debenedetti. Fluctuation Simulations and the Calculation of Mechanical Partial Molar Properties. *Mol. Sim.*, 2:33–53, 1989.

[117] D. Saumon and G. Chabrier. Fluid hydrogen at high density: The plasma phase transition. *Phys. Rev. Lett.*, 62:2397–2400, May 1989.

[118] K. Sawada and T. Fujimoto. Effective ionization and dissociation rate coefficients of molecular hydrogen in plasma. *J. Appl. Phys.*, 78(5):2913–2924, 1995.

[119] D. A. Reed and G. Ehrlich. Surface diffusion, atomic jump rates and thermodynamics. *Surface Science*, 102(2-3):588–609, 1981.

[120] R. B. Bird, W. E. Stewart, and E. N. Lightfoot. *Transport phenomena*. John Wiley & Sons, 1960.

[121] J. N. Butler and R. S. Brokaw. Thermal Conductivity of Gas Mixtures in Chemical Equilibrium. *J. Chem. Phys.*, 26:1636–1643, 1957.

[122] R. B. Bird, W. E. Stewart, and E. N. Lightfoot. *Transport phenomena*. John Wiley & Sons, 2nd. edition, 2006.

[123] R. Taylor and R. Krishna. *Multicomponent Mass Transfer*. Wiley, New York, 1993.

[124] R. Skorpa, J.-M. Simon, D. Bedeaux, and K. Kjelstrup. The reaction enthalpy of hydrogen dissociation calculated with the Small System Method from simulation of molecular fluctuations. *Phys. Chem. Chem. Phys.*, 16:19681–19693, 2014.

[125] F. Muller-Plathe. A simple nonequilibrium molecular dynamics method for calculating the thermal conductivity. *J. Chem. Phys.*, 106(14):6082–6085, 1997.

[126] F. J. Uribe, E. A. Mason, and J. Kestin. Thermal conductivity of nine polyatomic gases at low density. *J. Chem. Phys. Ref. Data*, 19:1123–1136, 1990.